Pulse dynamics in mode-locked high energy laser oscillators

Von der Fakultät für Mathematik und Physik
der Gottfried Wilhelm Leibniz Universität Hannover
zur Erlangung des Grades

Doktor der Naturwissenschaften
- Dr. rer. nat. -

genehmigte Dissertation

von
Dipl.-Phys. Martin Siegel
geboren am 17.07.1979 in Mannheim

2009

Referent: Prof. Dr. U. Morgner
Korreferent: PD. Dr. D. Ristau
Tag der Promotion: 11.11.2009

für Steffi

Kurzfassung:

Martin Siegel
Pulsdynamik in modengekoppelten Hochenergie-Laseroszillatoren

Modengekoppelte Hochenergie-Laseroszillatoren bieten die Möglichkeit, Femtosekunden-laserpulse mit Pulsenergien von einigen Mikrojoule und Repetitionsraten im Megahertz-bereich zu erzeugen. Sie können dadurch als Strahlquellen für verschiedenste Anwendungen von der Atomphysik über die Biologie bis hin zur Medizin und Materialbearbeitung dienen.

In der vorliegenden Doktorarbeit wurde die Pulsdynamik von verschiedenen Lasersystemen untersucht, um mit Hilfe von numerischen Simulationen und experimentellen Ergebnissen Aussagen über die weitere Energieskalierbarkeit dieser Systeme zu gewinnen. Besonderes Augenmerk wurde dabei auf auftretende Limitationen sowie Möglichkeiten diese zu umgehen gelegt. So gelang es durch die numerische Modellierung eines Yb:KYW Scheibenlasers mit Cavity-Dumping, die experimentell beobachteten Limitierungen theoretisch zu erklären. Dies ermöglichte es Wege zu finden, diese in zukünftigen Lasersystemen zu vermeiden. Die numerischen Ergebnisse zeigen, dass es so möglich sein wird, die erreichbare Pulseenergie deutlich zu steigern.

Des Weiteren wurde erstmalig eine detaillierte Untersuchung zum 'chirped-pulse'-Betrieb in Ytterbium Lasern durchgeführt. Basierend auf experimentellen und numerischen Daten konnte ein besseres Verständnis dieses Operationsregimes erlangt werden. Hiermit gelang es zu zeigen, dass auf Ytterbium basierende Scheibenlaser im positiven Dispersionsbereich außerordentliches Potential für eine weit reichende Energieskalierung bieten.

Schließlich konnte ein Titan-Saphir-Lasersystem aufgebaut werden, das es erstmalig erlaubt Pulsenergien von mehr als einem Mikrojoule direkt aus einem Titan-Saphir-Oszillator zu erzeugen. Hierzu kam das Konzept des Cavity-Dumpings mittels eines akusto-optischen Modulators in Kombination mit einem KLM und SESAM modengekoppelten chirped-pulse Laseroszillator zum Einsatz. Abschließend wird ein für dieses System entwickelter kryogener Nachverstärker sowie die Planungen für zukünftige Anwendungen in der Erzeugung von hoher harmonischer Strahlung vorgestellt. Die Ergebnisse dieser Arbeit erlauben ein deutlich besseres Verständnis des chirped-pulse Regimes und zeigen dessen enorme Bedeutung und Potential für zukünftige Entwicklungen. Dies wird es ermöglichen Spitzenintensitäten zu erzielen, die nie zuvor mit Laserpulsen direkt aus dem Oszillator erreicht werden konnten.

Schlagworte: Modenkopplung, Scheibenlaser, Titan-Saphir Laser

Abstract:

Martin Siegel

Pulse dynamics in mode-locked high energy laser oscillators

Mode-locked high energy laser oscillators offer the possibility to generate femtosecond laser pulses with energies on the microjoule level and repetition rates in the MHz regime. This makes them suitable for a variety of applications in areas ranging from atomic physics over biology up to medicine and material processing.

In this thesis the pulse dynamics of several different laser systems were investigated using numerical and experimental methods. The goal of these investigations was to find out more about the energy scaling properties of these systems. Special regard was put on possible limitations and ways to avoid them. Doing so allowed to find a theoretical explanation for experimental limitations observed in an Yb:KYW thin disk oscillator with cavity-dumping. As a result of this it was possible to identify ways of overcoming these limitations in future systems. The numerical results show that a significant increase of the pulse energy can be achieved in future systems.

In addition to this for the first time a detailed investigation of the chirped pulse regime in Yb-based lasers was done. Based on the comparison of experimental and numerical results it was possible to achieve a better understanding of this operation regime. Using these results it was also possible to show that Yb-based thin disk oscillators operating in the chirped pulse regime, have extraordinary potential for further energy scaling.

Finally it was also possible to develop the first Ti:sapphire laser system capable of generating pule energies in excess of one microjoule directly from the Ti:sapphire oscillator. To this end the concept of cavity-dumping with an acousto-optic modulator was used in a chirped pulse oscillator with both Kerr-lens and SESAM mode-locking. Lastly a cryogenic post-amplifier developed for this laser system is discussed and the plans for a first application in high harmonic generation are presented. The results of this thesis allow an improved understanding of the chirped pulse regime and show its importance as well as the potential for future developments. Using the results of this thesis it will be possible to reach peak intensities so far never achieved with pulses from a laser oscillator.

Key words: mode-locking, thin disk laser, Ti:sapphire laser

Contents

1 Introduction

In recent years ultrashort femtosecond laser systems have gone from being used solely in a handful of research laboratories to being used all over the world for applications ranging from fundamental physics like high harmonic generation and metrology over applications in biology (CARS) and medicine (LASIK) up to industrial applications like material post-processing in the automotive industry.

As the number of possible applications for this kind of lasers continues to grow with each passing year, so does the demand for new systems able to provide shorter pulses, higher pulse energies or faster repetition rates. Consequently the investigation and development of new femtosecond laser sources has long been one of the most active research areas in the optical sciences. In terms of the pulse duration, techniques such as SESAM and SESAM mode-locking have made it possible to routinely generate pulses with durations of only a few femtoseconds [Spe91, Rau08] from laser oscillators. For applications demanding higher pulse energies than those available from standard femtosecond oscillators while still requiring ultrashort pulse durations, the most common systems used are based on the chirped pulse amplification (CPA) method [Str85]. The main advantage of the CPA technique is the excellent energy scaling ability which allows to reach pulse energies ranging anywhere from the microjoule level up to several hundred Joules [Hec06].

The drawbacks of the CPA technique are on the one hand rather complex and expensive setups and more importantly the fact that the repetition rates are typically limited to the kHz-regime. The latter being the result of the high power pump lasers required for the amplification process which typically cannot operate at higher repetition rates. However as MHz repetition rates offer advantages for many applications in terms better of statistics, signal-to-noise ratio or processing time there is a great deal of interest in the development of high repetition rate high energy laser sources. Amongst other things the development of such laser sources makes it possible to generate high harmonic EUV radiation with MHz repetition rates which can then be studied with much better statistics in order to understand the underlying fundamental physical processes.

To this end much research has been done in recent years on high energy laser oscillators capable of delivering femtosecond laser pulses with pulse energies on the microjoule level at MHz repetition rates. By employing techniques like cavity-dumping, which increase the outcoupling ratio, or implementing long-cavity concepts, which increase the cavity length in order to achieve higher pulse energies at the expense of the average power, it was possible to raise the pulse energy available from femtosecond oscillators by about three orders of magnitude from the nanojoule to the microjoule level.
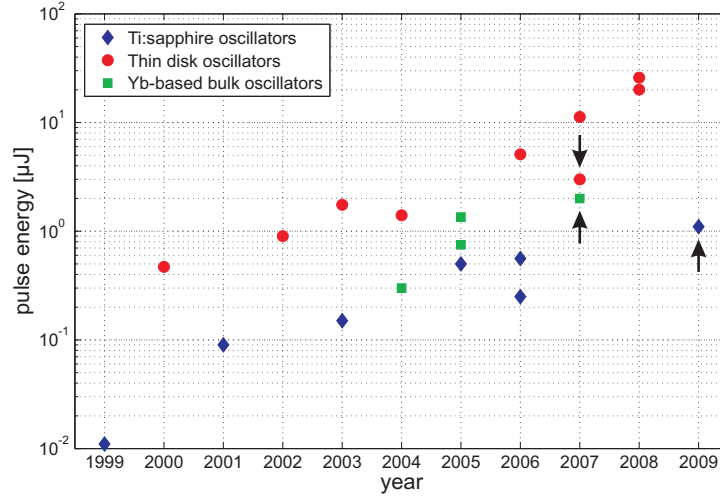
Figure 1.1: Evolution of high energy laser oscillators from 1999-2009 [Süd08, Kow06, Kil04b, Cho01, Pal07a, Sie09]. The three systems that are subject of this thesis are marked with arrows.

This development is illustrated in Fig. 1.1 which shows the evolution of high power femtosecond lasers over the course of the last decade. Aside from the traditional workhorse, the Ti:sapphire oscillators, in recent years Yb-doped gain media like Yb:YAG or Yb:KYW have become increasingly important for the generation of high energy laser pulses. While these crystals cannot compete with Ti:sapphire in terms of the emission bandwidth, they do offer a large advantage because they can be directly pumped with commercially available laser diodes. Together with the invention of the thin disk laser [Gie94], this made it possible to employ pump powers much higher than any currently available for Ti:sapphire systems. As a result, the highest pulse energies from femtosecond oscillators are currently generated with laser systems based on Yb-doped gain media.

Parallel to this, Ti:sapphire oscillators still play an important role as they are currently the only systems capable of delivering high pulse energies with pulse durations below 100 fs. For these systems, too, the pulse energy has drastically increased over the last decade from little more than 10 nJ [Cho99] up to pulse energies of more than one microjoule as a result of this thesis [Sie09].

Despite these successes, energy scaling is still one of the most important issues when it comes to current research in laser development. Amongst the key issues faced by current high energy oscillators are limitations that occur in the form of nonlinearities which can destabilize the laser operation and prevent further increases in the pulse energy. A possible solution to this is operation in the chirped pulse regime which can significantly reduce the nonlinearities in the laser cavity.

In this thesis, the pulse dynamics and energy scaling properties of different high energy laser oscillators are investigated both numerically and experimentally. To this end the

first chapter will give an introduction to the theoretical background required for the understanding of the remainder of this thesis. The second chapter will then introduce key methods for the energy scaling of femtosecond lasers like cavity-dumping or operation in the chirped pulse regime in more detail. Following this, a numerical investigation into the pulse dynamics of an Yb:KYW thin disk oscillator with cavity-dumping is presented. Modeling the laser system allows to gain a greater understanding of the processes which limit the pulse energies currently available from this system and to find ways for future improvements. Next to this the possibility of using Yb-based thin disk lasers operating in the chirped pulse regime for energy scaling purposes is investigated for the first time. Numerical simulations modeled after existing laser systems are used to show the great potential this kind of laser systems offers when it comes to generating highly energetic femtosecond pulses.

In the final experimental chapter the first Ti:sapphire oscillator capable of generating pulse energies in excess of one microjoule is introduced. Besides details of the experimental setup this chapter also presents experiments which help to better understand the intra-cavity dynamics and to gauge the possibilities of energy scaling in future systems. Lastly a cryogenic cw post-amplifier setup is presented which can be used to further increase the available pulse energy.

The thesis then concludes with a recapitulation of the achieved results and an outlook about how the results can be used to enable the generation of even higher energetic pulses in future systems. Finally the first planned application of the microjoule Ti:sapphire laser in an experiment about plasmon enhanced high harmonic generation in EUV region will be presented.

2 Principles of Laser dynamics and mode-locking

To allow better understanding of the main part of this thesis, which often relies on a number of rather fundamental equations, the following chapter is intended to give a recollection of some of the basic theoretical background to lasers in general and mode-locked femtosecond lasers in particular. The first section introduces the essential equations governing the dynamics of any laser oscillator, the rate equations as well as some dynamic processes like Q-switching and relaxation oscillations. The properties and special dynamics of mode-locked oscillators are presented in the third section of this chapter. After discussing the effects of dispersion on a mode-locked laser, the so-called 'Master equation of mode-locking' will be introduced as will the most common techniques and mechanisms for mode-locking solid-state laser oscillators. As the goal of this chapter is only to give a short overlook over topics required for the understanding of this thesis the presentation will be rather condensed and by no means complete. For a more detailed and also broader treatment of these topics the reader is referred to standard textbooks such as those by Svelto [Sve98], Koechner [Koe06] or in the case of femtosecond lasers by Diels and Rudolph [Die06]. A particularly thorough derivation can also be found in [Ell03].

2.1 Basic Laser dynamics

2.1.1 Rate equations

The basic dynamics of any laser system are governed by a set of two coupled differential equations, the so-called rate equations. Fig. 2.1 shows the schematic of a 4-level system as is typical for many common solid-state laser materials, e.g. Ti:sapphire. To achieve the necessary electron inversion between the laser levels 3 and 2, it is required that the lifetime of the energy levels 4 and 2 are negligible compared to the lifetime of the upper laser level 3. In a 4-level laser system these transitions are typically intra-band phonon transitions which for our purpose can be viewed as instantaneous. Because of this the time constants T_{43} and T_{21} are neglected in the further treatment of the system. By increasing the pump rate R, a stronger inversion can be created. As noted the actual laser transition takes place between the levels 3 and 2, hence T_{32} is denominated as τ_L, the lifetime of the laser material. If a photon created from this transition is reflected back into the crystal this photon can now induce stimulated emission, i.e. the emission of a second photon of equal frequency, phase and spatial direction. This then leads to the light amplification typical for any laser.
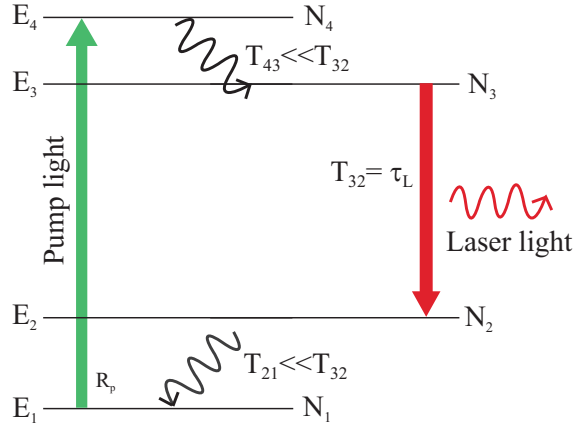
Figure 2.1: Schematic drawing of a four level laser system. The pumplight excites electrons from the groundlevel E_1 to the E_4, laser action takes place between the upper laser level E_3 and the lower laser level E_2. Both of which are linked to the other levels by vibronic transitions.

Using this schematic level system, it is possible to derive the two rate equations governing the laser system. As this derivation can be found in most of the standard textbooks on lasers, e.g. [Sve98, Koe06], it is not given here. Instead below, the final equations are given in a form that is best suited for the experimentalist as it involves parameters accessible in real lasers rather than somewhat more abstract numbers like the number of electrons in a given laser state.

$$\frac{d}{dt}g = -\frac{g - g_0}{\tau_L} - \frac{gP}{E_{sat,L}} \tag{2.1}$$

$$\frac{d}{dt}P = (g - l)\frac{P}{T_{rep}} \tag{2.2}$$

Here T_{rep} is the cavity round-trip time, l the losses of the resonator and P is the laser power. Eq. (2.1) describes the dynamic of the single pass gain g of the laser while eq. (2.2) shows the temporal evolution of the laser power. The remaining parameters are the small signal gain coefficient of the laser:

$$g_0 = \frac{\sigma_L \tau_L R_P}{2A_{eff}} \tag{2.3}$$

and the saturation energy of the laser:

$$E_{sat,L} = \frac{\hbar m \omega_L}{\sigma_L} A_{eff} \tag{2.4}$$

Here σ_L denotes the stimulated emission cross section of the laser material, A_{eff} the effective mode area, R_P the pump rate, $\hbar$ the Planck constant, m the number of passes

trough the laser medium and ω_L the laser frequency.

While this model is somewhat simplified, as it omits possible vibrational transitions between the two laser levels which can occur in laser gain media, it nevertheless describes the fundamental dynamics of a four level laser system and can be used to model most laser oscillators accurately.

Steady state operation

To get a better understanding of some of the processes in a laser oscillator it is helpful to look at the steady state regime in which the power of the oscillator is constant over time or mathematically speaking $\frac{d}{dt}P = 0$. Looking at the rate equations there now exist two solutions for eq. (2.2): First a trivial solution where $P = 0$ and no laser action takes place and a second where the gain is equal to the losses of the resonator $g_s = l$. With this eq. (2.1) becomes:

$$P = P_{sat}\left(\frac{g_0}{l} - 1\right) \tag{2.5}$$

As can be seen there exists a threshold $g_0 = l$ below which no laser operation is possible. For $g_0 > g_s$ the gain in the oscillator is sufficient to allow the laser to emit power which will rise linearly with g_0. At some point, a steady state of operation will be reached for which the saturated gain offsets the cavity losses during each roundtrip, $g_s = l$. As a measure of how far above the threshold the current regime of laser operation is, the so-called pump parameter is defined as $r = g_0/g_s$. Lastly since the stimulated emission during the laser process results in a reduction of the lifetime of the upper laser level, the stimulated emission lifetime τ_{stim} is defined as:

$$\tau_{stim} = \frac{\tau_L}{r} \tag{2.6}$$

Relaxation oscillations

In any laser oscillator there is a direct coupling between the inversion of the laser medium and the number of photons in the oscillator. This coupling, while necessary for the operation of the laser, results in a special type of damped oscillations which are called relaxation oscillations. Basically these oscillations can be understood as energy that is oscillating between gain material and laser photons. Relaxation oscillations will always arise at the start up of a laser before the system reaches steady state operation. More importantly however during steady state operation any perturbations of the laser will also give rise to relaxation oscillations as they represent a natural resonance of the dynamic system. Because of this any periodic perturbations with a frequency close to that of the relaxation oscillations can result in dynamical instabilities of the laser. An example of such a periodic perturbation is for instance cavity-dumping which will be dealt with in great detail later in this thesis.

For a 4-level system the frequency of the relaxation oscillations is given by:

$$f_{relax} = \frac{1}{2\pi} \left[\frac{r(r-1)l}{\tau_L T_{rep}} \right]^{1/2} = \frac{1}{2\pi} \left[\frac{g_0(\frac{g_0}{l} - 1)}{\tau_L T_{rep}} \right]^{1/2} \tag{2.7}$$

and the damping time is described by:

$$t_0 = 2\frac{\tau_L}{r^2} = 2\tau_L \left(\frac{l}{g_0} \right)^2 \tag{2.8}$$

The derivation of these equations as well as a more detailed description of the relaxation oscillations can be found in [Sve98]. Looking at eq. (2.7) and (2.8) the importance of small signal gain and losses with respect to the relaxation oscillations becomes obvious. The higher the gain and the lower the losses, the more stable a laser oscillator will be against relaxation oscillations stemming from perturbations during the steady state operation.

2.1.2 Q-switching

As can be seen in the previous paragraph the dynamics and the stability of any given laser oscillator is greatly dependent on the interplay between gain and losses in the laser cavity. This becomes even more obvious when looking at the dynamics behind the so-called Q-switching regime in laser oscillators. As in the previous sections only a brief overview over some of the key features of Q-switching will be given here, a much more in-depth description of the process can for instance be found in [Sve98] or [Mor03].
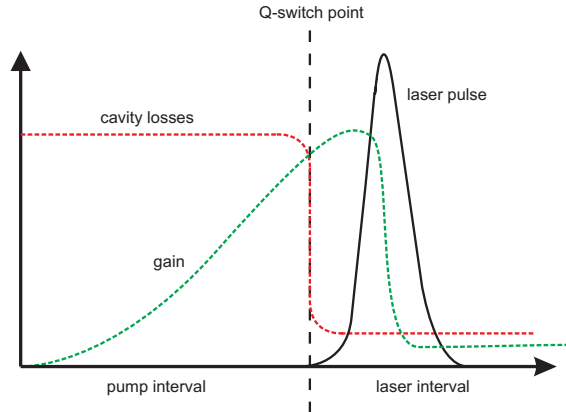
Active Q-switching

Figure 2.2: Schematic of the laser dynamics in the case of active Q-switching. [Kel02]

For an optical resonator, the quality or Q-factor represents a measure of the power losses per round trip and is defined as:

$$Q = \frac{\omega_L T_{rep}}{l} \tag{2.9}$$

where ω_L is the center wavelength of the laser. As the term suggests, Q-switching is a process where changes in the resonator Q-factor result in a changing behavior of the laser itself. The reason for this lies in the dynamic coupling between the gain saturation and the laser field, which do not necessarily react on the same timescale. This is illustrated in Fig. 2.2, the gain is saturated by pumping the laser medium in a cavity with relatively high losses during the pump interval. Due to the low Q-factor of the cavity no laser action is possible during this period. When the laser medium is close to saturation, the losses are reduced by means of an active switch (hence the term active Q-switching) and the cavity is suddenly far above the laser threshold. As a result, in this laser interval the number of photons in the laser field increases quickly due to the high gain of the saturated laser medium in combination with the low losses of the cavity and can far exceed the steady state limits. As the number of photon grows rapidly, the gain in the laser medium is depleted quickly and soon drops below the laser threshold at which point the laser action once again ceases. The end result of this is the formation of a short, high energy laser pulse which can be used to achieve higher intensities than in the steady-state regime. The pulse duration, pulse energy and the possible repetition rates are subject to the parameters of the laser cavity, the gain medium, the pump source and the switch employed in the Q-switching. Typical pulse durations for active Q-switched lasers are in the nanosecond range but pulses down to the ps regime have also been shown [Zay95]. The achievable pulse energies vary widely from system to system, but can reach several Joules in high power applications. Similarly the repetition rates vary from kHz for lower energies to below one Hertz for the highest pulse energies.
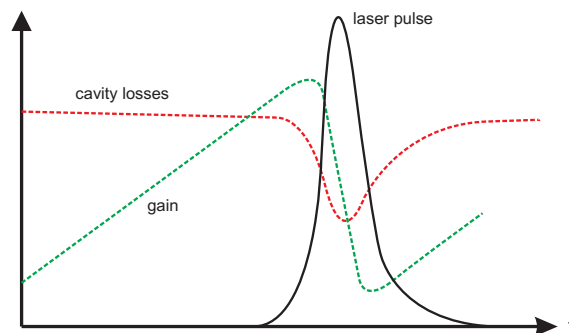
Passive Q-switching

Figure 2.3: Schematic of the laser dynamics in the case of passive Q-switching. [Kel02]

Instead of using an active switch to change the Q-factor of a cavity, it is also possible to use nonlinear intra-cavity elements to achieve a similar effect. This method is called 'passive

Q-Switching'. In this case the nonlinear element needs to act as a saturable absorber, inducing losses at low intensities while saturating for higher intensities. Consequently the laser will operate in the high intensity Q-switched regime rather than in the low intensity steady state.

To understand the effect of a saturable absorber in the case of passive Q-switching it is necessary to look at the relaxation oscillations of the laser. In the steady state regime these oscillations are damped with a time constant given by eq. (2.8). In the case of passive Q-switching the highest of these oscillations will saturate the absorber and consequently their damping will be reduced. Fig. 2.3 shows the dynamics of this process: As a result of pumping, the gain of the laser increases until the laser threshold is achieved. At this point the intensity of the laser field rises quickly and causes the absorber to saturate which reduces the losses. Consequently the number of photons in the laser field rises so rapidly that the gain is depleted far below the laser threshold, the laser action stops and the next cycle starts. Like in the case of active Q-switching the end result is a short, but intense, laser pulse.

Q-switching instabilities in mode-locked Lasers

While Q-switching as discussed above is an important tool for the generation of high energetic laser pulses, it also often poses a problem in passively mode-locked laser oscillators. Here it can occur as an undesired side effect of the loss modulation required in the mode-locking process. The reason for this is that the loss modulation is nothing but a modulation of the cavity Q-factor and as such can also result in unwanted Q-switching instabilities. If the modulation becomes too high, the damping of the relaxation oscillations becomes too weak and the undamped oscillations can lead to Q-switching. Instead of producing stable laser pulses with a frequency of f_{rep}, the laser will then generate bursts of laser pulses with at a far lower frequency and with varying pulse energy. In order to better understand and to avoid these instabilities a qualitative criterion against Q-switching instabilities has been developed in Ref. [Kär95] and extended in [Hön99]. This criterion can be given as:

$$E_p^2 > E_{sat,L}E_{sat,A}\Delta R \qquad (2.10)$$

Here E_p is the pulse energy of the mode-locked laser, $E_{sat,A}$ is the saturation energy of the absorber while ΔR is its modulation depth. To stay within the scope of this thesis an in-depth mathematical derivation of this criterion will be skipped and the reader is referred to the cited literature.

To better understand the physics behind this criterion it is helpful to remember that passive Q-switching is mainly governed by two factors: The damping of the relaxation oscillations and the dynamic of the gain. An increased damping or a quicker gain dynamic will lessen the likelihood for Q-switching instabilities. A reduction in the damping or a slower gain dynamic will increase the tendency for Q-switching. Looking at eq. (2.10) it

is now possible to identify the influence of each term.

The most obvious way of increasing stability against Q-switching in a mode-locked laser is to increase the left side of the inequality, the pulse energy. This can be understood by the fact that an increase in pulse energy always is the equivalent of raising the pump rate r. As can be seen from eq. (2.8) an increased pump rate means that the damping of the relaxation oscillations will get stronger and hence the stability against Q-switching increases.

The second parameter is the saturation energy of the laser $E_{sat,L}$. Looking at eq. (2.4) this parameter includes parameters of the laser medium such as σ_L and ω_L but also the effective mode area A_{eff}. Since the material parameters of the laser medium are fixed for any given material, the only accessible parameter is the mode area. By looking at eq. (2.3) it can be seen that a reduced mode area results in a higher small signal gain. From eq. (2.1) it is obvious that an increased small signal gain leads to a quicker gain dynamic and as has been noted above a quicker gain dynamic stabilizes the laser against Q-switching.

The final two parameters in eq. (2.10) are parameters that describe the behavior of the saturable absorber. $E_{sat,A}$ is the saturation energy of the absorber and is defined as:

$$E_{sat,A} = \phi_A A_{eff,A} \tag{2.11}$$

where ϕ_A is the saturation fluence of the absorber while $A_{eff,A}$ is the effective mode area on the absorber. Since the saturation fluence again is a material parameter and is fixed for a given absorber the most easily accessible parameter is the mode area. As is the case with the saturation energy of the laser, a smaller mode area on the absorber will suppress Q-switching instabilities. This is easily understood as a smaller mode area at a fixed pulse energy ensures that the absorber will saturate faster and more thoroughly which reduces the losses in the cavity.

Easiest to understand is the influence of the modulation depth ΔR. This parameter essentially describes the losses inflicted by the absorber or in other words the modulation of the Q-factor. Obviously if this modulation is reduced, Q-switching becomes less likely.

The stability criterion as given in eq. (2.10) is a helpful tool in the development of ultra-short pulsed laser systems, especially those lasers that rely on a saturable semiconductor absorber mirror (SESAM) for mode-locking. In a real life experiment usually not all of the parameters in eq. (2.10) are exactly known, nevertheless even in this case the stability criterion can often be used to help identify the cause of mode-locking instabilities and show ways to overcome these problems. One such case will be treated later in this thesis, in chapter 4.2.

3-Level and Quasi-3-level systems

Besides the 4-Level systems described in the section above, there also exist many laser media that feature either a 3-level or a quasi-3-level system some of which will be treated

in this thesis. In a 3-level system the laser transition takes place between the upper laser level and the ground state, while in a quasi-3-level system the lower laser level is so close to the ground state that it can be populated by simple thermal excitation. Because of these differences in general eq. (2.1) and (2.2) have to be adapted to accurately describe the dynamics of lasers based on such three-level and quasi-3-level gain media. For an in-depth description of 3-level systems and the changes required for the treatment of such materials the reader is referred to textbooks such as [Koe06] where this is treated in great detail. Dynamically the reabsorption in a quasi-3-level system does simply result in additional losses which reduce the small-signal gain. Because of this in a numerical treatment of the laser dynamics it is possible to use the same equations as in the case of a 4-level system as long as the small-signal gain is adapted accordingly. This has been done as part of the numerical modeling shown later in this thesis.

2.2 Ultra-short laser pulses

While pulsed lasers with pulse durations down to the nano- and picosecond range can be achieved with Q-switching mechanisms, pulse durations in the femtosecond range can only be generated by the technique of mode-locking. The focus of this section will be on the underlying physics behind mode-locking as well as techniques that are used for the generation of these ultra-short laser pulses. It also has to be noted that while both active and passive mode-locking techniques exist, this section will mainly deal with the passive techniques, as these are the ones used for the ultra-short pulse laser development described in this thesis.

The key for the understanding of femtosecond laser pulses is the so-called 'time-bandwidth product':

$$\Delta\tau_{puls} \cdot \Delta\nu = const. \tag{2.12}$$

This relation is a special form of Heisenbergs Uncertainty Principle and describes the relation between pulse duration and optical bandwidth of a mode-locked laser pulse. In order to achieve the shortest possible pulses it is necessary to have a frequency spectrum which is as broad as possible. Consequently rather than having a single optical frequency, as is the case for an ideal continuous wave laser, an ultra-short mode-locked laser pulse is formed by a large number of different frequencies.

2.2.1 Optical pulses and dispersion

While eq. (2.12) shows that a broad frequency spectrum allows a short pulse duration, the broad frequency spectrum associated with a femtosecond laser pulse also makes it especially susceptible to dispersion. Consequently when the pulse propagates in any kind of medium other than vacuum one needs to consider the effect of chromatic dispersion. In

any medium the speed of light is reduced by the wavelength dependent index of refraction $n(\nu)$:

$$c = \frac{c_0}{n(\nu)} \tag{2.13}$$

with c_0 the speed of light in vacuum. Since the index of refraction is different for different frequencies of light, optical frequencies which form a femtosecond laser pulse will all travel with different velocities which results in an overall temporal broadening of the pulse.

To better understand the effects of dispersion it is helpful to look closer at the laser pulse itself. Mathematically a laser pulse can be written as a superposition of plane waves:

$$E(z,t) = \frac{1}{2} \left[\int_0^\infty \hat{E}(\omega') e^{i(\omega' t - k(\omega')z)} d\omega' + c.c. \right] \tag{2.14}$$

Assuming one defined polarization state and omitting the complex conjugate (c.c.) part of the equation for simplicity, we can now use the coordinate transformation $\omega' = \omega_0 + \omega$ in order to arrive at:

$$E(z,t) = \frac{1}{2} \int_0^\infty \hat{E}(\omega_0 + \omega) e^{i((\omega_0+\omega)t - k(\omega_0+\omega)z)} d\omega \tag{2.15}$$

$$= \underbrace{\left(\int_0^\infty \hat{E}(\omega_0 + \omega) e^{i\omega t} e^{-i\Delta k(\omega)z} d\omega \right)}_{envelope} \underbrace{\left(e^{(i\omega_0 t - k(\omega_0)z)} \right)}_{carrier} e^{i\phi_{CEO}} \tag{2.16}$$

with the propagation constant $\Delta k(\omega) = k(\omega_0 + \omega) - k(\omega_0)$. Lastly by introducing the complex amplitude A(z,t) it is now possible to separate the electric field into the pulse envelope and the carrier-oscillation:

$$A(z,t) = \frac{1}{\sqrt{2Z_F}} \int_0^\infty \hat{E}(\omega_0 + \omega) e^{i\omega t} e^{-i\Delta k(\omega)z} d\omega \tag{2.17}$$

$$E(z,t) = \sqrt{2Z_F} A(z,t) e^{(i\omega_0 t - k(\omega_0)z)} e^{i\phi_{CEO}} \tag{2.18}$$

Using the factor $\sqrt{2Z_F}$ (with Z_F the dielectric impedance) ensures that $|A(z,t)|^2$ can be regarded as the intensity of the pulse. The phase factor ϕ_{CEO} is called the carrier envelope offset phase and describes the position of the electric field carrier below the pulse envelope.

Following eq. (2.16) the effects resulting from propagation in a dispersive medium on a

laser pulse are governed by the phase term $\phi = \Delta k(\omega)z$. By expanding this term into a series it is possible to understand the effects of dispersion:

$$\phi(\omega) = \Delta k(\omega)z \tag{2.19}$$

$$= \left.\frac{\partial k(\omega)z}{\partial \omega}\right|_{\omega_0} (\omega - \omega_0) \;+\; \frac{1}{2}\left.\frac{\partial^2 k(\omega)z}{\partial \omega^2}\right|_{\omega_0} (\omega - \omega_0)^2 \;+\; \frac{1}{6}\left.\frac{\partial^3 k(\omega)z}{\partial \omega^3}\right|_{\omega_0} (\omega - \omega_0)^3 + ...$$
$$\tag{2.20}$$

In this series, the coefficients of the series correspond with the different orders of dispersion:

$$D_1 = \left.\frac{\partial \phi}{\partial \omega}\right|_{\omega_0} = \left.\frac{\partial k(\omega)z}{\partial \omega}\right|_{\omega_0} (\omega - \omega_0) = \frac{z}{v_g} = group\ delay\ (GD) \tag{2.21}$$

The first order term is the group delay (GD) with the group velocity v_g, as a result of the group delay the whole pulse will be delayed in time.

$$D_2 = \left.\frac{\partial^2 \phi}{\partial \omega^2}\right|_{\omega_0} = \frac{1}{2}\left.\frac{\partial^2 k(\omega)z}{\partial \omega^2}\right|_{\omega_0} (\omega - \omega_0)^2 = group\ delay\ dispersion\ (GDD) \tag{2.22}$$

The 2nd order term shown above corresponds to the group delay dispersion (GDD). In contrast to the GD, all higher order terms result in a temporal broadening of the laser pulse. This broadening of the pulse is symmetrical for the GDD, but for the 3rd order dispersion (TOD) shown below as well as for still higher orders leads to irregular effects like pulse steepening.

$$D_3 = \left.\frac{\partial^3 \phi}{\partial \omega^3}\right|_{\omega_0} = \frac{1}{6}\left.\frac{\partial^3 k(\omega)z}{\partial \omega^3}\right|_{\omega_0} (\omega - \omega_0)^3 = third\ order\ dispersion\ (TOD) \tag{2.23}$$

As can be seen from the series expansion in eq. (2.20), the influence of the different dispersion orders is strongly dependent on the frequency bandwidth of the laser pulse. Because of this, the dispersion management becomes increasingly important for femtosecond laser pulses, especially ultra-short pulses with pulse durations below 10 fs.

2.2.2 Principles of mode-locking

As discussed in the previous section, a laser pulse can be described as a coherent superposition of plane waves with different frequencies. The mathematical formula for such a laser pulse was given in eq. (2.14). The question now is, how this mathematical descrip-

tion transfers to a real laser system and how such a coherent superposition of waves can be achieved in such a system?

To answer this question it is necessary to first look at the parameters that govern the frequency range of plane waves in a laser oscillator. One obvious factor in this is the emission bandwidth of the gain medium which sets an upper limit for the frequency range that can be amplified by the laser process. The other factor is the resonance condition given by the oscillator length:

$$f_m = mc/2L \tag{2.24}$$

with m the number of the cavity mode, f_m the frequency of the m-th cavity mode, c the speed of light and L the length of the cavity. In any given laser cavity only frequencies fulfilling this condition can form longitudinal standing waves and thus become part of the laser process. Usually in laser oscillators the relation between these two conditions is such that the emission bandwidth is broader than the minimal frequency spacing of $c/2L$ and as a result a number of different frequencies, the so-called laser modes, will be amplified in the laser. Generally these laser modes will have a randomly distributed phase with respect to each other which inhibits stable pulsed operation. To overcome this it is necessary to lock the phase relation between the different laser modes in such a way that all modes interfere constructively. Assuming N resonator modes are locked with constant phase, each having the same intensity $\hat{A}/\sqrt{N}$ equation (2.18) can be rewritten to give the electric field of the resulting laser pulse:

$$E(T) = \frac{\hat{A}_0 \sqrt{2Z_F}}{\sqrt{N}} \sum_{m=0}^{N-1} e^{im2\pi(f_R - f_0)t} \tag{2.25}$$

with f_0 the center frequency of the gain medium. To illustrate the importance of mode-locking for the pulse duration as well as the achievable intensities, a short example is shown in Fig. 2.4.

The intensity of the laser pulses increases linearly with the number of phase-locked laser modes. As a result already for a relatively small number of modes as in this example the increase is easily visible. By comparison the number of modes locked in a typical ultrashort Ti:sapphire oscillator is on the order of several times 10^5.

2.2.3 Passive mode-locking

As derived in the previous section the technique of mode-locking allows for the generation of ultra-short intense laser pulses by establishing a fixed phase relation between the different longitudinal resonator modes. Experimentally this can be achieved either by different means: Both active and passive mode-locking techniques are used to generate ultra-short laser pulses. Since the lasers used in the course of this thesis are all based on passive mode-locking techniques, the focus in the following sections will be on topics relating to these passive methods. Further information on active mode-locking can be in found for
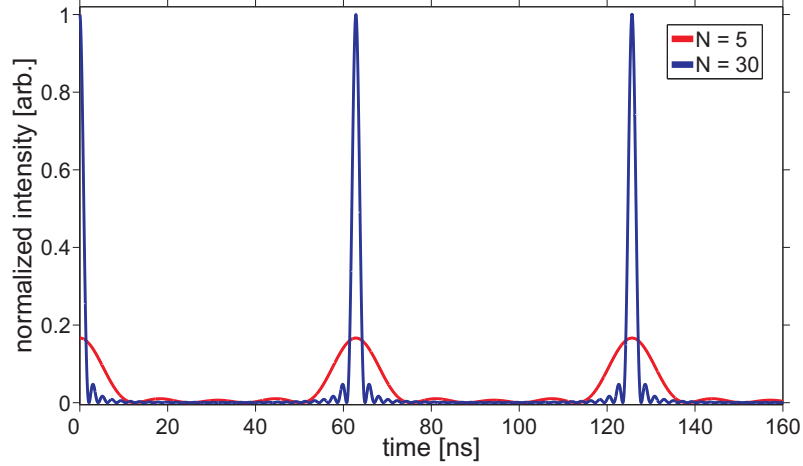
Figure 2.4: Simple numerical example of the peak intensities resulting from mode-locking. The intensity scales linearly with number of modes which can be seen when comparing the red peaks (N=5) with the blue ones (N=30).

instance in textbooks such as [Die06]. The basis for both techniques is a loss modulation. In passive mode-locked lasers the laser pulse itself generates the loss modulation by means of a saturable absorber that is inserted into the oscillator. The saturable absorber creates losses inside the optical cavity that are dependent on the intensity of the laser meaning they can be saturated and disappear by an intense laser pulse on the absorber. The result of this is that the pulse operation regime is energetically favored over the cw-regime which will stabilize the mode-locking.

In the next sections a theoretical description of mode-locking will be presented as well as a number of different experimental methods that can be used to generate ultra-short laser pulses.

2.2.4 Master equation

An analytical treatment of the mode-locking process was first described by Haus in 1975 [Hau75a, Hau75b, Hau75c] when he developed a Ginzburg-Landau type equation, the so-called master equation of mode-locking. In this representation it is possible to describe the various higher order terms that have an influence on the pulse envelope. One common form of this equation can be given as:

$$T_{Rep}\frac{\partial A(T,t)}{\partial T} = \left[g(T)-l+(\frac{g}{\Omega_g^2}+\frac{1}{\Omega_{sf}^2})\frac{\partial^2}{\partial t^2}+i\sum_{n=2}^{\infty}D_n^z(-i\frac{\partial}{\partial t})^n-q(t,T)-i\gamma|A(t,T)|^2\right]A(t,T)$$

$$(2.26)$$

The terms included in this representation are as follows:

- g(T) - gain of the laser as defined in eq. (2.1)

- l - losses of the system

- $(\frac{g}{\Omega_g^2} + \frac{1}{\Omega_{sf}^2})\frac{\partial^2}{\partial t^2}$ - gain filtering resulting from the gain bandwidth of the laser material (Ω_g) as well as effects stemming from other spectral filters (Ω_{sf})

- $i\sum_{n=2}^{\infty} D_n^z(-i\frac{\partial}{\partial t})^n$ - the different orders of dispersion

- q(t,T) - time dependent losses of the saturable absorber which follow an equation similar in form to eq. (2.1)

- $i\gamma|A(t,T)|^2$ - self-phase modulation (SPM) term with the SPM coefficient $\gamma = \frac{2\pi n_2}{\lambda A_{eff}}$. n_2 is the nonlinear index of refraction.

No analytical solution for the full master equation has been found. However by omitting the dissipative terms resulting from gain and losses as well as limiting dispersion to the GDD the equation becomes of the form of a Nonlinear Schrödinger Equation. In this form an analytical solution can be readily found as is shown i.e. in [Ell03]. Using the full equation it is possible however to use numerical methods for modeling the dynamics of many laser systems accurately. Looking at the different terms, it can be seen that in this form the master equations not only includes the gain and absorber dynamic of the laser, but also higher order dispersion and self phase modulation as well as filter terms that result from the materials used in the oscillator. If necessary the master equation can be further extended to include terms for Raman effects or other higher order effects which may then be used to model more complex laser dynamics. However in general the form presented in eq. (2.26) is sufficient for adequate modeling of most laser systems as will be discussed in more detail in Chapter 4. A detailed mathematical description of the master equation can be found in a number of standard textbooks. After this brief introduction to the theoretical background of mode-locking the next section introduces several mechanisms for achieving mode-locking experimentally.

2.2.5 Mode-locking mechanisms

As has been discussed in previous sections passive mode-locking techniques rely on an intensity dependent loss modulation created by a saturable absorber inside the cavity, which makes it energetically favorable for the laser to operate in the pulsed regime. Since the stability of the pulsed-regime is a direct result of this loss modulation the relaxation time of the saturable absorber is of key importance to the achievable pulse durations. Generally for solid-state lasers saturable absorbers are divided into two distinct groups: slow and fast saturable absorbers both of which are shown in Fig.2.5.
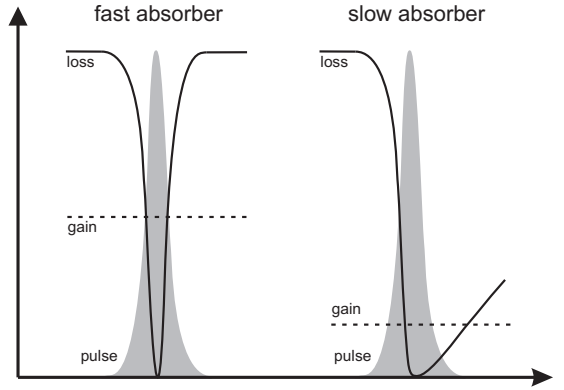
Figure 2.5: Time dynamics in solid-state lasers with fast and slow saturable absorbers. The left hand side shows the fast saturable absorber which follows the laser pulse almost instantaneously. On the right the dynamic resulting from a slow saturable absorber with a relaxation time of several picoseconds is shown.

In this nomenclature a fast saturable absorber has a relaxation time τ_A which is much shorter than the pulse length of the mode-locked pulse $\tau_A << \tau_{FWHM}$. This is shown in the left hand side of Fig.2.5, in this case the absorber losses follow the laser pulse instantaneously. As a result the width of the gain window is only determined by the length of the mode-locked laser pulse allowing for the shortest possible laser pulses. The fastest currently known saturable absorber used in femtosecond lasers is the Kerr lens effect used in the so-called 'Kerr lens mode-locking (KLM)' which will be discussed later in this section. By comparison for a slow saturable absorber $\tau_A >> \tau_{FWHM}$ the width of the gain window is determined by the relaxation time of the absorber. Mathematically the saturation of any of these absorbers can be described as:

$$\frac{\partial}{\partial t} q(t,T) = -\frac{q(t,T) - q_0}{\tau_{abs}} - q(t,T)\frac{|A(t,T)|^2}{E_{sat,A}} \tag{2.27}$$

with q(t,T) the saturable losses of the absorber, q_0 the unsaturated loss coefficient, $|A(t,T)|^2$ the laser power and $E_{sat,A}$ the saturation energy of the absorber. Instead of using the saturation energy it is often more convenient to look at the saturation fluence of the absorber, which is defined as:

$$\Phi_{abs} = \frac{E_{sat,A}}{A_{eff,A}} \tag{2.28}$$

where $A_{eff,A}$ is the effective mode area on the absorber.

SESAM mode-locking

In modern picosecond and femtosecond solid-state lasers the most common example of a slow saturable absorber is probably the so called semiconductor saturable absorber mirror

(SESAM) [Kel96]. The typical design of a SESAM is such that it consists of a dielectric Bragg mirror into which one or more quantum well absorber layers are embedded. In this case the saturable absorption effect relies on the saturation of the semiconductor quantum well. At the low intensities typical for the cw-regime the SESAM induces losses to the resonator because of intraband transitions in the quantum well layers. However in the pulsed regime the increased intensities become high enough to saturate the transition, resulting in a depletion of the lower states in the quantum well. As a result of this optical bleaching the losses of the SESAM are reduced for a window of time dictated by the relaxation time of the quantum well layers. Looking at eq. (2.27) there are three key parameters that need to be kept in mind when using a saturable absorber such as a SESAM in a passively mode-locked laser, namely the saturable losses, the saturation fluence and the relaxation time. One of the great advantages of a SESAM is that both the saturable losses and the saturation fluence are well defined by the properties of the quantum well layers. This makes it possible to create SESAMs with different loss modulations and saturation fluences depending on design parameters of the quantum well layers such as thickness, location inside the Bragg structure or material. Typical relaxation times for SESAMs are usually in the picosecond regime, making them well suited for the generation of pulses with similar durations. More information about the design properties of SESAMs as well as a more detailed description of the physics involved can for instance be found in [Gra06].

Soliton mode-locking

Despite their relatively long relaxation times, SESAMs have also become one of the most prominent tools for generating femtosecond laser pulses. This is made possible by an effect called soliton mode-locking, in which the interplay between GDD and self-phase modulation results in the creation of a soliton-like pulse. The first successful experiments with solitary mode-locked lasers were done by Mollenauer et al. in 1980 [Mol80, Mol84] who used propagation in an anomalous dispersive fiber in a coupled cavity to create a solitary pulse and stabilize the mode-locking of the laser cavity. Since then it has been shown that soliton mode-locking can be used in conjunction with any type of saturable absorber as long as the necessary conditions for solitary pulse formation are met and the intra-cavity GDD is negative. As a result solitary pulses have become a very important feature in laser optics with applications ranging from telecommunications to femtosecond solid-state lasers. Some aspects of soliton theory as well as some effects that are of importance for the work presented in this thesis will be explained in the following paragraphs. However a much more thorough introduction to optical solitons can be found in a number of works such as [Agr95, Kär95].

   The key feature of soliton mode-locked lasers is that the pulse duration inside the laser cavity is no longer governed by the relaxation time of the absorber, but is instead determined by the so soliton condition unless limited by the bandwidth of the laser medium. The soliton condition or area theorem used to describe a solitary pulse mathematically is

given as:

$$\hat{P}\tau_{pulse}^2 = 1.7627 \cdot O^2 \frac{|\beta_2|}{\gamma} \tag{2.29}$$

which links the peak power $\hat{P}$ to the pulse duration, the GDD β_2 and the Kerr non-linearities represented by the SPM coefficient γ. The factor O gives the soliton-order for the fundamental soliton. Using the factor of 1.7627, the pulse shape of a solitary laser pulse can be described as a $sech^2$, which is very convenient in the mathematical description of the soliton-like pulses. As for any soliton, the solitary laser pulse maintains its spectral and temporal shape as it propagates through the laser cavity. Perturbations of the pulse which would normally cause it to deviate from the current pulse shapes are counteracted by the nature of the fundamental soliton. In these cases the laser pulse can shed energy to the continuum in order to once again fulfil the area theorem and become a fundamental soliton. As a result of the stable nature of the fundamental soliton, the pulse duration in a soliton mode-locked oscillator is no longer determined by the relaxation time of the saturable absorber, but rather by the area theorem itself. As has been mentioned at the beginning of this paragraph this makes it possible to achieve pulse durations in the femtosecond regime despite the fact that the gain window given by the absorber is on the order of several picoseconds. Another noteworthy effect of soliton mode-locking in an oscillator stems from the fact that inside a laser cavity built up by discrete optical elements, there will be periodical perturbations of the soliton. These can result in an interaction between the soliton and the dispersive continuum, formed by the energy shed away as a result of the perturbation. When the phase relation between the two reaches 2π for an optical frequency narrow sidebands will occur in the optical spectrum of the solitary pulse, the Kelly sidebands [Kel92]. An example for a laser spectrum with Kelly sidebands is shown in Fig. 2.6 [Ste08].

To understand the importance of these sidebands it is helpful to introduce the dispersion length L_D as well as the non-linear length L_{NL}:

$$L_D = \frac{\tau_{pulse^2}}{|\beta_2|} \qquad L_{NL} = \frac{1}{\gamma\hat{P}} \tag{2.30}$$

With this, the area theorem for the fundamental soliton (O=1) can be rewritten as:

$$L_D = L_{NL} \tag{2.31}$$

As strong Kelly sidebands indicate strong perturbations of the solitary pulse, this means that at some points in the resonator there is a substantial difference between L_D and L_{NL}. Experimentally the most common explanation for this is that at least at one point in the resonator strong non-linearities are induced on the laser pulse which are counteracted elsewhere in the resonator by respective values of the β_2 in order to be able to fulfill the area theorem. For increasing perturbations, the Kelly sidebands will continue to grow
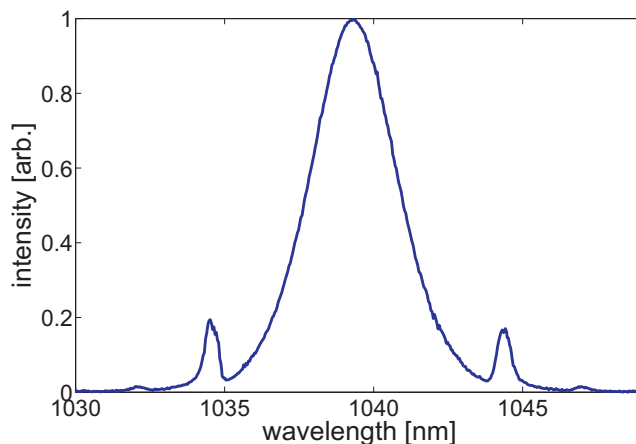
Figure 2.6: Sample spectrum of a KYW oscillator taken from [Ste08]. Two sets of Kelly sidebands are visible in the wings of the spectrum. The first set appears as sharp peaks while a second set of sidebands appears more drawn out. The measurement of the height and width of the sidebands is limited by the resolution of the spectrometer.

until the disturbance is too strong for the soliton-like pulse to compensate and the laser will then become unstable.

As has been noted above, in theory the duration of the laser pulse in a soliton mode-locked oscillator should decrease for higher pulse energies in accordance with eq. (2.29) until the limit presented by the emission bandwidth of the laser material. In reality however it has been noticed that if the pulse energies become too high it is not possible to reach this limit even if enough negative second order dispersion is inserted into the oscillator to fulfill the soliton condition [Bra91, Bra92b]. This is of special concern for high power femtosecond oscillators with intra-cavity pulse energies in excess of 10 μJ where this effect becomes especially pronounced [Süd08]. Instead of further pulse-shortening the pulse splits up into multiple pulses with longer durations.

The reasons for this effect are not entirely understood at this point. However several possible explanations exist: One possible explanation is that at the peak intensities reached by these oscillators, the solitary pulse is no longer able to balance the perturbations created by the discrete distribution of the optical elements in the resonator. Because of this the pulse can no longer form a fundamental soliton and loses stability. Another possible explanation looks at the two-photon absorption in the SESAM. At high enough peak intensities it is possible to start inducing two-photon absorption in the absorber at which point the reflectivity actually drops for higher intensities [Tho99]. As a result it may be energetically better for the laser pulse to split into two or more multiple pulses which do not have enough intensity to initiate two-photon absorption and are thus experiencing lower losses. Experimental verification of either theory is difficult as any high energy mode-locked oscillator is a strongly coupled system and variation in any one pa-

rameter, especially any parameter regarding the saturable absorber, drastically influences most other laser parameters simultaneously.

As has already been mentioned, a key requisite for soliton mode-locking is a negative intra-cavity GDD. However for pulses with a duration of only a few femtoseconds and GDD values close to zero, the laser will exhibit a different behavior, which is called dispersion managed mode-locking. In this regime the pulse starts to exhibit temporal breathing while propagating through the cavity and cannot be described as a solitary pulse anymore [Che99].

Yet another operation regime exists for positive values of the intra-cavity GDD. In that case the laser pulses will become strongly chirped and the resulting type of lasers are called chirped pulse oscillators. As this class of lasers plays an important role for this thesis, a detailed description of this type of lasers will follow in Chapter 3.

Kerr Lens mode-locking

The fastest currently known saturable absorber is based on the optical Kerr effect. This effect describes the intensity dependence of the refractive index given by:

$$n(\mathbf{r},t) = n_0 + n_2 \cdot I(\mathbf{r},t) \tag{2.32}$$

with n_2 the non-linear index of refraction for a given material. When looking at the time domain, the result of the Kerr nonlinearity is the 'self phase modulation', which results in the generation of new frequency components and will be discussed later. On the other hand in the spatial domain, the result of the Kerr-effect is that a Gaussian beam with sufficient intensity will experience a Gaussian gradient of the refractive index with an effect similar to that of a classical lens. In terms of mode-locking, the most important feature of the Kerr-effect is that the response of the refractive index has a time constant which is quasi instantaneous with respect to the laser pulse. The Kerr-effect alone however does not represent a saturable absorber, as it does not à priori involve a loss modulation. In order to employ the intensity dependent refractive index as a saturable absorber it is once again necessary to ensure that the low intensity cw-light does experience more losses than the mode-locked laser pulse which has sufficient intensity to initiate a change in the refractive index. A relatively simple way to achieve this is to use hard aperture Kerr lens mode-locking (KLM). For this an aperture, i.e. an iris diaphragm, is inserted into the oscillator at a specific location where the Kerr lens can decrease the beam radius. The diameter of the open aperture is then chosen such that it corresponds to the reduced beam radius of a high intensity laser pulse as opposed to the larger radius of the cw-light. The result is the required loss modulation favoring the pulsed light over the low intensity cw-light thus forming a saturable absorber and ensuring mode-locked operation of the laser. [Bra92a, Bra93]

Another possible implementation is the so-called soft aperture Kerr lens mode-locking [Spe91, Pic93, Cer94a, Cer94b]. Here no additional element is needed inside the resonator

as the necessary modulation is created directly inside the laser. The difference is that here instead of using a loss modulation the gain is modulated, yet the result is exactly the same. Experimentally this is made possible by choosing the resonator design in such a way that, under cw-operation, the laser beam inside the gain medium has a larger diameter than the pump beam. As a result the laser beam cannot use all of the inversion created by the pump. This is shown on the left hand side of Fig. 2.7. If however an intensity spike forms inside the oscillator, either because of random noise or as the result of a short intentional perturbation of the laser cavity, the increased peak intensities will lead to the formation of a Kerr lens. When adjusted correctly, this Kerr lens will enhance the overlap between pump beam and laser beam in the gain medium by reducing the beam waist of the laser. Consequently the laser will now experience a higher gain which means the pulsed regime is again energetically favored over cw-operation. This situation is shown on the right hand side of Fig. 2.7.

Today the quasi-instantaneous nature of the Kerr effect has resulted in making it the foremost experimental technique for the generation of ultra-short femtosecond laser pulses. With the help of soft aperture mode-locking it has been possible to routinely generate sub-10 fs pulses from Ti:sapphire laser oscillators as well as the shortest laser pulses from a laser oscillator with a pulse duration of only 3.7 fs [Rau08].

2.2.6 Self-phase modulation

As mentioned in the previous section, the Kerr-effect results in self-focusing in the spatial domain and in self-phase modulation in the time domain. Eq. (2.32) shows that the effect
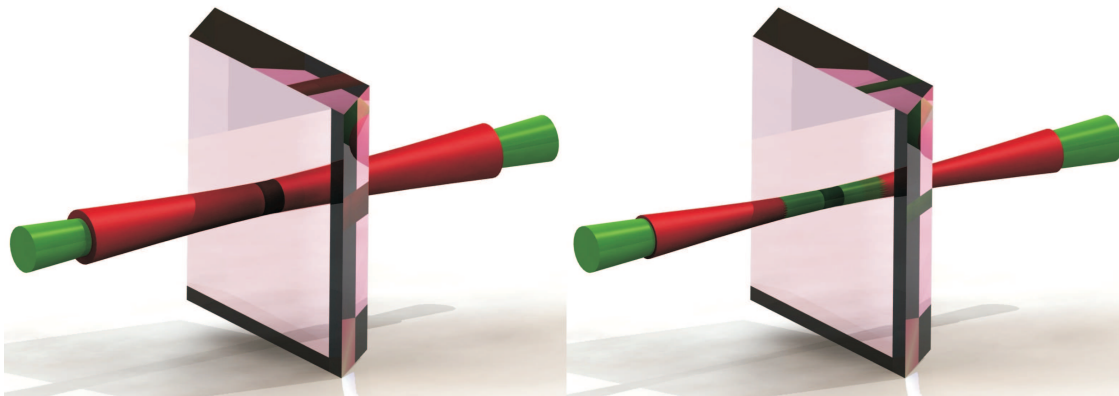
Figure 2.7: Schematic principle of soft aperture Kerr lens mode-locking. The left hand side of the figure shows the laser in cw-operation. The red laser beam is noticeably larger than the green pump beam. As a result not all of the inversion created by the pump can be used. On the right hand side the laser is operating in the pulsed regime, the overlap between pump beam and laser beam is increased, allowing the laser to experience a higher gain.

is strongly dependent on the peak intensities of the laser pulse, hence the importance for high power ultrashort oscillators.

As it is a result of the optical Kerr-effect, self-phase modulation will occur in any nonlinear medium given sufficiently high intensities. While self-phase modulation does not change the temporal pulse envelope, it results in the generation of new frequency components on the edges of the fundamental pulse spectrum and induces a frequency chirp in the pulse. The maximum phase shift occurring at the center of the pulse can be described as:

$$\phi_{max} = \frac{2\pi n_2}{\lambda A_{eff}} \cdot \hat{P} L_{eff} = \gamma \hat{P} L_{eff} \tag{2.33}$$

with L_{eff} the length of the nonlinear medium and γ the SPM coefficient. This phase then acts on the temporal pulse envelope adding a phase shift to it:

$$A(t') = A(t) e^{-i\gamma |A(t)|^2} \tag{2.34}$$

A schematic of the frequency generation is shown in Fig. 2.8. The dotted black curve shows the fundamental laser spectrum.

As can be seen from this figure it is possible to increase the spectral width of a given laser pulse drastically using SPM. An example for the frequency chirp resulting from SPM is given in Fig. 2.9 which shows how the frequencies arrange under the envelope in case of a Gaussian pulse shape.
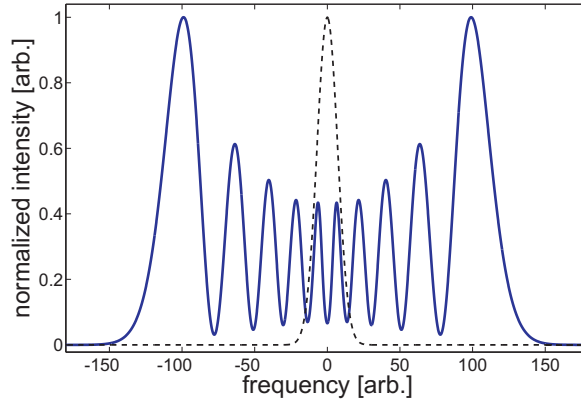

Figure 2.8: Schematic of frequency generation via SPM. The dotted black curve signifies the initial fundamental laser spectrum while the blue curve shows the significantly broadened spectrum due to SPM. For this example ϕ_{max} is set to 9.5π
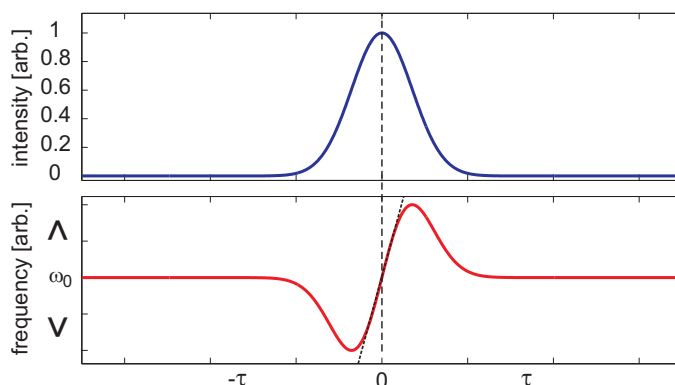
Figure 2.9: Schematic diagram of the frequency chirp in a Gaussian pulse created by SPM. The upper picture shows the temporal envelope of the laser pulse, while the lower depicts the frequency shift resulting from the SPM. Lower frequencies are shifted to the front of the pulse while higher ones are shifted to the back. Between these is a region of nearly linear frequency chirp allowing for relatively easy temporal compression of the pulse.

The upper picture shows the temporal pulse shape of the laser pulse while the lower shows the frequency distribution resulting from the SPM. While the lower frequencies will shift to the front of the pulse, the higher ones shift towards its back. Also visible in the the diagram is that the frequency shift in the middle of the pulse is linear. This fact combined with the spectral broadening makes it possible to use SPM in order to shorten laser pulses significantly below their original Fourier-limit.

Effect of pulse shape and chirp

Because the Kerr-effect is a direct result of the pulse intensity all its associated effects are strongly dependent on the temporal shape of the pulse. As such the situation described above is true for unchirped Gaussian or nearly Gaussian pulse shapes but changes for different pulse shapes and pulse chirps.

In order to achieve a more general understanding it is helpful to not only look at Gaussian pulses, but also at super-Gaussian pulses described by:

$$A(t) = \exp\left[-\frac{1 + iC}{2}\left(\frac{t}{t_0}\right)^{2m} \right] \tag{2.35}$$

with C, the so-called chirp factor and m, a parameter that controls the steepness of the edges. As can be seen, for $m = 1$ and $C = 0$ the resulting pulse shape is an unchirped Gaussian pulse.
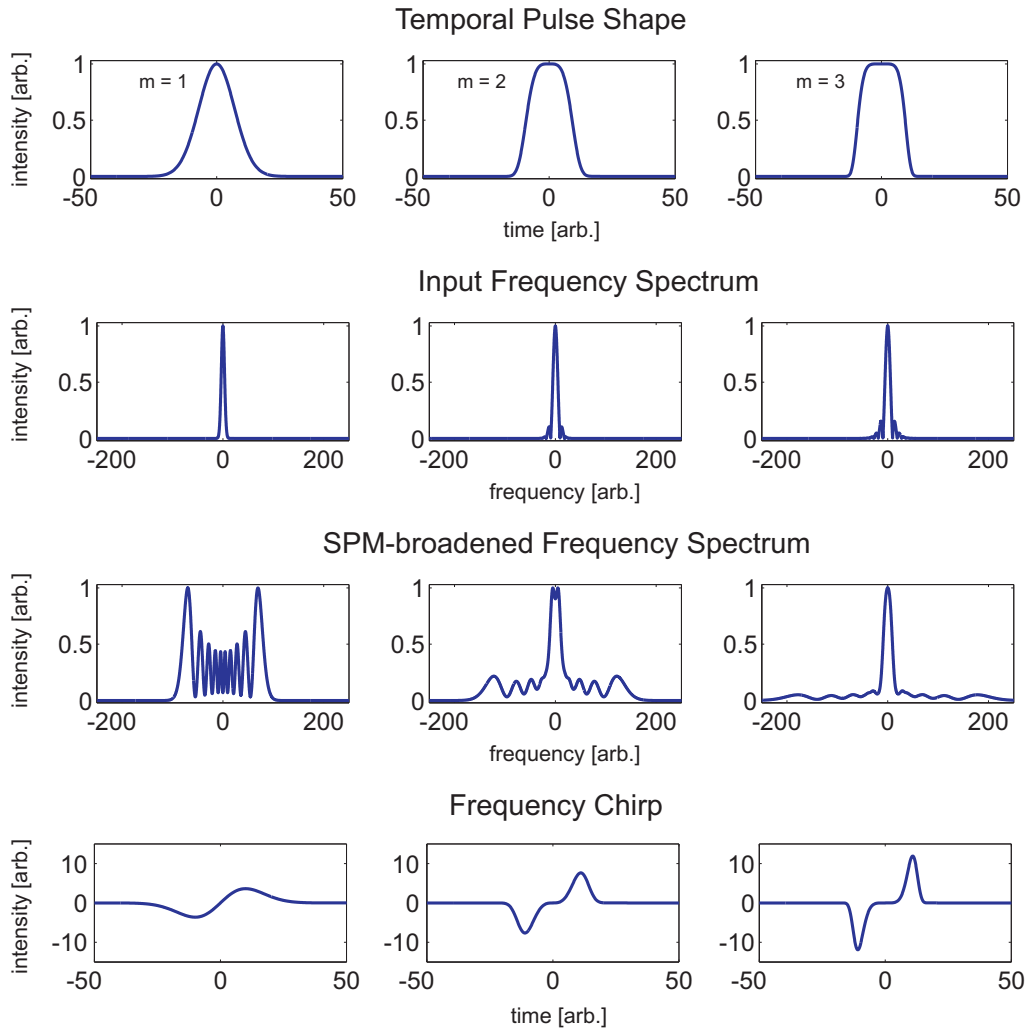
Temporal Pulse Shape

Input Frequency Spectrum

SPM-broadened Frequency Spectrum

Frequency Chirp

Figure 2.10: Schematic of the SPM induced effects depending on different pulse shapes. The left column showing the effects for a perfect Gaussian pulse while the middle and right column depict the effects for super-Gaussian pulses with m = 2 and m = 3. The nonlinear phase again is set to $\phi_{max} = 9\pi$

Fig. 2.10 shows how the effects of SPM change when the pulse deviates from pure Gaussian-shape as the edges of the pulse steepen increasingly while the pulses are still unchirped because of this for all pulses in this figure C=0. The left column of the figure shows the frequency broadening and chirp of a Gaussian pulse while the other two columns show the effects for pulses with m=2 and m=3 respectively. The impact of the pulse shape is severe both in terms of spectral broadening and of frequency chirp. As can be seen from the figure, steeper pulse edges result in an increased spectral width. However the intensity of the newly generated frequencies is far lower than in the case of a pure Gaussian

pulse. More importantly the pulse chirp gets more pronounced in the pulse wings and becomes nonlinear even in the middle of the pulse. As a result pulse compression to the Fourier-limit becomes more difficult experimentally in this case.

Since much of this thesis deals with chirped pulse oscillators, it makes sense to look at the effects an initial chirp has on the results of SPM. Again using Gaussian and super-Gaussian pulses this is done in Fig. 2.11 by varying the chirp factor from C=-10 to C=10.

The top of the figure shows the effects on a Gaussian pulse. In terms of the spectral form, the most obvious effect is that a negative chirp results in an increased peak structure of the spectrum while a positive chirp has the opposite effect and results in a smoothing out of the oscillations normally associated with SPM-induced spectral broadening. This is the result of an interaction between the initial chirp of the pulse with the frequency chirp induced by the SPM [Agr95]. Looking at the spectral width it can be seen that a negative chirp leads to an decrease in width for a Gaussian pulse compared to the unchirped case. For high enough values of negative chirp it is even possible to achieve an overall spectral compression of the pulse. The chirp also has significant effects on the frequency chirp after the SPM as it strongly increases the nonlinear chirp in the wings of the pulse making it much harder to recompress. The lower part of the figure shows the effects of an initial chirp on a super-Gaussian pulse with m=3. As can be seen qualitatively the effects are very similar to the pure Gaussian pulse. However the effect on the frequency spectrum is less severe while the chirp becomes more nonlinear.
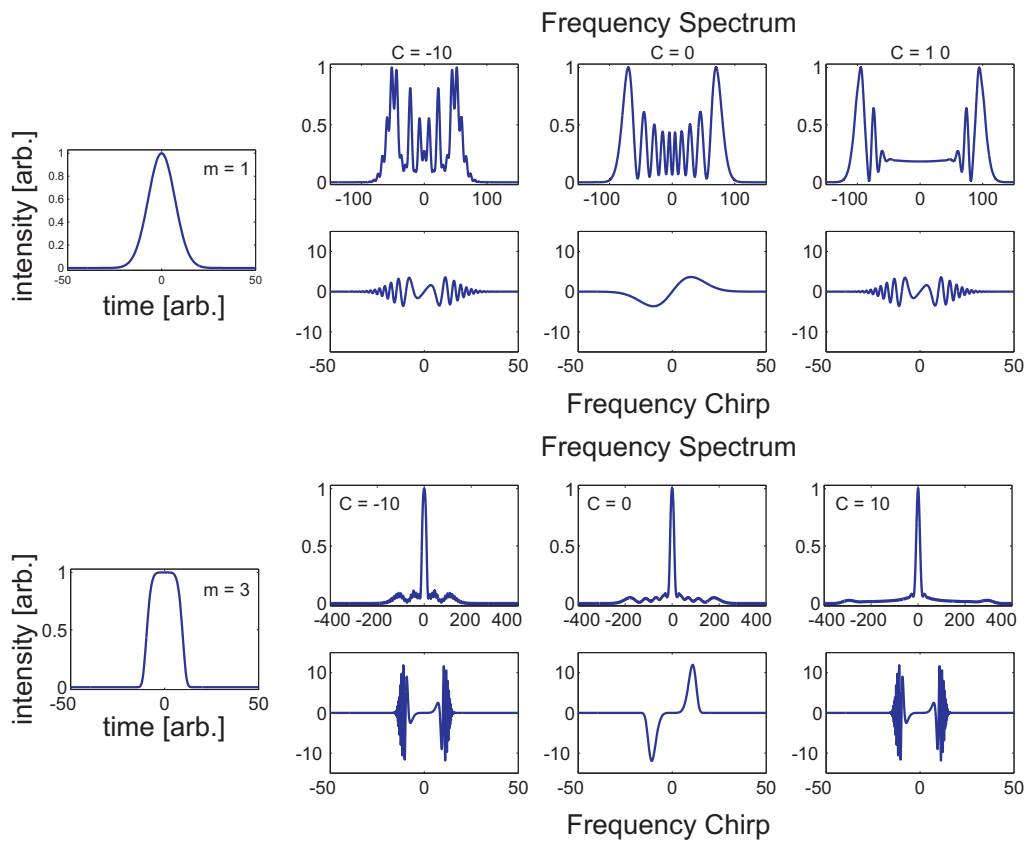
Figure 2.11: Variation of SPM induced effects for a Gaussian (m = 1) and super-Gaussian (m = 3) pulse given different initial chirps of the pulse ranging from C = -10 to C = 10. The nonlinear phase is same as in the previous examples.

2.3 Laser materials

Over the years a wide range of different materials has successfully been used to build laser oscillators and the number continues to grow as material research is still one of the most productive areas in laser science. Nevertheless when it comes to high power solid state femtosecond oscillators there are only a number of materials that have been proven to be suited as gain media for this specific kind of lasers. Besides Ti:sapphire, numerous Yb-doped gain media have become increasingly important for the development of high power laser oscillators. In this section some basic facts and material properties of the gain media used in this thesis will be presented in order to enable the reader to better understand the later parts of this work.

2.3.1 Ti:sapphire

Since the minimal achievable pulse duration in mode-locked lasers is determined by the time bandwidth product given in eq. (2.12) any gain medium for femtosecond lasers is required to have a broad emission spectrum. Because of this many current femtosecond lasers are based on a Ti:sapphire crystal (Al_2O_3) which has one of the broadest emission spectra of all currently available laser materials. Some of the material parameters of this gain medium are listed in Tab. 2.1, for a more detailed description of the crystal structure and other parameters, the reader is referred to the cited literature.

Property	Value
Index of refraction	1.76
Nonlinear index of refraction [cm^2/W]	$3 \cdot 10^{-16}$
Peak absorption [nm]	495
Peak emission [nm]	795
σ_L [cm^2]	$3 \cdot 10^{-19}$
Fluoresence lifetime [μs]	3.15
β_2 [fs^2/mm]	61.2
Thermal conductivity [W/mK]	27.21

Table 2.1: Optical and spectroscopical parameters of Ti:sapphire at room temperature [Mou86, Smo98, Koe06]

The emission spectrum of Ti:sapphire spans 128 THz or 270 nm and the shortest pulses achieved with a Ti:sapphire oscillator have a Fourier-limit of 3.7 fs [Rau08]. A schematic of the absorption and emission spectra of Ti:sapphire is shown in Fig. 2.12 a) along with a depiction of the pump and emission lines of the laser built in this thesis.
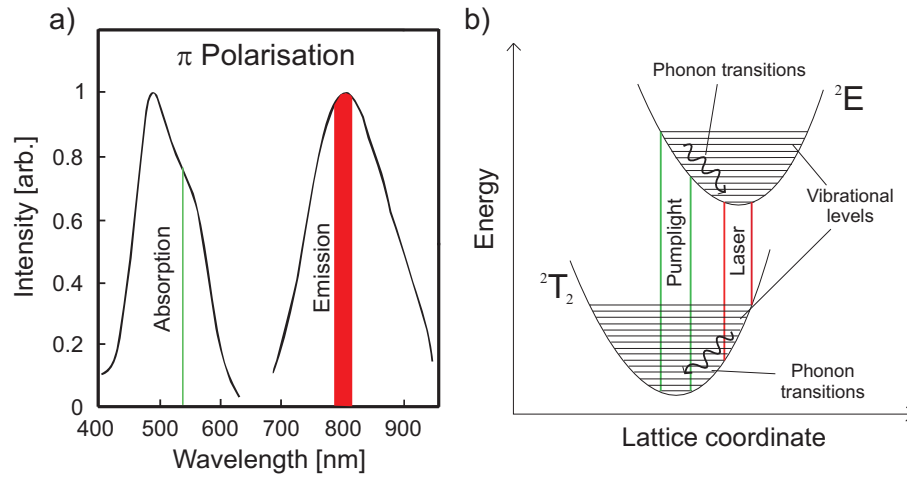
Figure 2.12: a) Level scheme of the Ti:sapphire crystal; b) Absorption and Emission spectra for the Ti:sapphire crystal. The green and red line represent the pump wavelength and the spectra of the Ti:sapphire laser oscillator built as part of this thesis.

Fig. 2.12 b) shows a schematic of the 4-level system in a Ti:sapphire crystal. As can be seen the level structure is made up of two electric states ($^2T_2$, ^2E) which both are strongly broadened by vibrational levels. Absorption of pump light takes place in the lowest vibrational level of the $^2T_2$ state and the electrons are pumped into the excited vibrational levels of the ^2E state. From these states the electrons quickly decay via phonon transitions into the lowest vibrational level. Without laser action, the electrons decay into excited vibrational levels of the $^2T_2$ state via spontaneous emission. At room temperature, the lifetime of this process is about 3.15 μs. However because of a vibrational decay channel between the upper and the lower state, the upper state lifetime is temperature dependent. This becomes especially important for high power laser systems where the crystal may be strongly heated by the pump absorption. A measurement of the temperature dependence of the upper state lifetime is shown in Fig. 2.13. While the lifetime is is nearly constant at 3.8 μs below 200 K it shortens considerably for higher temperatures and above 600 K the decay is almost instantaneous. The origin of this behavior can be found in the increased non-radiative phonon transitions as the lifetime of the spontaneous decay has been shown to be temperature independent [Alb86]. Nevertheless this change in the lifetime is an important effect in high power laser systems as the increase in non-radiative transitions can lessen or even deplete the inversion of the laser medium.

Thermal properties

Besides its good spectral properties Ti:sapphire has another material property that makes it suitable for high power femtosecond lasers: The thermal conductivity. At room temperature Ti:sapphire boasts a thermal conductivity of 27.21 W/mK which is significantly higher than that of many other gain media (e.g. Yb:YAG 14 W/mK, Yb:Glas 0.85 W/mK).
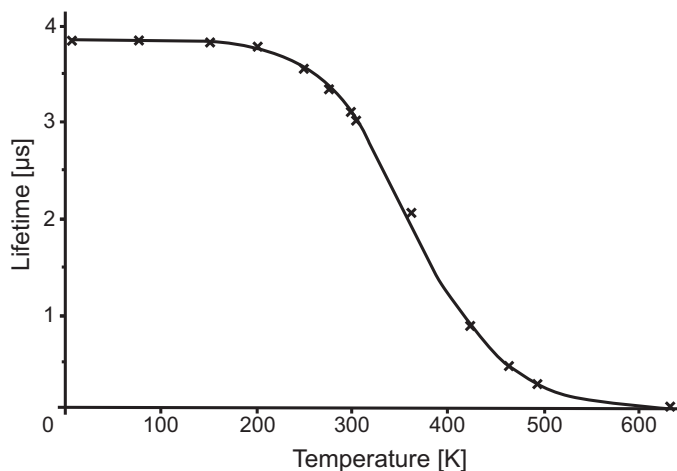
Figure 2.13: Temperature dependence of the upper state lifetime in Ti:sapphire [Alb86]

Furthermore the thermal conductivity of Ti:sapphire is also highly temperature dependent which is illustrated in Fig. 2.14. Below temperatures of 200 K, the thermal conductivity rises rapidly before reaching a peak at about 70 K. Thanks to this property it is possible to use liquid nitrogen cooling of the Ti:sapphire crystal in order to ensure efficient heat removal which allows high pump powers for high power laser oscillators or amplifiers.

Pump sources

While Ti:sapphire offers an extremely broad emission spectrum along with other useful material parameters for use in laser oscillators, there is one major drawback to its use in high power oscillators: At the pump wavelength around 495 nm there are currently no high power diodes which could be used for pumping Ti:sapphire oscillators. While there has been some progress in the area of directly diode pumped Ti:sapphire lasers in recent years no real breakthrough has been achieved so far [Mac09]. As a result Ti:sapphire oscillators still rely on pumping by either frequency doubled solid-state lasers or by argon-ion lasers. Both of which are rather expensive and limited in terms of available pump power. Currently the highest available CW pump lasers for Ti:sapphire laser oscillators are limited to 20 W from a single pump source. Pump lasers with higher output powers do exist, but these are pulsed systems with repetition rates in the kHz-regime. Furthermore because of their beam profiles these systems are generally not suited for use in Kerr-lens mode-locked oscillators.
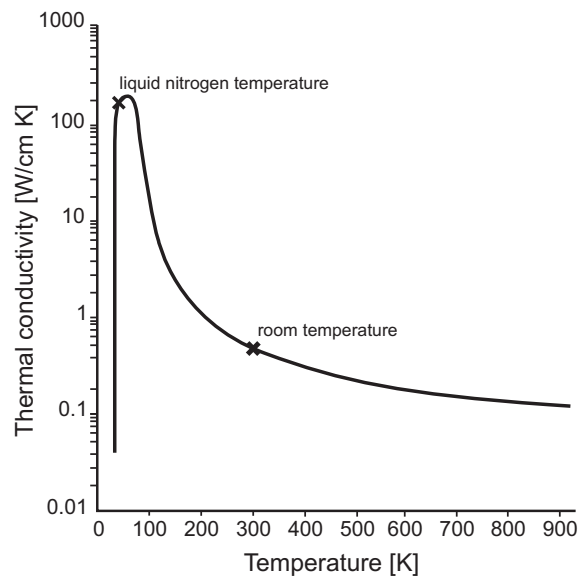
Figure 2.14: Temperature dependence of the thermal conductivity of Ti:sapphire [SG04]

2.3.2 Ytterbium-doped materials

Over the last decade, laser oscillators based on gain media doped with the rare earth metal Ytterbium have become increasingly important in the field of high power femtosecond oscillators and have also been used as part of this thesis. Yt^{3+}-ions are used as dopant in many different host materials ranging from a number of glasses (mainly for fiber lasers) to crystals like, amongst others, yttrium aluminium garnet (YAG), vanadate (YVO_4), monoclinic potassium double tungstates ($KY(WO_4)_2$, $KLu(WO_4)_2$, KGW) or sesquioxides. In contrast to Ti:sapphire, these gain media typically have absorption wavelengths in the near infrared where suitable high power laser diodes are available.

All of these doped materials share a couple of material properties that make them well suited for use as laser gain media. Probably the most prominent feature of this group of gain media is their pronounced quasi-three-level behavior which is founded in their rather simple level structure. Especially important for the laser operation is also the fact that all Yb-doped materials exhibit a small quantum defect allowing for high efficiencies and reducing the thermal load in the crystal furthermore losses due to excited state-absorption and quenching are minimal. Lastly, while their gain bandwidth is not nearly as large as that of Ti:sapphire it nevertheless is broad enough to allow for the generation of laser pulses in the femtosecond regime. The combination of these properties with the possibility of a rather simple and comparably cheap diode pumping scheme make Yb-doped gain media a strong competitor in the field of high power femtosecond oscillators.

Besides the general characteristics each group of Yb-doped materials has certain proper-

ties that depend on the structure of the host material and greatly influence the possible use in laser oscillators. Because there is such a huge variety of Yb-doped gain media this thesis cannot give an overview over all of them however information on most Ytterbium-doped materials can be readily found in standard textbooks or various scientific publications [Kru00, Koe06, Pet07, Hau02, Liu09, Sel06]. Instead, the main characteristics of those two Yb-doped media that were used as part of this thesis will be presented.

Ytterbium tungstates

Both Yb-doped gain media used here are based on tungstate compounds as host materials and are part of the family of Ytterbium tungstates. The tungstates offer a nice compromise in terms of emission bandwidth and thermal conductivity allowing them to generate shorter pulses than with Yb:YAG while at the same time allowing higher pump powers than can be employed with Yb:glass. It is this combination that make them of special interest in the development of high power femtosecond laser oscillators. One drawback for the experimental use of Yb:tungstates is the fact, that they display a distinct anisotropy resulting in different physical properties for each of the crystal axis. One of the main effects is a strong tendency to form a thermal lens when heated because of the different thermal expansion coefficients of the axis. This has to be taken into account when cutting the crystals for use in a laser oscillator as well as when designing the optical cavity itself. A more thorough discussion of the properties of Ytterbium-tungstates can for instance be found in [Pal09].

For the lasers discussed in this thesis two different tungstates were used: KYW which is short for $KY(WO_4)_2$ and KLuW, short for $KLu(WO_4)_2$. In table 2.2 the most important properties of these two crystals are presented:

Property	Yb:KYW	Yb:KLuW	Source
Index of refraction [@ 1μm]	2.06	2.08	[Kil05a, Pet07]
n_2 [cm^2/W]	$15 \cdot 10^{-16}$	not measured so far	[Sel06, Pet07]
Peak absorption [nm]	981	981	[Pal09]
Peak emission [nm]	1040	1040	[Pal09]
σ_L [cm^2]	$1.33 \cdot 10^{-20}$	$1.24 \cdot 10^{-20}$	[Kul97, Pet07]
τ_{sp} @300 K [μs]	300	254	[Gri05, Pet07]
β_2 [fs^2/mm]	143	115	[Pal09]

Table 2.2: Optical and spectroscopical parameters of Yb:KYW and Yb:KLuW. Unless otherwise noted the values given are for room temperature and laser operation on the N_m axis

While some of the parameters, like the spectral data for absorption and emission, are known with great precision other parameters are still unknown or known with little certainty. Most notable amongst these is the non-linear index of refraction, where the

publicized values differ by more than a factor of two [Kil05a]. Other uncertainties concern the fluorescence lifetime which depends strongly on the doping concentration and on any possible impurities in the crystal and can thus also vary to some degree. Nevertheless the values given in table 2.2 give a general overview of the important properties of these crystals.

3 Energy scaling of femtosecond solid-state lasers

As has already been discussed in Chapter 1, the development of high energy laser femtosecond laser sources with pulse energies on the microjoule level and repetition rates on the order of 1 MHz or above is of great interest for a variety of applications both in fundamental science and in industrial applications. However when trying to reach these parameters there are certain experimental and theoretical challenges that have to be overcome in order to allow operation in this regime.

The previous chapter introduced the most important theoretical principles necessary for the understanding of the work done in this thesis. In the following chapter the most important experimental techniques for the energy scaling of femtosecond laser systems will be discussed as will some key challenges resulting from the energy scaling.

The first concept will be that of the thin disk laser which is used later in this thesis as basis for the Yb:KYW oscillator presented in Section 4.2. Following that the concept of the long-cavity laser will be introduced. As part of this the optical setup of the so-called 'Herriott-cell' will be explained, which is important for the understanding of the lasers presented in Section 4.3 and Chapter 5. Lastly the concept of cavity-dumping will be introduced which is used in all experimental laser setups discussed in the later parts of this thesis.

Following the introduction of the different energy scaling concepts, challenges emanating from nonlinear effects will be discussed as will the different operation regimes used for the lasers discussed in thesis. The chapter will then conclude with a short comparison of energy-scaling in solid state bulk and fiber lasers.

3.1 Power scaling: Challenges and Concepts

In general the challenges that are encountered during the power scaling of femtosecond solid-state lasers can be roughly divided into two distinct groups: On the one hand the fact that the pump source and in many cases also the femtosecond laser itself are required to operate at rather high average powers compared to standard ultrashort pulse oscillators, which does result in challenges concerning the thermal properties of the laser. On the other hand high pulse energies at ultrashort pulse durations lead to very high peak intensities inside the laser cavity which will also affect the laser operation when the pulse is propagating through nonlinear material. Any attempt at energy scaling in a pulsed laser oscillator is governed by the following equation:

$$E_p = \frac{\bar{P}}{f_{rep}} \tag{3.1}$$

with $\bar{P}$ the average output power of the laser. As can be seen, in order to increase the pulse energy one can either attempt to increase the average power or to reduce the repetition rate.

3.1.1 Scaling the average output power

While the scaling of the average output power may seem like the most straight forward way of achieving higher pulse energies in reality this does pose several challenges. Important applications of high energy femtosecond lasers, like for instance micro-machining, rely on the fact that these systems deliver high peak intensities without the kind of thermal load created by cw-lasers of similar intensity. By raising the average output power in order to achieve higher pulse energies this important advantage of femtosecond lasers is diminished or even lost.

Because of this the scaling of the average output power alone will always be a limited means of scaling the pulse energy of femtosecond oscillators. Nevertheless in combination with other concepts it can prove valuable for the development of high energy femtosecond oscillators.

However there remain two other issues: One is the availability of high power pump sources required to increase the average output power of any laser system. The other is the question of how to apply high pump powers to the gain medium without introducing thermal effects that can destabilize the laser oscillator.

Pump sources

In the case of Ti:sapphire lasers the strongest currently available cw-pump sources are limited to 20 W of pump power at 514 nm[1] and to 18 W at 532 nm[2]. Higher pump powers can currently only be achieved by using pulsed laser sources which operate at repetition rates in the kHz-regime and have beam profiles that prohibit the use of such lasers for Kerr-lens mode-locking making them unsuitable for the generation of ultra-short femtosecond laser pulses. This limitation currently forms the main obstacle in terms of power scaling in Ti:sapphire laser oscillators.

For Yb-doped gain media the situation is different. Here it is possible to employ extremely high pump powers of several hundred Watts and more by using commercially available diode lasers. A drawback to this is that high power diodes in general consist of multiple diode emitters bundled together. The result of this is that the beam profile and the brightness of such systems are generally worse than those achieved by solid state

---

1   SLT Gemini 20 W
2   Coherent Verdi V-18

lasers. Regardless of this the power scaling for such system is not generally limited by the available pump powers it does however pose other problems, namely the thermal load in the gain medium.

Thermal load

Any increase in the pump power inevitably results in a higher thermal load in the laser gain crystal. This is mainly due to the inevitable quantum defect, the difference between pump and laser wavelengths but also due to the fact that not all of the inversion will be depleted in the laser process. The main issue with regards to a high thermal load in the gain medium is that it will lead to the formation of a strong thermal lens and will destabilize the laser oscillator. This is of special importance for the Yb-tungstates which, because of their anisotropic nature, have different coefficients for the thermal conductivity and thermal expansion in each of the three crystal axis.

As a result increased pump powers requires that the heat removal away from be sufficiently efficient in order to avoid detrimental thermal effects. In the case of Ti:sapphire this is relatively easy because the already high thermal conductivity of the crystal can be further improved by cooling the crystal to lower temperatures as has already been discussed in section 2.3.1. For Yb-doped gain media the situation is different: Here the thermal conductivity is relatively low. Even for materials like the Yb-tungstates which have some of the highest thermal conductivities of all Yb-doped gain media, the coefficient is almost an order of magnitude lower than that of Ti:sapphire. As a result special measures to ensure optimal heat flow have to be taken when building high power Yb-based oscillators which lead to the development of the thin disk laser concept [Gie94] which is nowadays used both for high power cw- and pulsed-lasers.

3.1.2 Thin disk oscillators

As the name suggests, the active medium in a thin disk laser is a thin plate of crystal mounted on a heat sink. The large surface ratio of the disk, created by the difference between disk diameter (several mm) and thickness (usually 50-300 μm) allows for a much more efficient heat removal. Fig. 3.1 shows an example of thin disk pumping module as described in [Pal09].

Because of the short length of the gain medium in a thin disk laser, it is necessary to optimize the pumping scheme such that despite the relatively low single pass absorption enough inversion is created to allow laser action. To this end the pump module is designed in such a way as to allow for several pump passes through the thin disk. This way it is possible to achieve overall absorption in excess of 80% which is similar to that in standard bulk oscillators. A more detailed description of thin disk pump chambers and other characteristics of this laser type can be found in [Pal09, Gie07]. The great advantage of the thin disk setup is that by combining the much improved heat removal with a large spot size on the disk drastically reduces the problem of the thermal load and allows the
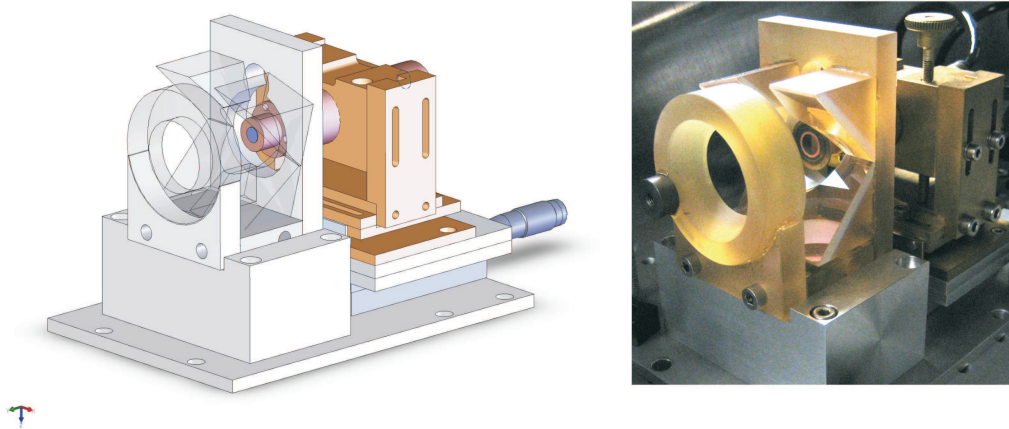
Figure 3.1: Diagram of a home made thin disk pump-module taken from [Pal09]. On the left hand side a technical drawing of the design can be seen while the right hand side shows the actual module. The disk mounted on the heat sink can be seen in the middle of each picture.

use of much higher pump powers. For cw-lasers this new technique has in recent years enabled the generation of average powers on the kW-level [Ste00] and industrial laser systems with average powers of up to 16 kW are currently commercially available[1]. While the limitations created by the thermal load have thus been drastically lessened for cw-lasers, one key problem remains with regard to using it for the power scaling in ultrashort pulse lasers: As has been discussed previously one of the main advantages of pulsed lasers over cw-lasers is that pulsed lasers can be used for micro-machining and other purposes because they can deliver high intensities without the thermal damage created by the high average output power from cw-lasers. This advantage would be lost if energy scaling in pulsed laser oscillators would be done only by scaling the pump power.

3.1.3 Scaling the repetition rate

As a result of the issues discussed above the energy scaling in ultrashort lasers is usually not done by only scaling the pump power, but rather by a combination of increasing the pump power while at the same time scaling down the repetition rate. While overall the goal is still to have MHz repetition rates, standard ultrashort pulse oscillators typically have repetition rates on the order of 50 to 100 MHz so there is some room for scaling. Eq. 3.1 shows that by reducing the repetition rate down to a few MHz it is possible to increase the pulse energy by up to two orders of magnitude while still achieving the goal of keeping the repetition rate at the MHz level. Since a reduction in the repetition rate also results in a decrease in the average output power the combination of reducing the

---

1   Trumpf TruDisk 16002

repetition rate and increasing the pump power opens up a way for further energy scaling in ultrashort pulse oscillators while still keeping the output power levels moderat.

3.1.4 Long cavity oscillators

Since the repetition rate of a linear cavity is defined as

$$f_{rep} = \frac{c}{2 \cdot l_{res}} \tag{3.2}$$

where l_{res} is the length of the cavity, the intuitive way to decrease the repetition rate is simply to increase the length of the oscillator. Keeping in mind that a repetition rate of 10 MHz already equals a resonator length of 15 meters it becomes clear that reducing the repetition rate is not without problems either. The challenge of course is to extend the cavity in such a way that it does not affect resonator stability or lead to excessive space requirements.

Cavity extension by use of a Herriott cell

An established way to allow an extension of an optical cavity while still keeping the cavity design simple and compact enough for stable pulsed laser operation is the use of a Herriott cell [Her64].

In this device two spherical mirrors are used in such a way as to reflect the laser beam back and forth between them before it exits after a set number of reflections thus creating an optical delay line. Fig. 3.2 shows a rendered drawing of a Herriott-cell with four reflection on each mirror. What makes the Herriott cell special is the fact, that the two mirrors are aligned in such a way that the geometrical properties of the incoming laser beam are exactly preserved in the outgoing beam. In order to achieve this it is necessary for the mirrors to be separated by a fixed distance l_{HC} given by:

$$l_{HC} = \frac{R_1 + R_2}{2} \pm \frac{1}{2}\sqrt{R_1^2 + R_2^2 + 2R_1 R_2 \cdot cos\left(\frac{\mu\pi}{\nu}\right)} \tag{3.3}$$

In this equation R_1 and R_2 define the radii of curvature of the two mirrors, μ is the number of rotations the beam makes around the center axis of the cell and ν is the number of reflections on each mirror. For practical purposes only such configurations where μ and ν do not share any prime factors are of actual use in order to avoid having the beam retracing the same path inside the cell again and again. It is also useful to introduce the angle Θ_{HC} defined as:

$$\Theta_{HC} = 2 \cdot \frac{\pi\mu}{\nu} \tag{3.4}$$

This angle signifies the angle between two successive reflections on the same mirror and is thus very helpful for the experimental realization of the cell. More about the principles
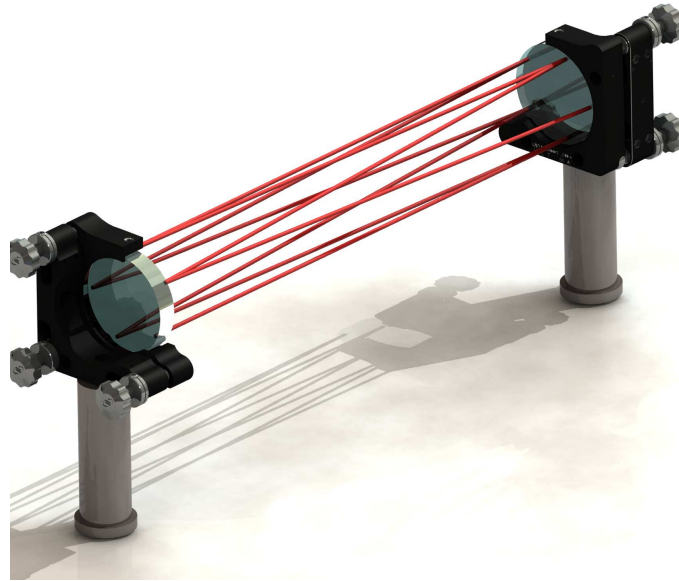
Figure 3.2: Image of a Herriott-cell with 4 reflections on each mirror. The mirrors used to couple into and out of the cell are omitted for clarity.

behind this concept as well as a more detailed investigation of these kind of multi-pass cells can for instance be found in [Dew02, Dew06a, Kow06].

Experimental realization

In recent years using a Herriott cell as means of extending the laser cavity has lead to a number of remarkable advances in the field of high energy laser oscillators. Starting in 1999 with the work of Cho et al., Herriott cells have been used in Ti:sapphire oscillators in order to increase the pulse energy [Cho99]. Over the years the pulse energy was successfully scaled up by the use of this concept [Cho01, Shc01, Kow03]. However for pulse energies exceeding several 100 nJ it was found that it becomes impossible to keep the laser in stable single pulse operation due to excessive nonlinearities that occur when operating in the traditionally used solitary regime. A solution to this problem is to operate the laser in the positive dispersion regime which results in a drastic reduction of the nonlinear effects [Fer04]. Using this approach pulse energies up to 500 nJ have been reached in recent years [Dew06b, Nau05]. This will be discussed in more detail later in this chapter in section 3.2.

Besides the use in Ti:sapphire oscillators, in recent years the concept of the long cavity oscillator has also been used sucessfully in Yb-based lasers. Here it is of special interest to combine the power scalability of the thin disk concept with the cavity extension by the Herriott cell. By introducing a Herriott cell into a thin disk cavity it was for instance possible to achieve up to 11 μJ of pulse energy from an Yb:YAG oscillator at a repetition

rate of 4 MHz [Mar06, Mar08]. However like in Ti:sapphire at some level the nonlinearities in the oscillator become so high that stable single pulse operation becomes impossible so that here as well operation in the positive dispersive regime becomes a viable alternative. Table 3.1 shows an overview over some of the key systems that have been investigated using this technique so far.

Source	Gain Material	Pulse Energy	Pulse Duration	Repetition Rate
[Cho99]	Ti:sapphire	11 nJ	16.5 fs	15 MHz
[Cho01]	Ti:sapphire	90 nJ	80 fs	4 MHz
[Shc01]	$Cr^{4+}:Mg_2SiO_4$	17 nJ	40 fs	26.5 MHz
[Kow03]	Ti:sapphire	150 nJ	43 fs	5.85 MHz
[Fer04]	Ti:sapphire	220 nJ	30 fs	11 MHz
[Nau05]	Ti:sapphire	505 nJ	45 fs	2 MHz
[Dew06b]	Ti:sapphire	560 nJ	50 fs	6 MHz
[Mar06]	Yb:YAG	5 μJ	800 fs	12.3 MHz
[Mar08]	Yb:YAG	11.3 μJ	791 fs	4 MHz
[Neu08]	Yb:YAG	25.9 μJ	980 fs	2.7 MHz

Table 3.1: Summary of existing long-cavity laser systems.

Active multipass cell

The last system mentioned in table 3.1 is using a concept that is very similar to that of the Herriott cell and is capable of generating the highest pulse energies currently available from femtosecond oscillators. By employing a so-called active multi-pass cell (AMC) in which the laser cavity is folded around the thin disk gain medium a pulse energy as high as 25.9 μJ with a pulse duration of 928 fs has been achieved by Neuhaus et al. in [Neu08]. In effect the AMC is a multipass cell built in such a way that the multiple passes through the gain medium allow for outcoupling percentages in excess of 70%. The advantage of the high outcoupling ratio is that the nonlinearities inside the cavity are reduced, which in combination with double chirped mirrors still allows operation in the solitary regime despite the high pulse energies. More details of this novel technique can be found in [Neu09]. While this newly developed system does deliver the highest pulse energies so far generated with a laser oscillator the long pulse durations do pose a considerable drawback compared to other concepts.

3.1.5 Cavity dumping in mode-locked lasers

Besides the extension of the cavity by using a multipass cell discussed above, there is also another way to increase the pulse energy by reducing the repetition rate. Using the experimental technique of cavity dumping it is possible to reduce the repetition rate

without actually having to increase the cavity length. Standard laser oscillators make use of a partially reflecting mirror to couple out the laser pulse. In order to use cavity dumping, this mirror is replaced by a standard high reflective mirror to achieve a closed cavity. The outcoupling of the pulse is then realized by means of either an acousto-optical (AOM) or electro-optical modulator (EOM) which can be used to 'dump' a part of the resonator energy out after a fixed number of roundtrips inside the cavity. This results in a virtual extension of the cavity defined by the frequency with which the pulse is coupled out via the modulator. Besides virtually extending the cavity, the main advantage of cavity-dumping is that it allows for much higher outcoupling ratios when compared to standard oscillators. Fig. 3.3 shows a schematic of the effect this outcoupling procedure has on the internal pulse energy.

As shown in that figure, the dumping occurs at a point in time when the intra-cavity pulse energy is highest. Then after the dumping process, the pulse energy starts to grow again over a number of passes through the cavity until the next dumping process starts. The dumping depth or dumping ratio describing the percentage of intra-cavity pulse energy that is coupled out is then described as $\frac{a}{b}$ as can be seen from the picture. When using an acousto-optical modulator the dumping is achieved by creating a grating structure inside the AOM by injecting it with an acoustic wave that diffracts part of the laser pulse into the first grating order where it can then be guided out of the cavity with a simple mirror. In contrast the electro-optical modulator uses the electro-optical effect, where a high voltage is applied to the EOM in order to turn the polarization of the laser pulse which can then be coupled out using a thin film polarizer (TFP). Regardless of which method is used for the cavity dumping process this technique for increasing the pulse energy does involve actively changing the intracavity pulse dynamics. Because of this it is helpful to take a closer look at this process.

Dynamics of cavity dumping

In order to achieve the highest possible pulse energies it is necessary to understand the importance of the dumping frequency and its influence on the cavity dynamics. As explained in section 2.1.1 every laser oscillator has a characteristic eigenfrequency describing the frequency of the relaxation oscillations, the value of which is defined by equation (2.7).As a result of this, the system will be especially susceptible to any perturbations occurring with a similar frequency. Experimentally this can result in period doubling preventing the laser from generating a constant pulse energy. For the dumping process this means that the dumping frequency ideally should be either much smaller or much larger than the relaxation frequency:

$$f_{dumping} \ll f_{relax} \ll f_{dumping} \tag{3.5}$$

If the dumping frequency is much slower than the relaxation frequency it is possible to achieve very high dumping ratios up to nearly 100%. However since typical relaxation
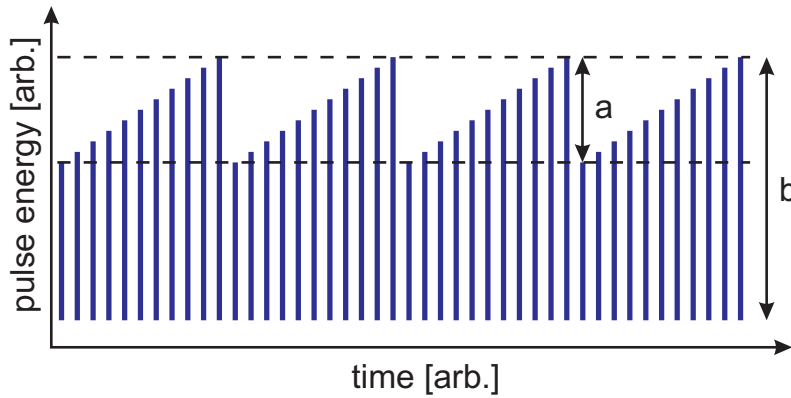
Figure 3.3: Schematic figure showing the dynamic of the intra-cavity pulse energy during cavity-dumping

frequencies are in the kHz regime the respective dumping frequencies have to be of the order of only a few kHz or below. In this case any oscillations occurring because of the dumping will dissipate and the laser has sufficient time to reach the steady state again prior to the next dumping cycle. As a result this mode of operation is generally called the relaxed regime. An example for this regime taken from a numerical simulation done as part of this thesis is shown in Fig. 3.4 to better illustrate the dynamic of this regime.

The dumping process does in fact lead to a relaxation oscillation. However because of the low dumping frequency and the low cavity losses between dumping cycles this oscillation can dissipate before the next dumping is initiated. While this regime allows for very high outcoupling ratios and consequently high pulse energies it is of lesser interest with regards to this thesis as it is intrinsically limited to a repetition rate in the low kHz range. In the case that $f_{dumping} \gg f_{relax}$ the pulse dynamic changes drastically. Fig. 3.5 shows a numerical simulation of this regime for laser parameters that were otherwise the same as in the previous figure. In the top picture the overall dynamic of the system can be seen from starting the laser until stable cavity dumped operation has been reached. Initially the laser is started with the cavity dumper turned off. As a result the laser starts without perturbation and after a short period of relaxation oscillations reaches the steady state. After 10.000 cavity roundtrips the dumping is turned on. In this regime the dumping cycle is so short that only the first perturbation of the laser leads to the start of relaxation oscillations while none of the following dumping processes lead to further oscillations. The high frequency with which the perturbation occurs prevents it from coupling to the relaxation frequency of the oscillator. This is similar to the classical case of two coupled pendulums where a periodic perturbation of one pendulum does not affect the system as a whole if it is too different from the eigenfrequency of the system [Kil04a].

A close up of the intra-cavity pulse energy during the relaxation oscillations can be seen in the lower left part of the figure, with the dots marking the individual cavity roundtrips. The cavity dumping, which in this model takes places every 17th roundtrip, continues
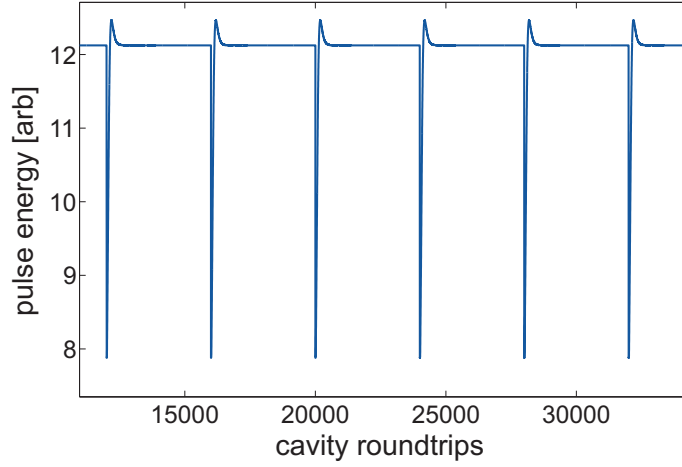
Figure 3.4: Numerical simulation of the relaxed dumping regime. After the cavity dumping occurs the laser lapses into a short period of relaxation oscillations which have enough time to dissipate before the next dumping cycle starts

during the oscillation without initiating further oscillations. However the extra losses created by the high frequency dumping reduces the damping of the oscillations and as a result they are much more pronounced than in the relaxed regime. Once the oscillations have dissipated after about 12.000 cavity roundtrips, the laser reaches a quasi-steady state regime depicted in the lower right part of Fig. 3.5. In this state the intra-cavity dynamic is periodically linked with the dumping cycle ensuring that each outcoupled laser pulse is equal. The maximum pulse energy that can be coupled out of the oscillator is smaller than in the relaxed regime. However still far larger than would be possible with a standard outcoupling mirror while allowing for repetition rates in the MHz regime.

Looking at the maximum intra-cavity pulse energy with dumping and without it is obvious that as a result of the additional losses introduced by the dumping the maximum energy is reduced. Experimentally this can be counteracted by increasing the pump power. Which will bring the intra-cavity pulse energy closer to the original value again and allow for a further increase of the dumping ratio. By carefully increasing the pump power along with the dumping ratio it is thus possible to maximize the outcoupled pulse energy.

In case the laser is operating in the solitary regime, there is another frequency that has to be considered. As discussed in section 2.2.5 if the soliton is facing a perturbation from the fundamental soliton mode it tries to dissipate energy so that it can once again reach the fundamental soliton order. This dissipation happens in such a fashion that the soliton order as well as the pulse energy and pulse duration is oscillating around N=1. The frequency of this oscillation is determined by:

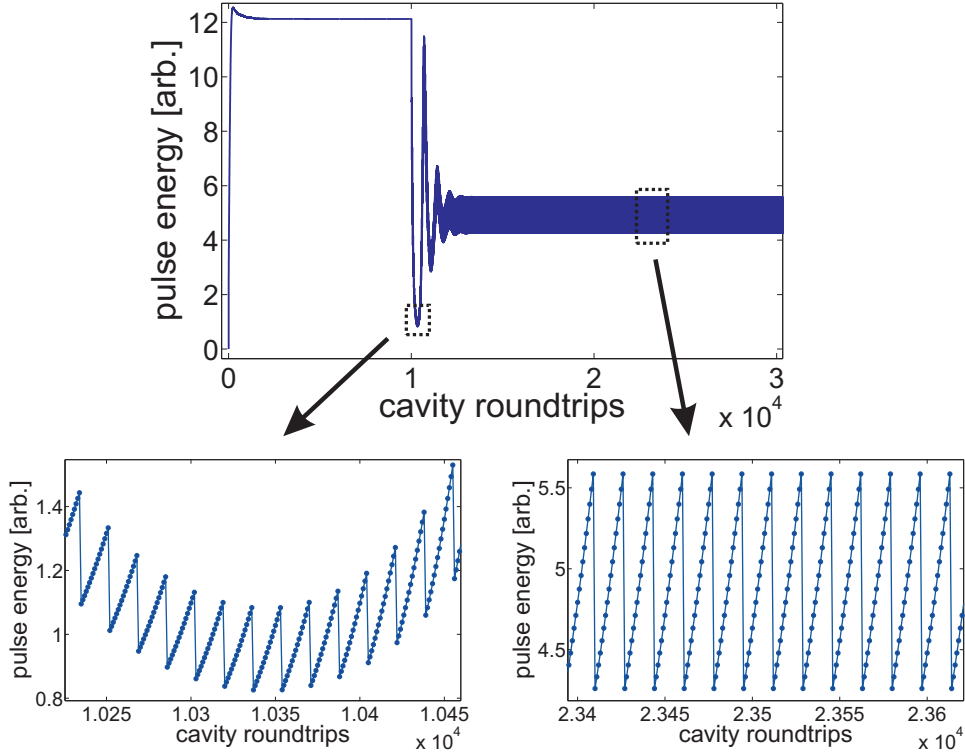$$f_{soliton} = \frac{1}{4\pi}\gamma f_{rep}\hat{P} \tag{3.6}$$

Figure 3.5: Dynamics of the transient dumping regime. The topmost picture shows the cavity dynamic over 30000 roundtrips, with the dumping turned on after 10000 roundtrips. The lower two pictures are outtakes that show a close-up of the dynamics during the initial relaxation oscillations and during quasi-steady state operation.

Since the main perturbation of the soliton in a cavity dumped oscillator is obviously going to be the dumping process, the importance of this frequency can be easily understood. If $f_{dumping}$ is slower than $f_{soliton}$ the result can be complex dynamical processes preventing the laser from reaching stable operation [Kil05a].

Consequently in order to minimize dynamical instabilities resulting from the dumping process the dumping frequency should be chosen such that:

$$f_{dumping} \gg f_{soliton} \qquad f_{dumping} \gg f_{relax} \tag{3.7}$$

If this condition is met the laser will operate in the transient regime described above which allows high dumping ratios at MHz repetition rates. In this regime neither the relaxation oscillations nor the soliton oscillations will affect the stable operation of the laser. However even in this regime instabilities may occur as the laser may switch to q-switched mode-locked operation if the dumping ratio is too high.
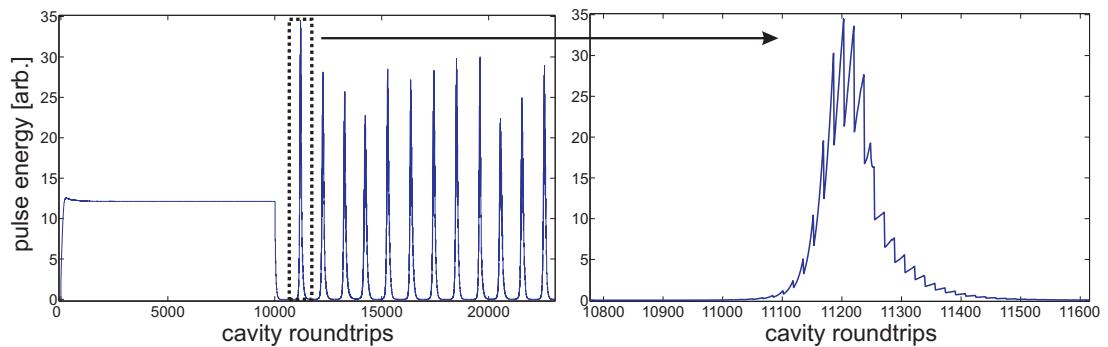
Figure 3.6: Q-switching instabilities caused by excessive dumping ratios. The gain cannot compensate the additional losses from the cavity dumping and the laser falls below the Q-switching threshold and starts emitting random bursts of laser pulses. The right hand side shows a closeup of such a burst where the modulation resulting from the cavity dumping is still visible.

If the dumping ratios are so high that the losses induced cannot be compensated for by the gain of the system and the laser falls below the Q-switching threshold described in eq. (2.10), the laser will then start to display irregular Q-switched behavior which is shown in Fig. 3.6. After the cavity dumping has been turned on after 10000 cavity roundtrips, the pulse energy rapidly decreases because of the added losses until at some point the laser action stops. As described in section 2.1.2, the laser then starts to operate in the q-switch regime and emits burst of mode-locked pulses. The enlarged image of such a burst in right hand side of Fig. 3.6 shows that in these bursts the effect of the cavity dumping can still be seen by the typical saw-toothed dynamic which is superimposed on the Q-switching dynamic. While this can in theory be reversed by simply lowering the dumping ratio, experimentally this can lead to problems as the high peak intensities that may occur as a result of the Q-switching can lead to damage in the optical components especially if a SESAM is used as saturable absorber.

Experimental realization

Table 3.2 shows an overview of cavity dumped mode-locked laser systems that have been realized in the past years.

Source	Gain Material	Pulse Energy	Pulse Duration	Method	Repetition Rate
[Ram93]	Ti:sapphire	100 nJ	50 fs	AOM	950 kHz
[Psh93]	Ti:sapphire	60 nJ	13 fs	AOM	200 kHz
[Gib96]	Ti:sapphire	212 nJ	17 fs	EOM	1 kHz
[Bal97]	Ti:sapphire	40 nJ	13 fs	AOM	1 MHz
[Kil04b]	Yb:glass	400 nJ	300 fs	EOM	173 kHz
[Kil05b]	Yb:KYW	1 μJ	380 fs	EOM	1 MHz
[Zho06]	Ti:sapphire	450 nJ	60 fs	AOM	800 kHz
[Pal07b]	Yb:KYW	3 μJ	680 fs	EOM	1 MHz
[Pal07a]	Yb:KYW	2 μJ	420 fs	EOM	1 MHz
[Sie09]	Ti:sapphire	1.1 μJ	(74 fs)	AOM	1 MHz

Table 3.2: Overview of cavity dumped laser systems. The last three systems printed in green are treated in this thesis. The two Yb:KYW based systems were the subject of numerical investigations while the Ti:sapphire system was developed in the course this thesis. When the pulse duration is given in parenthesis, no recompression of the pulses has been shown. The number given then refers to the Fourier-limit of the optical spectrum.

Cavity-dumping has been used in Q-switched lasers for a long time. The use in mode-locked lasers however has not really been probed until about 15 years ago. Nevertheless it soon became apparent that by using this technique it is possible to reach pulse energies that were until then not available from laser oscillators. The first experiments using cavity-dumping were mainly done with Ti:sapphire lasers and using an AOM as dumping mechanism [Ram93, Psh93, Bal97] with the exception Gibson et al. who used an EOM [Gib96]. Looking at the numbers in Table 3.2 it can be seen that the main limitation of all EOM cavity-dumped lasers has long been the repetition rate which was limited to the kHz regime. Only in recent years the development of faster EOM driver electronics that are able to reach switching frequencies of up to 1 MHz and beyond allowed the development of laser systems with higher repetition rates. [Kil05b, Pal07b, Pal07a]. By contrast AOMs have long allowed for higher dumping frequencies, yet in these systems the dumping ratio is generally smaller than in EOM cavity-dumped systems because of the limited diffraction efficiency of the Bragg-cell. Nevertheless, for Ti:sapphire system AOMs are still the main cavity dumping technique owing to the fact that the Bragg-cell induce less material dispersion into the laser cavity compared to the long non-linear crystals used in the most effectiv Pockels-cells.

The combination of virtually extending the laser cavity while at the same time allowing for higher outcoupling ratio enables cavity dumped laser systems to generate similar pulse energies as in long-cavity oscillators at lower internal peak intensities. Still even for these systems nonlinear effects eventually become the main source for instabilities when scaling to higher pulse energies. These nonlinearities, their effects and ways to avoid them will

be discussed in the next section.

3.2 Nonlinear effects and operation regimes

As has already been mentioned in the previous sections, at some point excessive nonlinearities become the main difficulty in further increasing the pulse energy of femtosecond laser pulses. The reason for this lies in the combination of the phase shifts induced by the Kerr-effect and material dispersion from the cavity elements.

3.2.1 Optical wave breaking

As already discussed in section 2.2.6 the SPM resulting from the optical Kerr-effect does not by itself influence the temporal envelope of a laser pulse. However for femtosecond laser pulses, the effects of SPM and GDD inside a nonlinear medium cannot be viewed independently. Instead one has to consider that GDD and SPM act on the pulse at the same time during the propagation through the medium.

While the SPM itself does not alter the temporal pulse shape, the resulting frequency chirp does make it strongly susceptible to temporal pulse shaping by the GDD. The combination of the linear chirp induced by the GDD and the often highly non-linear chirp resulting from the SPM can lead to the effect that different parts of the pulse propagate at different speeds, overtake and even interfere with each other. This so-called optical-wave breaking can lead to strong perturbations of the temporal pulse shape and ultimately the division into multiple pulses [Tom85, Agr95]. Given the intensity dependence of the SPM and the resulting frequency chirp, wave-breaking is of special concern in high energy laser oscillators and is one of the strongest limiting factors for energy scaling in femtosecond oscillators.

3.2.2 Negative dispersive or solitary regime

In the solitary regime the combined effects of GDD and modest SPM are actually a requirement for the formation and propagation of the optical solitons [Agr95]. However at higher intensities the growing Kerr-nonlinearities result in ever stronger perturbations of the soliton. This is further aggravated by the discrete nature of the cavity elements which force the soliton to go through a series of changes during each cavity roundtrip. Using eq. (2.33), the sum of the nonlinearities in the laser cavity can simply be expressed as:

$$\phi_{max,total} = \sum_i \gamma_i \hat{P}_i L_{eff,i} \qquad (3.8)$$

In general the main contribution to this term will be the phase acquired in the gain medium and any possible other nonlinear crystals included in the cavity (e.g. the Pockels-cell in the case of EOM cavity-dumping). For standard femtosecond oscillators this can be compensated for by adding more negative second order dispersion to the oscillator with

chirped mirrors or prisms. However for high energy laser oscillators the situation becomes more complex. In the case of high power Kerr-lens mode-locked lasers a problem arises from the fact that in order to achieve stable mode-locking a tight focus inside the laser crystal is needed which gives rise to a high nonlinear phase. Eventually the nonlinear phase becomes so high that optical wave-breaking occurs inside the nonlinear medium before it can be compensated by chirped mirrors. A similar problem arises in Yb-based laser oscillators for very high pulse energies. While these oscillators do not normally rely on Kerr-lens mode-locking, for peak intensities of around 10 MW even the contribution of the residual gas inside the oscillator becomes significant. At this point the nonlinear phase effects actually become extremely susceptible to pressure fluctuations caused by the air flow inside the cavity which makes it almost impossible to compensate the effects with standard measures. One possible solution for this is to operate the laser in a vacuum or a noble gas atmosphere which eliminates or severely reduces Kerr-nonlinearities in the residual gas [Mar06, Mar08, Pal07b] making it again possible to compensate the remaining nonlinear phase by using chirped mirrors. Another possible solution is the implementation of the active-multi-pass cell which has already been discussed above [Neu08].

3.2.3 Positive dispersive or chirped pulse regime

While the negative effects of the excessive nonlinearities can be counteracted in the solitary regime the fact remains that to do so requires some rather complex experimental methods (e.g. using an airtight box). In 1993 Proctor et al. came up with a way to avoid the problem of excessive nonlinearities by operating the laser in the positive dispersion regime rather than in the negative [Pro93]. In the negative dispersion regime, the pulse typically has a duration close to the Fourier-limit while traveling inside the cavity. By contrast when the laser is operated in the regime of net positive intra-cavity dispersion the pulse in the cavity is heavily chirped and the pulse duration increases significantly. Since the increase in pulse duration directly leads to a proportional decrease in peak intensity it is thus possible to strongly reduce the Kerr-nonlinearities acting on the pulse. Because of the chirped laser pulses this type of laser is commonly called chirped pulse oscillator (CPO). The drawback of the CPO technique is that the pulses coming out of the laser cavity are strongly chirped and will typically have pulse durations of a couple of picoseconds. Consequently it is necessary to recompress the pulses to reach pulse durations close to their original Fourier-limit, which can be done either by using a prism or a grating compressor.

Pulse formation in the chirped pulse regime

In terms of the temporal pulse shaping, the positive dispersion regime also differs from the solitary regime. The area theorem which determines the pulse duration in the solitary regime does not apply in the positive dispersive regime. Consequently the chirped pulse duration is mainly determined by the saturable absorber and the temporal broadening resulting from the positive intra-cavity GDD. In case of a SESAM mode-locked CPO,
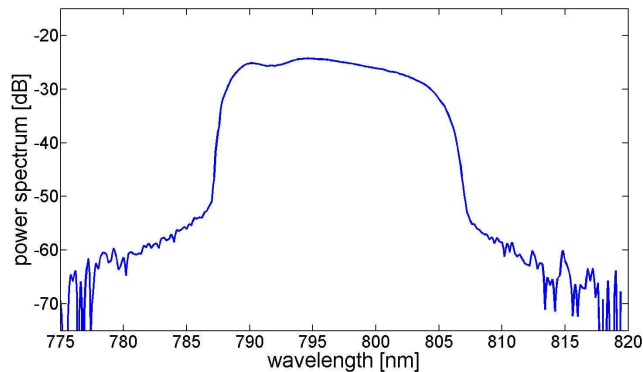
Figure 3.7: Example of a typical spectrum from a chirped pulse oscillator as shown in section 5.2.

the pulse chirp will usually be determined by the relaxation time of the SESAM which usually is on the order of several picoseconds. However, this is also influenced by the saturation parameter of the SESAM, stronger saturation tends to lead to longer pulse durations because the gain window defined by the absorber will become wider.

In the spectral domain a typical feature of a chirped pulse oscillator is the nearly rectangular or in some cases even M-shaped spectrum, an example of which is shown in Fig. 3.7. Since the dynamics of the CPO are closely linked to its unique spectral shape it is important to understand the effects which lead to it.

Generally speaking a chirped pulse oscillator can be seen as a combination of several discrete elements: A saturable absorber, the gain medium, dispersive elements and an outcoupler which are shown in Fig. 3.8.

A qualitative explanation for the evolution of the spectral shape requires looking at the combined effects of these elements. The pulse is initially formed by the saturable absorber as explained in section 2.2.5. However unlike in the solitary regime there is no dispersion compensation in place to keep the pulse phase flat and the temporal duration short as it travels through the laser cavity which leads to the chirping of the pulse. As a result when this chirped pulse travels through a Kerr-medium the effects of SPM are different than for an unchirped laser pulse as outlined in section 2.2.6. If the ratio between chirp and nonlinear phase is chosen correctly this results in spectra such as those shown in
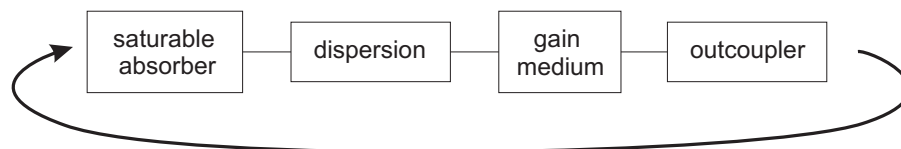

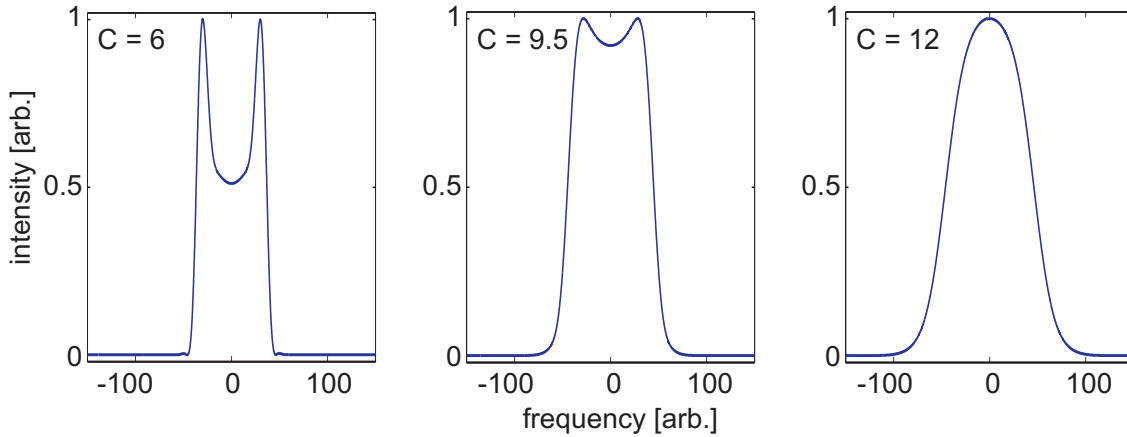**Figure 3.8:** Diagram of a standard CPO

Figure 3.9: Qualitative examples of spectral shaping in CPOs by SPM. From left to right the chirp factor increased from 6 to 12. The nonlinear phase used in this example is 1.9π.

Fig. 3.9. Here the chirp factor is increasing from left to right starting with C = 6. As can be seen a small chirp factor results in an M-shaped spectrum, as the chirp factor increases, the spectral form changes into a π-like form before finally becoming more and more parabolic in shape. On the other hand experimentally when the pulse chirp is too low, the spectrum will start to show signs of optical wave breaking, which cannot be seen in the simple model used for Fig. 3.9.

In order to achieve a quantitatively correct understanding of the pulse dynamics it is necessary to include several other effects such as the gain dynamics, the emission bandwidth, the absorber dynamics, higher order dispersion and other effects of the Kerr-nonlinearity inside the crystal like self-steepening.

A possible analytical solution to this problem has been presented in the past by Kalashnikov et al. [Kal09, Kal05]. Another way to model the pulse dynamics in CPOs quantitatively is to use a numerical simulation based on the split-step fourier method which has been done in this thesis and will be presented in chapter 4 [Sie08].

Experimental realization

Since the first implementation of a Ti:sapphire CPO in 1993 [Pro93] this technique has made it possible to drastically increase the pulse energy output generated by Ti:sapphire oscillators and has also been successfully implemented in lasers based on other gain materials such as Yb:KYW [Pal07a, Pal08]. Table 3.3 shows a summary of some key CPOs developed in recent years. As the CPO concept can easily be combined with any of the other scaling concepts presented above many of the laser systems have already been quoted in the respective sections. As can be seen from the table, especially for Ti:sapphire oscillators there has been a great increase in interest in the CPO concept in recent years as the increase in pulse energies, has made the handling of the Kerr-nonlinearities ever

more important.

Source	Gain Material	Pulse Energy	Pulse Duration	Repetition Rate
[Pro93]	Ti:sapphire	not given	13 fs	not given
[Cho01]	Ti:sapphire	90 nJ	80 fs	4 MHz
[Fer04]	Ti:sapphire	220 nJ	30 fs	11 MHz
[Nau05]	Ti:sapphire	505 nJ	45 fs	2 MHz
[Dew06b]	Ti:sapphire	560 nJ	50 fs	6 MHz
[Zho06]	Ti:sapphire	450 nJ	60 fs	800 kHz
[Pal07a]	Yb:KYW	2 μJ	420 fs	1 MHz
[Pal08]	Yb:KLuW	274 nJ	5 ps (450 fs)	34.7 MHz
[Sie09]	Ti:sapphire	1.1 μJ	5-6 ps (74 fs)	1 MHz

Table 3.3: A summary of chirped pulse oscillators developed in recent years. The last three systems printed in green are subject of this thesis. When the pulse duration is given in parenthesis, no recompression of the pulses has been shown. The number given then refers to the Fourier-limit of the optical spectrum.

In general Ti:sapphire based CPOs are using either pure Kerr-lens mode-locking or a hybrid mode-locking technique based on Kerr-lens mode-locking and a SESAM. Because of the lower peak intensities associated with the chirped pulse regime, the effectiveness of the Kerr-lens is somewhat reduced. As a result CPOs relying solely on Kerr-lens mode-locking are generally not self-starting or intra-cavity prisms have to be used to start the laser in the solitary regime and then use the prisms to change the operation into the positive dispersive regime. Using a SESAM to help start the mode-locking process enables the laser to be self-starting and become more stable against perturbations [Cho01]. In this respect it needs to be noticed that the dynamic of the saturable absorber in the positive dispersive regime does not only influence the temporal evolution of the laser pulse but can also have strong effects on the spectral shape. If the chirp factor of the pulse is high enough so that the pulse duration exceeds the relaxation time of the SESAM it can even act as a spectral filter. In SESAM mode-locked oscillators in the negative dispersion regime soliton mode-locking is usually used in order to help stabilize the mode-locking and to reduce the pulse duration below that achievable with the SESAM alone. Since solitons require negative dispersion to form, this can obviously not be done in the positive dispersion regime. As a result the SESAM needs to have a higher modulation depth in order to make up for the absence of the stabilizing effect otherwise provided by the soliton.

The dynamic of the individual CPO systems as well as further energy scaling possibilities will be treated in chapters 4 and 5.

3.3 Comparison to fiber lasers

Given the nature of chirped pulse oscillators and their importance energy scaling in solid-state laser oscillators it may be interesting and helpful to make a brief comparison between the power scaling in solid-state lasers and modern fiber oscillators. Like for solid-state femtosecond oscillators the scaling of the pulse energy is one of the most active research areas in fiber optics as well. Inherently nonlinearities resulting from Kerr-nonlinearities are a major problem in the development of high energy femtosecond fiber lasers and as a result numerous schemes to overcome the limitations presented by this problem have been researched in recent years.

While the fact that the laser pulses in a fiber oscillator have to traverse far greater lengths of nonlinear material is an obvious drawback in terms of energy scaling, fiber oscillators have two big advantages in terms of dealing with nonlinearities: First of all because the pulse propagates almost completely in optical fibers, the nonlinearity is spread far more evenly throughout the oscillator as compared to the discrete nature of nonlinearities in a solid-state laser cavity. Second, the fiber technology makes it possible to easily change the dispersion regimes inside the cavity by simply using a different fiber.

These two advantages make it possible to not only use the chirped pulse technique in fiber oscillators, but to actually go further and reach the wave-breaking free regime where the laser pulse travels inside the optical fiber as a so-called similariton [And93, Ild04a, Dud07]. In this operation regime the gain, the Kerr-nonlinearity and the positive dispersion can interact in such a way as to generate pulses which have a parabolic intensity profile in the frequency domain and a frequency chirp that is not only entirely linear, but also is completely independent of the Kerr-nonlinearity. As a result optical wave-breaking is avoided regardless of the peak intensities while the pulse propagates through the nonlinear medium in a self-similar fashion[1]. Herein lies the main difference between the wave-breaking free regime and the chirped pulse regime. In the latter, wave-breaking is avoided by reducing the Kerr-nonlinearities through lowering the peak power whereas in the former, the non-linearities still exist, but do simply not lead to optical wave-breaking.

While there is still some ambiguity in the naming of the operating regime ('wave-breaking free', 'self similar', 'all-normal dispersive') it is nevertheless quite clear that the development of fiber oscillators with net positive dispersion has helped boost the available pulse energy from below nJ-levels close to the μJ-level in recent years [Ort09, Rue08].

With respect to this thesis an interesting question is whether it is possible to transfer the developments made for fiber oscillators to standard solid-state oscillators in order to reach a similar operation regime. To this end the main obstacle is the discreteness of the cavity elements and the fact that the high values of GDD and propagation lengths required for the formation of similaritons cannot be easily reached in a solid-state oscillator. It needs

---

1 The term 'self-similar' describes a certain transient behavior observed in a number of physical systems. An extensive definition as well as a mathematical treatment of this can be found in [Bar96] hence the pulses are called similaritons.

to be noted however that even in fiber oscillators a pure similariton is never achieved and in fact many of the self-similar properties of wave-breaking free regime are already even when the pulse is relatively far from the similariton solution [Rue08]. Interestingly it has been shown in the past that theoretically it should be possible to achieve an intermediate regime in Ti:sapphire oscillators which would emulate the wave-breaking free regime in fiber oscillators. Theoretically this should allow the generation of chirped laser pulses with a Fourier-limit of 10 fs and pulse energies of 1 μJ [Ild04b]. However experimentally a realization of such a laser system is difficult because it would require very accurate control of the intra-cavity GDD down to below 10 fs^2 over a frequency range sufficiently broad to support a Fourier-limit of 10 fs which is difficult to achieve with current technologies. Consequently no experimental realization of such a laser system has so far been reported.

4 Numerical investigation of energy scaling in Yb-based femtosecond oscillators

Having introduced the most important principles of mode-locking and energy scaling in solid-state laser oscillators in the previous chapters, in this chapter numerical investigations done as part of this thesis will be presented. The simulations were used to better understand the intra-cavity dynamics of existing laser systems allowing to identify limitation as well as possible ways to increase their performance. Besides this the simulations were used to investigate what possible results can be expected from combining the thin disk laser concept with operation in the chirped pulse regime. First the basics of the simulations will be explained along with a brief overlook over the computational implementation.

The second section presents the results of a numerical investigation into the pulse dynamics of an Yb-KYW think disk oscillator with cavity-dumping. Based on the numerical results limitations of the experimental setup presented in [Pal07a] are identified and ways for further energy scaling are deduced.

Following that a more fundamental investigation of the energy scaling properties of Yb-based chirped pulse oscillators is shown. Here a special focus was put on the possibility of implementing an Yb-based thin disk chirped pulse oscillator in order to generate high pulse energies.

4.1 Numerical model

The mathematical foundation of the numerical simulations presented in this chapter is the master equation of mode-locking given in eq. (2.26). While the full master equation does not have an analytical solution it can be effectively modeled numerically by use of the split-step Fourier method [Har73].

4.1.1 Split-step Fourier algorithm

The idea behind the split step method is to divide the master equation into two parts: a nonlinear part which can be solved in the time domain and a linear term which can be solved in the frequency domain. In order to use this method to simulate the propagation of a laser pulse, the propagation length is divided into a finite number of individual steps. For each of these steps the nonlinear and linear terms are applied to the laser pulse in an alternating fashion. In order to link each step to the next a Fourier transformation is

needed to transfer the solution from the time domain to the frequency domain and vice versa. Using this approach it is possible to implement the propagation of a laser pulse through a cavity modeling each cavity element individually in the appropriate regime. If multiple effects occur in the same element these are considered one after the other. A more thorough and more mathematical description of the split-step Fourier algorithm can for instance be found in [Kil05a] or [Agr95].

4.1.2 Computational implementation

The split-step Fourier algorithm is based on propagating a laser pulse through the different cavity elements one after another taking into account their individual effects on the laser dynamics. For many laser systems it is actually possible to simplify this approach somewhat by summing up the effects of different elements into a single computational calculation. This way for instance the dispersion effects resulting from material dispersion and chirped mirrors can be combined into a total dispersion and need to be calculated only once in the simulation. In most cases using this method makes it possible to significantly speed up the simulation process while sacrificing very little in terms of accuracy. There are however some cases, especially for laser pulses shorter than 50 fs, when this method is unsuitable because the inaccuracies become too large. However as the laser systems subject of the numerical investigations generate pulse durations of several hundred femtoseconds this does not pose a problem. Consequently for this thesis, the dispersion as well as the losses were combined into blocks rather than treating each cavity element individually. On the other hand the nonlinearities stemming from the different nonlinear elements in the cavity were in fact calculated separately in order to achieve higher accuracy.
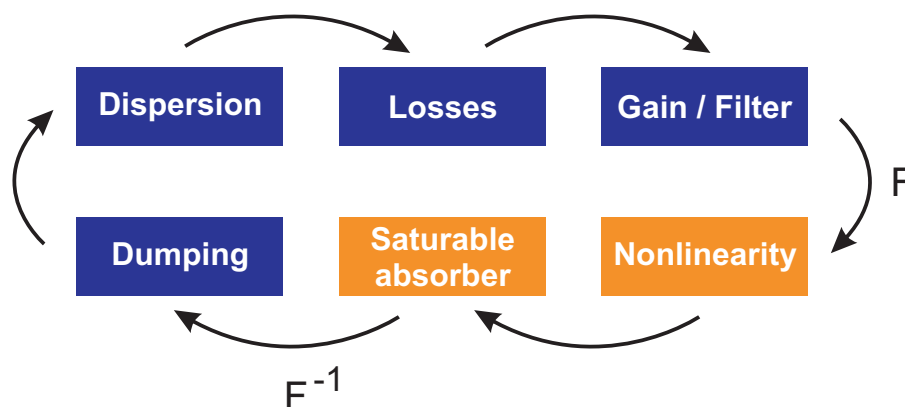

Figure 4.1: Flowdiagram for a standard split-step Fourier simulation of a cavity-dumped oscillator. F and F^{-1} signify a Fourier transformation and an inverse Fourier transformation respectively.

Fig. 4.1 shows a flowdiagram for a typical split-step Fourier algorithm used in the simulation of a typical SESAM mode-locked oscillator with cavity-dumping. The simulation takes into account a number of different effects:

- **Dispersion**
  The simulations done as part of this thesis include both the effects of GDD and TOD resulting from the material inside the laser cavity. This is done using the eqs. (2.22) and (2.23).

- **Residual losses**

- **Dynamic frequency dependent Gain**
  The gain of the system is described by eq. (2.1), in order to achieve the necessary frequency dependence, the calculations are done in the frequency domain and a Lorentz-curve is used in order to simulate the gain filtering effect.

- **Nonlinearities**
  As described in section 2.2.6 the self-phase modulation resulting from the Kerr-nonlinearities acts on the laser pulse according to eq. (2.34)

- **Saturable absorber**
  As already discussed in chapter 2, the dynamics of a saturable absorber inside a laser cavity can be described by eq. (2.27). Depending on the actual type of absorber, its saturable losses q(t) need to be calculated accordingly. Here the absorber is a slow saturable absorber, a SESAM. To describe the dynamics of the saturable losses of this type of absorber the following equation is used:

$$q(t,T) = q_0 \cdot \exp\left[-\frac{1}{E_{sat}} \int\limits_{-T_{Rep}/2}^{t} |A(t,T)|^2 dt\right] \tag{4.1}$$

- **Cavity-dumping**
  The cavity-dumping is numerically implemented as a constant periodic loss modulation occurring after a fixed amount of cavity roundtrips.

In order to facilitate a working computational implementation of the split-step Fourier method it is also necessary to define time a frequency windows consisting of N supporting points which can then be used in the calculations. By setting a fixed width T for the time window, the distance between the individual support points can be defined as follows:

$$\Delta t = \frac{T}{N} \qquad\qquad \Delta\omega = \frac{2\pi}{N\Delta t} \tag{4.2}$$

Implementing these elements and their respective mathematical descriptions in a programming language now allows for the simulation of a wide range of mode-locked oscillators. The accuracy of the numerical results then depends on a number of factors, some

linked to the experimental parameters but also others that are linked to the numerical implementation of the algorithm. The important numerical parameters that influence the accuracy are the number of supporting points used in the calculation as well as their distance from each other. Depending on the laser system in question, the experimental parameters and the nature of the investigation another point which can be important is the sequence in which the cavity elements are arranged. Because the numerical simulations done here are based on the parameters gathered from several laser systems the accuracies of these parameters are also influencing the accuracy of the numerical model. Any uncertainties affecting the results of the simulations done in this thesis are pointed out in the respective sections.

Having now briefly outlined the basic ideas behind the numerical model, the next sections will present the results of the investigations done as part of this thesis.

4.2 Investigation of cavity-dumping in thin disk oscillators

As has been outlined in chapter 3 numerous concepts for the power and energy scaling in mode-locked femtosecond lasers exist. Two particularly intriguing concepts are the thin-disk laser, allowing for higher pump powers compared to bulk lasers, and cavity-dumping, allowing for increased outcoupling ratios in comparison to standard outcoupling methods. Taking into account the recent achievements that have been made with either of these two concepts [Kil05a, Mar08], an obvious next step is to investigate the possibility of combining the two.
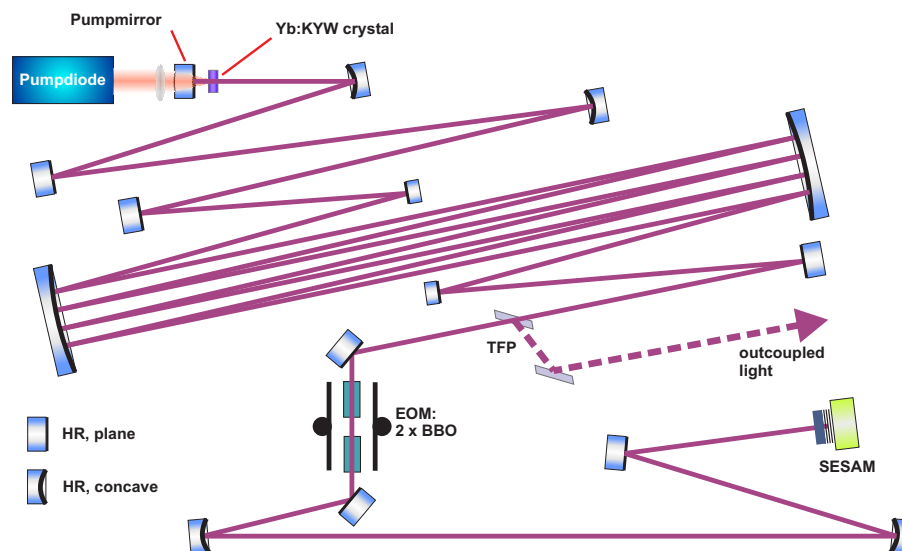

Figure 4.2: Schematic of the thin-disk oscillator with cavity-dumping as shown in [Pal07a, Pal09].

4.2.1 Laser setup

On the basis of the cavity-dumping scheme used in [Kil05a], a thin-disk laser with EOM cavity-dumping has been presented in 2007 [Pal07a, Pal09].

Fig. 4.2 shows the schematic experimental setup of this laser system. Since the experimental work on this laser has already been discussed in detail elsewhere [Pal07a, Pal09] only some fundamental aspects of the experimental setup will be discussed in this thesis. As gain medium an Yb:KYW thin disk is used, which is mounted in a commercially available thin disk module[1]. The disk itself has a thickness of 115 μm and a doping concentration of 10 at%. The pump source is a commercial 50 W laser diode[2] operating at a wavelength of 980 nm. The thin disk module allows for 24 passes of the pump light through the disk which leads to an overall pump absorption of 86%. As thin disk lasers are particularly susceptible to spatial hole burning and etalon effects [Pas01], a quadruple pass of the laser through the thin disk along with a birefringent filter (BRF) is used to counter these effects and guarantee stable mode-locked operation. For the cavity-dumping a BBO-based Pockels-cell[3] is used in combination with a thin film polarizer (TFP). The mode-locking of the laser is initiated by the use of a SESAM[4] and in addition to this a number of negative dispersive mirrors ensure that the soliton condition is met allowing the formation of an optical soliton which supports the mode-locking process. The total resulting cavity length for this setup is 9.36 m leading to an internal repetition rate of 16 MHz.

Some of the key results achieved with this laser system are summed up in Table 4.1.

Parameter	Value
Repetition rate	16 MHz
Dumping frequency	1 MHz
Pulse energy (air)	2.3 μJ
Pulse duration (air)	700 fs
Pulse energy (helium)	3 μJ
Pulse duration (helium)	680 fs
Dumping ratio	24%

Table 4.1: Summary of the results achieved with the Yb:KYW thin disk oscillator with cavity-dumping.

---

1   Technologiegesellschaft für Strahlwerkzeuge mbH
2   Jenoptik Jold-50-CPXF-2P
3   Cleveland Crystals
4   Batop GmbH

By using the Pockels-cell and the TFP for cavity dumping pulse energies of 2.3 μJ with a pulse duration of 700 fs could be generated at a repetition rate of 1 MHz. When trying to achieve higher pulse energies, two different problems came up: One problem is that the peak intensities inside the resonator become so high that the laser is actually susceptible to nonlinearities generated in air inside the cavity as already pointed out in section 3.2. As also explained in that section, this effect can be countered by flooding the laser cavity with Helium which reduces the nonlinear effects and allows to operate the laser at higher intra-cavity powers. Using this method it was possible to further scale the pulse energy to 3 μJ at pulse durations of 680 fs. The second problem preventing higher pulse energies however is directly linked to the cavity-dumping process. In previous cavity-dumped femtosecond lasers dumping ratios in excess of 50% could be shown [Kil05a] and even higher ratios close to 80% have been achieved at IQ. By comparison in the cavity dumped thin-disk oscillator the maximum dumping-ratio still allowing stable laser operation was found to be 23% despite the fact that with 13 μJ, the intra-cavity pulse energy is far higher than in the case of the bulk laser. Higher dumping ratios experimentally resulted in multiple-pulsing, Q-switching and other instabilities. Because this effect could not be readily explained experimentally. Numerical simulations were used as a means to investigate the cause of the limitations and to find ways to overcome them, this work was done as part of this thesis.

4.2.2 Comparing experiment and theory

The basis for the numerical modeling is the split-step Fourier algorithm introduced in the previous part of this chapter. As with any numerical simulations, special care has to be taken in order to ensure the validity of the model. Consequently a necessary first step in the investigation of the problem is to test the numerical model against the experimental realities and check if the model is able to reproduce the data gathered in the experiment.

To this end there are two logical starting points: On the one hand the thin-disk oscillator itself, on the other hand the Yb:KYW bulk laser used in previous cavity-dumping experiments [Kil04a, Kil04b, Kil05a, Kil05b]. The latter system is of interest not only because it is already well understood as the result of earlier investigations but also because a direct comparison between the two laser systems is of obvious value seeing how they are very similar in many aspects, except the dumping ratio and the way the gain medium is implemented into the oscillator.

Simulation of the Yb:KYW thin disk oscillator

As a first step the numerical simulation of the Yb:KYW thin disk oscillator was done using the known experimental values for the system. Table 4.2 shows both the parameters used in the simulation as well as the experimental parameters along with their uncertainties.

While some parameters like the repetition rate can be readily measured or are known with high certainty, some of the other parameters have to be estimated. The dispersion

Parameter	Experimental value	Numerical value
f_{rep}	16 MHz	16 MHz
β_2	-40000 fs^2 $\pm$ 2000 fs^2	-40000 fs^2
w_{BBO}	650 μm $\pm$ 65 μm	650 μm
w_{gain}	450 μm $\pm$ 23 μm	450 μm
w_{abs}	370 μm $\pm$ 14 μm	370 μm
w_{gas}	700 μm $\pm$ 35 μm	700 μm
l	4% $\pm$ 0.5%	4%
τ_{abs}	$\leq$1 ps	1 ps
ΔR	0.5%	0.6%
ϕ_{abs}	90 μJ/cm^2 $\pm$ 40 μJ/cm^2	90 μJ/cm^2
g$_{0,air}$	0.6	0.6
g$_{0,helium}$	0.7	0.7
Dumping Ratio	24%	24%

Table 4.2: Summary of the key experimental and numerical parameters for the Yb:KYW thin disk oscillator with cavity-dumping. The two different values for the small signal gain are the result of slightly different pump powers for air and Helium atmosphere.

value is taken as the sum of the design value of the negative dispersive mirrors that were used in the setup. Because of likely difference between design values and actual values an uncertainty of 5% is taken into consideration for this parameter. Radii for the laser beam in the different cavity elements are taken from a simulation done with a commercially available software[1] used to design the cavity prior to the experiment. Cavity losses are estimated using the known reflectivity of the cavity mirrors, the non-saturable losses of the cavity and some additional losses originating from the remaining cavity elements.

The SESAM parameters are taken from the specifications given by the manufacturer. The uncertainties for the modulation depth as well as the relaxation time are not readily known. Lastly the small-signal gain has been approximately calculated using the absorbed pump power [Pal09].

In terms of the numerical simulation, the experimental values given on the left hand side of the table were used as a starting point. w_{BBO}, w_{gain} and w_{abs} are the beam radii in the BBO-Pockels cell, the thin disk and the SESAM respectively. w_{gas} is the average beam radius in the residual gas of the cavity. Given the uncertainties, the parameters were then carefully varied to achieve a fit between experiment and simulation. As it turned out the most critical parameters in terms of pulse energy and mode-locking stability were the radius on the disk and the SESAM parameters. The best possible fit between model and
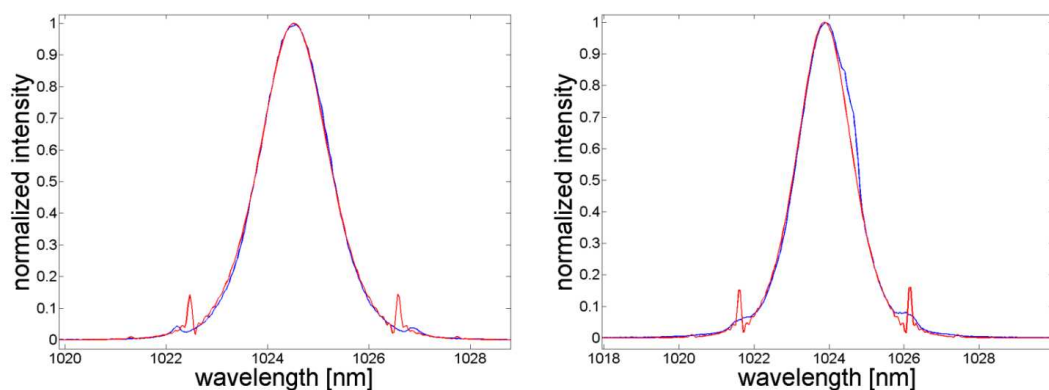
---

1 WinLase2

Figure 4.3: Comparison of the experimental (blue) and simulated (red) pulse spectra obtained for the Yb:KYW thin disk oscillator. The left hand side of the figure shows the pulse spectra for the laser operating in residual air while the right hand side shows the results for operation under a helium atmosphere.

experiment was achieved with the parameters on the right hand side of the table, after making small adjustments to the beam radius inside the EOM and the relaxation time of the SESAM. However as can be seen from the table, the parameters of the simulation and those of the experiment are in very good agreement. Except for the modulation depth where the uncertainty of the experimental value is not known, all other parameters are well inside the range of the uncertainties.

The results of the numerical simulation are shown in Fig. 4.3 and in Table 4.3. In terms of the pulse spectra the agreement between experiment and simulation is excellent both for the laser operating in air and in helium. The only notable deviation is for the Kelly-sidebands, while their position (which in this case is mainly determined by the dumping frequency) fits very well there is some discrepancy concerning their heights as

Parameter	Experimental value	Numerical value
Pulse energy (air)	2.3 μJ	2.3 μJ
Fourier limit (air)	698 fs	686 fs
Pulse duration (air)	700 fs	688 fs
Pulse energy (helium)	3.21 μJ	3.08 μJ
Fourier limit (helium)	630 fs	662 fs
Pulse duration (helium)	680 fs	692 fs

Table 4.3: Comparison between the experimental and numerical results for the Yb:KYW thin disk oscillator.

they are more pronounced in the simulated spectra. However since the Kelly-sidebands are extremely narrow this is the result of the limited spectral resolution of the spectrometer used in the experiment.

With respect to the pulse energy and duration there is also very good agreement in case the laser is operated in residual air. For the helium atmosphere there are some minor discrepancies between the numbers, but the agreement is still good and well within experimental uncertainties, especially in the case of the pulse duration.

Simulation of the Yb:KYW bulk oscillator

After the numerical model was successfully used to reproduce the results obtained experimentally with Yb:KYW thin disk oscillator the next step was to apply the model to the Yb:KYW bulk oscillator with cavity-dumping presented in [Kil05a]. As in the case of the thin disk oscillator the experimental parameters were used as starting point for the numerical model and slight adjustments within the limits of the experimental uncertainties were then made to achieve an optimal fit between experiment and simulation.

Table 4.4 shows a summary of key parameters and results achieved with the numerical model and using the experimental setup. Again the numerical model accurately reproduces the results obtained with the actual laser system which can also be seen when comparing the laser spectra in Fig. 4.4.
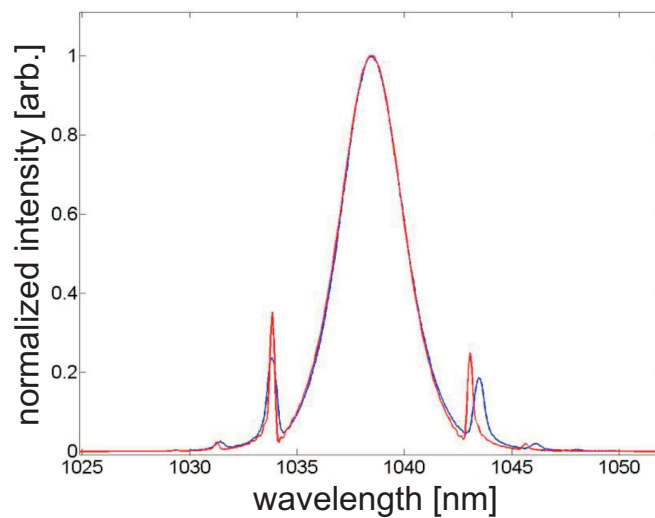
Figure 4.4: Comparison of the experimental (blue) and simulated (red) pulse spectra obtained for the Yb:KYW bulk laser with cavity-dumping.

Parameter	Experimental value	Numerical value
f_{rep}	17 MHz	17 MHz
β_2	-9200 fs^2 $\pm$ 460 fs^2	-9200 fs^2
w_{BBO}	650 μm $\pm$ 65 μm	650 μm
w_{gain}	120 μm $\pm$ 6 μm	110 μm
w_{abs}	375 μm $\pm$ 15 μm	370 μm
w_{gas}	700 μm $\pm$ 35 μm	700 μm
l	3% $\pm$ 0.5%	3%
τ_{abs}	5 ps	5 ps
ΔR	1.6%	1.6%
ϕ_{abs}	50 μJ/cm^2 $\pm$ 20 μJ/cm^2	50 μJ/cm^2
g_0	1.5	1.5
Dumping Ratio	53%	53%
Pulse energy	1.35 μJ	1.41 μJ
Pulse duration	390 fs	380 fs

Table 4.4: Comparison between experimental and numerical parameters and results for the Yb:KYW bulk oscillator with cavity-dumping. Further experimental parameters are taken from [Kil05a].

4.2.3 Numerical results

Instabilities

The accuracy the numerical model exhibited when used to model the two different laser systems discussed above gives a good indication that it is in fact well suited for the investigation of the pulse dynamics and limitations of cavity-dumping in thin disk oscillators. When simulating the Yb:KYW thin disk oscillator using the split-step method it turned out that like in the experiment, there is a limit to the dumping ratio that the system can sustain before becoming instable. In the simulations this ratio was found to be between 25% to 30% which is close to the 24% that were observed in the experiment.

Fig. 4.5 shows the results of both a stable simulation run and an instable one resulting in irregular Q-switched behavior of the laser oscillator. On the left hand side the dumping ratio is low enough for the laser to remain stable, while on the right hand side a higher dumping ratio leads to instabilities. As has been mentioned previously, in the experiment other types of instabilities will also occur for higher dumping ratios. Regarding this it needs to be noted that while the numerical model can accurately simulate stable laser operation and can also be used to determine the point at which instabilities tend to occur. However there will inevitably be differences between the simulations and the experiment when it comes to how the laser behaves after the onset of the instabilities. Looking at the
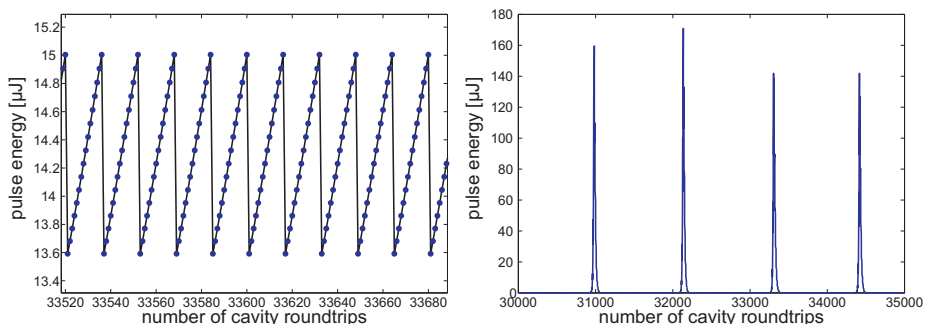
Figure 4.5: On the left hand side an example for stable cavity-dumping of the system is shown, while the right hand side depicts Q-switching instabilities resulting from excessive dumping ratios.

Q-switching instabilities shown in the right hand side of Fig. 4.5 one reason for this are the high pulse energies and peak intensities that can be generated during Q-switching. When these occur in the experiment they will often lead to damage to optical elements, especially the SESAM. Typically this will then lead to other instabilities like the formation of multiple pulses or cw-instabilities. This behavior can obviously not be reproduced easily by the split-step model. Another reason is that as a result of the equations forming the numerical model cw-instabilities can intrinsically not occur within the scope of this model.

Comparison between bulk and thin disk oscillator

Regardless the numerical model offers a good way to investigate the cause behind instabilities and the reasons for the limited dumping ratio. To this end it makes sense to first compare the parameters of the two different laser setups.

When looking at the parameters of the two setups, it turns out that the main difference between the two systems as far as the laser setup is concerned can be found in the mode diameter in the gain medium. While the focal radius inside the bulk crystal is relatively tight at 110-120 μm, the radius on the laser disk is more than four times that number. To investigate the impact the spot size has on the stability against cavity-dumping the numerical model was used to scan the mode radius on the gain medium over a wide range starting from 540 μm going down to 200 μm. The values of the remaining parameters are given in Table 4.2, all of which were kept constant during the simulation run. For each of the different mode radii the maximum dumping ratio was determined by subsequently scanning the dumping ratio to find out up until which ratio the laser remains in stable mode-locked operation. To do so each individual parameter set was run through a simulation lasting 400000 cavity roundtrips. For the first 10000 roundtrips the cavity was operated without cavity-dumping, only then the dumping was initiated. If the laser remained in stable mode-locked operation over the course of a complete simulation run, it is considered a stable system. On the other hand a laser which has not stabilized

after 400000 roundtrips or has shown periodic windows of instability typically does not become stable even for longer timescales making it possible to distinguish between stable and instable sets of parameters.

Fig. 4.6 shows the results of these simulations. The blue markers signify the maximum dumping ratio at which the laser remains stable for each of the different mode radii. As can be seen for high mode radii, there is a plateau of about 18% but as the mode size is decreased below 500 μm the maximum dumping level starts to rise linearly to values above 90% for mode radii below 200 μm.

Experimentally this means reducing the pump spot on the gain media along with the laser spot. However this cannot be readily achieved, because by simply reducing the mode area inside the gain medium at some point thermal damage would occur as a result of the increasing power density in the gain medium. In the case of the disk and the pump power used in the current Yb:KYW thin disk oscillator the maximum sustainable power density is given as 4 kW/cm^2 by the manufacturer which would allow for a minimum mode diameter of 350 μm. Consequently for smaller mode radii, the pump power would have to be reduced to avoid thermal damage.

When this is done in the simulation, it amounts to a transition from the high power thin disk regime with mode radii over 400 μm, down to the standard bulk oscillators with mode radii below 200 μm. At the lower end of the mode radii, the oscillator will then be able to sustain dumping ratios in excess of 50% however the achievable pulse energies will then also be reduced to a level of about one microjoule.

Qualitatively this can be understood by looking at the influence the mode area in the gain medium has on the small signal gain and the saturation energy of the system. Going back to Chapter 2, these parameters are defined by eqs. (2.3) and (2.4) which can be rewritten as:

$$g_0 = \frac{\sigma_L \tau_L R_P}{2 A_{eff}} = \frac{\sigma_L \tau_L R}{2 \pi w_{gain}^2} \tag{4.3}$$

$$E_{sat,L} = \frac{m \hbar \omega_L}{\sigma_L} A_{eff} = \frac{2 \pi m \hbar \omega_L}{\sigma_L} w_{gain}^2 \tag{4.4}$$

Following these definitions, the result of the increased mode area in the thin disk laser are a decrease in the small-signal gain and a rise in the saturation energy of the medium. The effect on the small-signal gain is somewhat reduced by the fact that thin disk setup allows for higher pump powers and consequently results in a higher pump rate. However since the effect of the pump rate is linear while the effect of the mode radius is quadratic the higher pumping rate cannot compensate the reduction of the small signal gain completely.

The importance of the reduced small-signal gain can be understood best by looking on the effect this has on the relaxation oscillations. By looking at eq. (2.8a) lower small-signal gain reduces the damping of the relaxation oscillations making the laser more susceptible
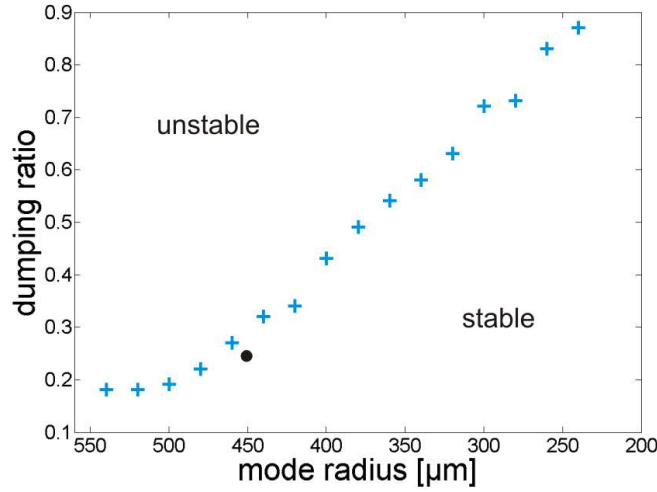
Figure 4.6: Simulated maximum dumping ratios for the Yb:KYW thin disk oscillator as a function of the mode radius on the laser disk. The black dot signifies the experimental parameters of the thin disk system.

to instabilities.

When it comes to the saturation energy its influence can be understood by going back to eq. (2.10), the stability criterion against Q-switching introduced in Section 2.1.2:

$$E_p^2 > E_{sat,L}E_{sat,A}\Delta R \tag{4.5}$$

As a result of the increased saturation energy in a thin disk oscillator, the threshold against Q-switching instabilities is higher. In a standard thin disk oscillator without cavity-dumping this is of little consequence because the intra-cavity pulse energy can easily be kept above this threshold because of the relatively low outcoupling percentages below 10%. With cavity-dumping however the pulse energy is drastically reduced every time the dumping is initiated. At that point the increased threshold in combination with the reduced damping of the relaxation oscillations will lead to q-switching instabilities for dumping ratios far lower than in the case of a bulk oscillator.

Influence of the SESAM parameters

Eq. (2.10) also points to two other factors that may be of interest in the investigation of the limitations of the cavity-dumping: The saturation energy of the absorber and its modulation depth. To find out how much influence these two parameters have on the maximum possible dumping ratio more simulation runs were made.
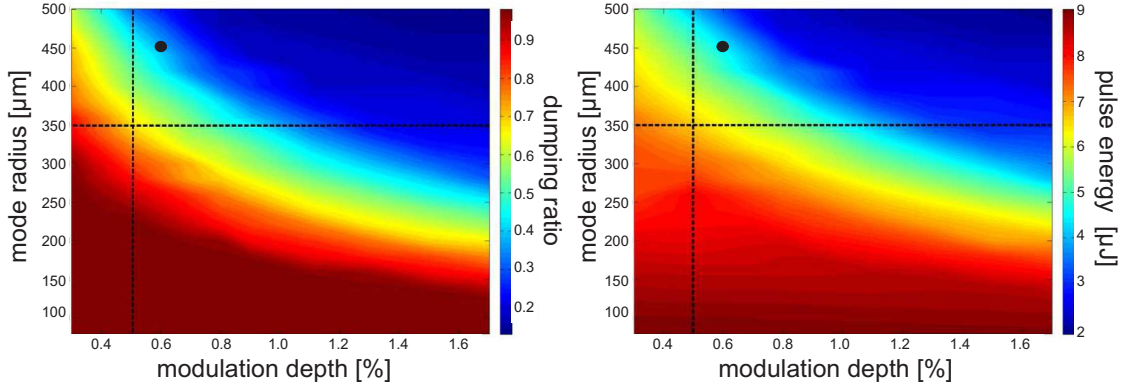
Figure 4.7: Left: Simulated maximum dumping ratio as a function of mode radius on the disk and modulation depth on the SESAM. The color bar indicates the maximum stable dumping ratio. Right: Resulting outcoupled pulse energies for the dumping ratios given on the left. Here the color bar gives the pulse energy in microjoule. The black dots mark the parameter region for the experimental setup.

The results of the first numerical investigation can be seen in Fig. 4.7. For this simulation run both the modulation depth of the SESAM and the mode radius on the laser disk were varied. The mode radius was scanned from 100 μm to 500 μm while the modulation depth was scanned from 0.3% up to 1.7%. The left hand side of the figure shows how the maximum stable dumping ratio changes in dependence on these two parameters while the right hand side shows what outcoupled pulse energies could be achieved with these dumping ratios. In each figure, the black spot signifies the parameter setting currently used in the oscillator.

As can be seen the modulation depth does in fact influence the achievable dumping ratio in a way that qualitatively agrees with eq. (2.10) in so far as an increase in modulation depth results in a decrease of the maximum dumping ratio. Furthermore the two dashed lines in the figures depict experimental limits: The vertical line results from the fact that experimentally no stable mode-locking could be achieved for SESAMs with modulation below 0.5% as the modulation depth was not strong enough to suppress cw-breakthroughs. The horizontal line is the already mentioned limit for the power density on the laser disk which is reached at a mode radius of 350 μm if the pump power is kept constant while decreasing the mode area. Taking these two things into account Fig. 4.7 does show how the available pulse energy could be increased through careful optimization of the laser system. The black spots mark the parameters of the current laser setup. By reducing the modulation depth and the mode area to the optimum it should be possible to move closer to the optimal operation point which would be at the crossing of the horizontal and vertical lines. As can be seen in the figure, this would make it possible to raise the dumping ratio closer to 40% and achieve pulse energies of 6 μJ.
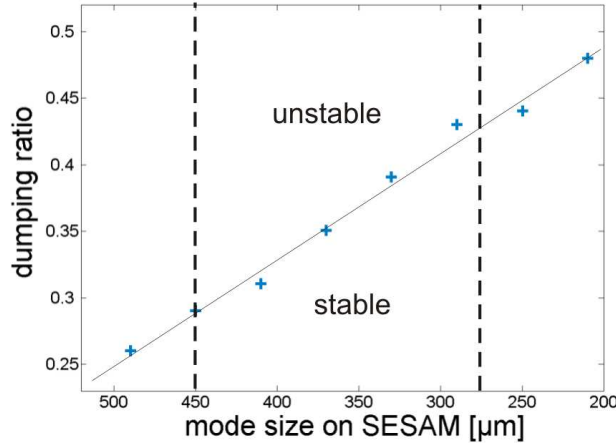
Figure 4.8: Maximum dumping ratio as a function of the mode radius on the SESAM. The two vertical lines depict experimental limitations. For mode radii above 450 μm no stable mode-locking was achieved while for mode radii below 270 μm the SESAM was destroyed.

The second SESAM parameter of importance is the saturation energy of the absorber. Using eq. (2.11) it becomes obvious that the saturation energy of the absorber is proportional to the mode radius on the absorber as well as its saturation fluence. The latter parameter however is a material parameter and closely linked to the modulation depth. Since we have already established that the modulation depth should be as small as possible, the mode radius on the absorber is left as the only accessible parameter. Consequently the influence of the mode radius on the SESAM was investigated by varying this parameter between 200 μm and 500 μm. As can be seen in Fig. 4.8 the stability against cavity-dumping in this case rises almost linearly with decreasing mode area which again agrees nicely with eq. (2.10). Also experimentally this parameter faces some rather tight limitations: For mode radii above 450 μm no stable mode-locking was possible because of cw-breakthroughs. On the other hand for mode radii below 270 μm the SESAM was destroyed by excessive laser intensities. These limitations make the mode radius on the SESAM a not so well suited parameter for the optimization of this particular laser system. This is further underscored by the fact that in general for all high power thin disk oscillators the SESAM has to be operated at energy fluences close to the damage threshold of the material leaving little room for optimization of the mode radius. Regardless of this the development of new SESAMs with higher damage thresholds may well make this a workable possibility for future system.

Influence of other parameters

In addition to the parameter scans described in the previous sections several other parameters were also varied widely in order to see what, if any, influence they have on the

dynamics of the laser system. Experimentally the second order dispersion was varied between -20000 fs^2 and -50000 fs^2, in the simulations it was changed over an even wider range from -10000 fs^2 to -150000 fs^2. In the numerical model various other parameters like the mode radius in the Pockels-cell as well as the cavity roundtrip were also changed. In the case of the latter the variation ranged from 50 ns to 80 ns. However neither of these variations had any discernible impact on the cavity-dumping.

Another obvious parameter that was changed is the dumping frequency. Both in the experiments and in the numerical model changing the dumping frequency between 350 kHz and 1.15 MHz, which is the highest frequency supported by the currently used EOM electronics, does not have any strong effect on the possible dumping ratios. For frequencies below 350 kHz the laser system becomes increasingly instable because the dumping frequency gets too close to the soliton frequency mentioned in 3.1.5, which can experimentally be estimated to be about 326 kHz [Pal09]. Lastly for frequencies around 10 kHz and below it becomes possible in the numerics to drastically increase the dumping ratio to values of 90% and above as the laser then operates in the relaxed dumping regime. However because of the extremely low repetition rate this regime is of little interest experimentally as has been noted before.

Conclusion

In conclusion the numerical model has successfully been used to investigate the limitations of cavity-dumping in thin disk laser oscillators. By scanning various parameters the cause of the limitations has been identified and possible options for the optimization of such laser systems have been developed which offer the potential to increase the pulse energy of future systems to 6 μJ or above [Sie07]. Regardless of this however the instabilities caused by the nonlinearities inside the resonator that were experienced during the development of this laser system have made it obvious that ultimately these nonlinearities will be the limiting factor on energy scaling in the soliton regime unless a way can be found to reduce them.

4.3 Numerical investigation of Ytterbium based chirped-pulse oscillators

As has already been discussed in Chapter 3, a possible way to reduce the nonlinearities in a high power femtosecond laser oscillator is to operate the laser with net-positive intra-cavity dispersion in the chirped pulse regime. With the growing interest in chirped pulse oscillators in recent years there have been a number of publications dealing with the modeling of Ti:sapphire based CPO systems [SC97, Kal05, Kal07, Kal08].

However as it turns out these publications and the dynamics and limitations predicted for the CPOs treated therein are very specific to the properties of Ti:sapphire systems and cannot be readily used to learn anything about the properties of CPOs based on other gain media. For instance, in the case of Ti:sapphire based CPOs it is found that

the higher order dispersion plays a crucial role in the pulse dynamics and are likely to ultimately be responsible for limitations to these systems. What this means for gain media like the Ytterbium tungstates, which have a much narrower bandwidth than Ti:sapphire and consequently are much less susceptible to higher order dispersion is a question that has not been looked into prior to the work done in this thesis. In the following sections the numerical model developed above is used to investigate the pulse dynamics for such systems, to compare the results to experiments and ultimately to make predictions for possible energy scaling of future systems.

4.3.1 Yb:KYW chirped-pulse oscillator with cavity-dumping

Laser setup
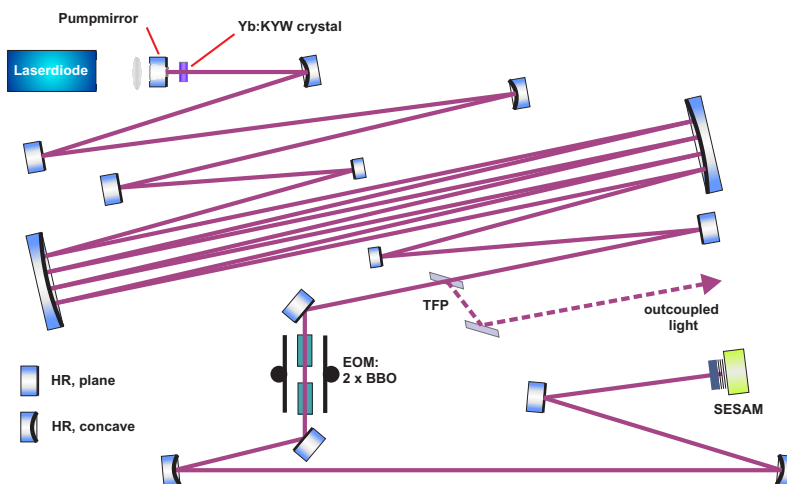
Figure 4.9: Schematic setup of the positive dispersive Yb:KYW oscillator with cavity-dumping [Pal09].

A combination of the concepts of cavity-dumping and chirped pulse operation has first been reported in 2006 by Zhou et al. for a Ti:sapphire laser with AOM cavity dumping [Zho06]. Another Ti:sapphire system will be discussed later in this thesis in Chapter 5. In contrast to these Ti:sapphire based systems Fig. 4.9 shows the setup of a Yb:KYW bulk laser with cavity dumping operating in the positive dispersive regime. This laser system has been developed as part of [Pal09] and has successfully been used to generate pulses of up to 2 μJ with pulse durations of 370 fs at a repetition rate of 1 MHz. Except for the fact that the laser operates in the positive dispersion regime, the experimental setup is very similar to the one used in [Kil05a] and [Emo06] for cavity-dumping of an Yb:KYW laser in the solitary regime. However by operating the laser in the positive dispersive regime it was possible to significantly increase the pulse energy.

As far as the experimental setup is concerned the main difference is that some of the

negative dispersive mirrors have been replaced in order to keep the intra-cavity dispersion positive rather than negative, another difference is the addition of a Herriott-cell in order to create a more compact setup. More about the experimental setup can be found in [Pal09].

Comparison between experimental results and numerical simulation

Having already successfully used the numerical split-step model to simulate pulse evolution in the solitary regime a logical starting point for the investigation of the positive dispersive regime was to go ahead and try to model the chirped pulse oscillator shown in Fig. 4.9. The procedures for the simulation were essentially the same as in the case of the thin-disk laser with cavity-dumping described in the previous section. Again the known experimental parameters were used as a starting point before fitting the numerical to the experimental results by varying the numerical parameters within the limits of the experimental uncertainties. It needs to be noted that experimentally the GDD of the laser cavity was varied in discrete steps, with stable mode-locked operation possible for GDD values from 250 fs^2 up to 2250 fs^2. The following comparison between experimental results and numerical simulations will treat an intermediate setup with an intra-cavity dispersion of 750 fs^2.

Parameter	Experimental value	Numerical value
f_{rep}	17 MHz	17 MHz
β_2	750 fs^2 $\pm$ 75 fs^2	800 fs^2
r_{BBO}	620 μm $\pm$ 62 μm	620 μm
r_{gain}	115 μm $\pm$ 12 μm	120 μm
r_{abs}	135 μm $\pm$ 14 μm	135 μm
r_{gas}	520 μm $\pm$ 52 μm	500 μm
l	3% $\pm$ 0.5%	2.5%
τ_{abs}	261 fs (fast) 4.3 ps (slow)	4 ps
ΔR	2-3%	2.5%
ϕ_{abs}	50 μJ/cm^2 $\pm$ 10 μJ/cm^2	40 μJ/cm^2
g_0	1.1	1.2
Dumping ratio	45%	45%

Table 4.5: Summary of the key experimental and numerical parameters for the Yb:KYW CPO with cavity-dumping

Table 4.5 shows both the experimental parameters as well as the parameters used in the numerical model. As can be seen the agreement between experiment and simulation is once again very good. The experimental parameters have been determined using ray-tracing software in the case of the radii, the design values of the chirped mirrors as

well as textbook values for the material dispersion of the cavity elements. The SESAM parameters were taken accordingly with information granted by the manufacturer except for the relaxation times which have been measured as part of a diploma thesis [Sch07]. The two relaxation times given in the table refer to the fact that the relaxation of the SESAM follows a double-exponential function describing the thermalization and recombination of the electrons in the absorber. For the numerical simulation only the longer time constant was used because for most SESAMs this still allows a good fit to the relaxation behavior.
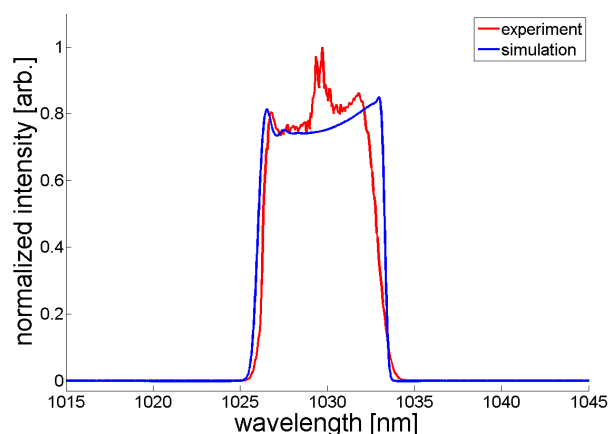
Figure 4.10: Comparison of the experimental and simulated pulse spectra obtained for the Yb:KYW CPO with cavity-dumping at an intra-cavity dispersion of 750 fs^2. For the numerical simulations a value of 800 fs^2 was used.

Fig. 4.10 shows both the experimental as well as the simulated spectrum. The slight tilt of the top of the spectrum is a direct result of the 3rd order dispersion the pulse picks up when propagating through the BBO in the Pockels-cell. The one feature not represented in the numerical simulation is the modulation in the middle of the spectrum. The most likely explanation for this feature in the experimental spectrum is that the laser was close to the onset of optical wave-breaking. Under these conditions other CPO systems have been known to exhibit similar spectral behavior [Kal05, Nau05, Kal07]. In the numerical simulation the laser was in fact exhibiting optical wave-breaking at a GDD value of 750 fs^2 and became instable. This is the reason why the numerical simulations were done for a GDD value of 800 fs^2 as indicated in table 4.5, which however is still well within the uncertainties of the experimental parameters.

Another interesting feature that is visible both in the simulated and the numerical spectrum is a slight modulation on the short wavelength side of the spectrum. The origin of this modulation is not completely understood but has also been described in other CPOs. By using the numerical model to investigate this feature it was found that it is sensitive to a variation of the SESAM parameters especially the relaxation time. One possible explanation is that it is a result of the chirped pulses interacting with the SESAM over a

time that is longer than the relaxation time of the SESAM.

There is also good agreement in terms of the pulse energy and pulse duration as outlined in Table 4.6. The agreement in terms of pulse energy and Fourier limit is excellent while the values for the chirped pulse duration differs by as much as 30%. However here it needs to be noted that the chirped pulse duration depends strongly on the relaxation time of the SESAM, the intra-cavity pulse energy and the GDD as outlined Sec. 3.2. This means that slight deviations in these parameters can result in additional deviations for the chirped pulse duration.

Fig. 4.11 shows the simulated and experimental spectrum for another configuration of the laser cavity with the intra-cavity GDD changed to 1250 fs^2. While there is still good agreement in terms of the spectral width, it is obvious that the numerical model cannot accurately reproduce the oscillations visible in the spectrum. It is notable that aside from the spectral width, the main difference in the experimental parameters of the laser is that the chirped pulse duration inside the laser cavity increases slightly due to the higher GDD. This does point to a possible explanation which may be found in the in the fact that the numerical model for the SESAM is somewhat simplified in contrast to the experimental reality. The most notable simplifications include the omission of two-photon absorption which occurs in the SESAM for high enough intensities and the fact that only one time constant is considered with respect to the relaxation time. Since this is only a minor detail in the scope of this thesis no further investigations into this topic were made. In the future, implementation of the second time constant as well as the two-photon absorption might allow to check this hypothesis.

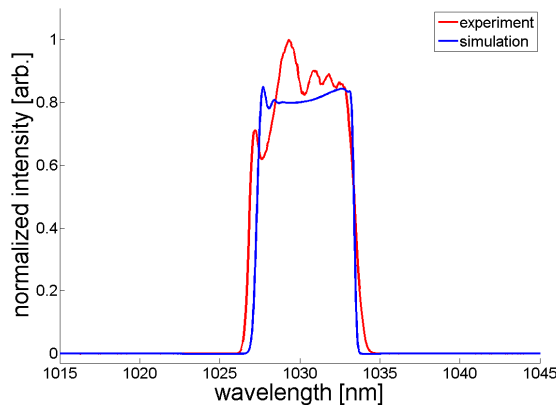As the oscillations significantly change the pulse spectra for higher values of intra-

Figure 4.11: Comparison of the experimental and simulated pulse spectra obtained for the Yb:KYW CPO with cavity-dumping at an intra-cavity dispersion of 1250 fs^2.

Parameter	Experimental value	Numerical value
Pulse energy	2.2 μJ	2.4 μJ
Fourier limit	400 fs	388 fs
Chirped pulse duration	5 ps	6.5 ps

Table 4.6: Comparison between the experimental and numerical results for the Yb:KYW CPO with cavity-dumping.

cavity GDD it may be interesting to study their origins in more detail in the future. One possible way of doing this might be to use the pump-probe setup developed in [Sch07] in order to measure the influence the chirped pulse durations has on the dynamics of the SESAM. However in order to achieve the required time resolution despite the picosecond pulse duration of the uncompressed CPO laser pulse it would be necessary to alter the setup. An elegant way of doing this would be to use a beam splitter prior to divide the CPO laser power in such a way that the main part remains chirped and can be used as pump beam while a small part is recompressed which could then act as the probe beam in the measurement setup. Alternatively it would also be possible to simply use a different femtosecond laser in the probe arm.

Besides the two sets of intra-cavity dispersion discussed so far a number of other setups were tested experimentally. As a result of these variations it was found that while the pulse energy and achievable dumping ratio all basically remained the same, the chirped pulse duration and the pulse spectrum changes significantly. Any increase in second order dispersion increases the chirped pulse duration while at the same time resulting in a narrowing of the laser spectrum and consequently a longer Fourier-limit [Pal09]. This behavior was readily reproduced in the numerical simulation as shown in Fig. 4.12. For this simulation all parameters except the intra-cavity dispersion were kept constant. As can be seen the spectral width decreases significantly as the GDD increases and the pulse chirp becomes stronger. For GDD values of lower than 750 fs^2 instabilities can occur as the result of optical wave-breaking which occurs when the pulse chirp is not sufficiently high to prevent excessive nonlinearities.

A possible qualitative explanation for the decreasing spectral width can be attempted by applying the SPM model of spectral shaping in the CPO regime to the results of the numerical simulation: As is known from Fourier-theory a high pulse chirp will change the temporal shape so that it becomes similar to its shape in the spectral domain. For a CPO this means that the laser pulse which initially can be seen as similar to a a Gaussian or sech-like shape becomes more rectangular with steeper edges. In terms of the SPM these steeper edges result in a behavior very similar to that of a chirped super-Gaussian pulse which has been described in Section 2.2.6. As can be seen there, in this case the spectral broadening becomes limited to creating a low intensity pedestal or stops completely. Because of the strong chirp the SESAM will then start to act as a frequency
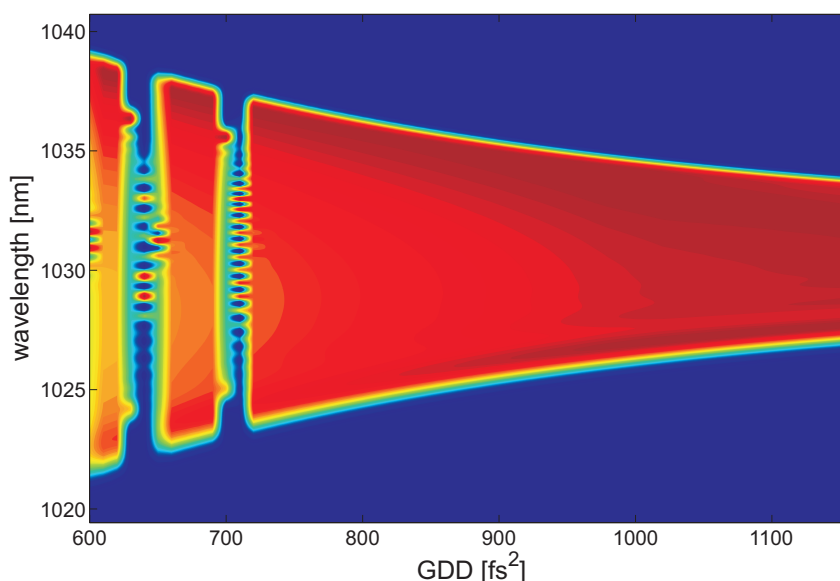
Figure 4.12: Evolution of the pulse spectrum in the Yb:KYW chirped-pulse oscillator for increasing GDD. The spectral bandwidth decreases significantly as the GDD is increased in the numerical simulations. The irregularities at certain low GDD values are instabilities resulting from optical wave-breaking.

filter and cut off the frequencies situated in the pedestal. As the pulse chirp increases further, more frequencies get cut off and the Fourier-limit increases.

4.3.2 Numerical investigation of power-scaling properties

As a result of the operation in the CPO regime, the limitations of the pulse energy resulting from the nonlinearities generated by the Yb:KYW bulk oscillator with cavity-dumping could successfully be eliminated. However the scaling properties of this system are currently limited because increasing pump powers lead to thermal lensing or even damage in the gain medium.

By using a thin disk instead of a bulk crystal these thermal issues could be resolved however as discussed above this would come at the expense of the dumping efficiency since a thin disk laser is not well suited for cavity dumping. Consequently the most promising system in terms of scaling properties may actually be a long-cavity thin disk CPO using a standard output-coupler rather than a cavity dumping scheme. In such a system the advantages of the thin disk setup could be combined with those of the CPO to solve the problem of nonlinearities which currently are the main limitation for standard high power thin disk oscillators operating in the solitary regime. However no such system has ever been investigated experimentally or theoretically prior to this thesis. In order to determine the actual energy scalability properties of such a system the split-step model

Parameter	Numerical value
f_{rep}	10 MHz
w_{gain}	620 μm
w_{abs}	380 μm
w_{gas}	690 μm
l	2%
τ_{abs}	1.4 ps
ΔR	2.5%
ϕ_{abs}	90 μJ/cm^2
$Outcoupling$	5%

Table 4.7: Parameters used for the simulation of a high power Yb:KLuW CPO.

was used to investigate such a system numerically. Parallel to this, a relatively low-energy version of a Yb:KLuW thin disk CPO was developed as a proof-of-principle model for this kind of oscillator [Pal08, Pal09].

The numerical parameters used for the simulation were based in part on the experimental parameters of this setup however a repetition rate of 10 MHz was assumed in order to implement a long-cavity design for energy-scaling purposes. The parameters used in the model are shown in Table 4.7. The outcoupling percentage was set to 10% which is similar to what has been reported in other high power mode-locked thin disk lasers [Mar06].

In order to investigate the scaling properties of this system, both the GDD and the pulse energy were varied over a wide range. As a first step the principal properties of such a laser system were tested for outcoupled pulse energies below 5 μJ. The results of this are shown in Fig. 4.13. The left hand side of the figure shows how the spectral shape of the laser pulses evolves for an outcoupled pulse energy of 2.1 μJ when the GDD is scanned from 855 fs^2 (which was the lowest numerical value at which stable mode-locking was achieved) up to 2000 fs^2 while all other parameters are kept constant. As is typical for chirped pulse oscillators and has already been discussed in Chapter 3.2 the broadest spectra are almost M-shaped and can be achieved for the lowest stable dispersion values.

When the GDD is increased the spectrum becomes narrower and changes into an almost rectangular shape before becoming almost parabolic at even higher levels. On the right hand side shows how the spectral shape behaves for three different dispersion levels (1050, 1620 and 2000 fs^2) and different pulse energies (0.5, 2.1 and 3.6 μJ). In principle the same spectral evolution as in the left figure can be seen, however it becomes obvious that the spectral shape and width are not only dependent on the GDD but also on the pulse energy. While a GDD of 1050 fs^2 is optimal at a pulse energy of 3.6 μJ the same GDD at lower pulse energies will result in much narrower spectra. On the other hand for a pulse energy of 2.1 μJ a dispersion of 855 fs^2 is sufficient to achieve the broadest spectra as seen on the
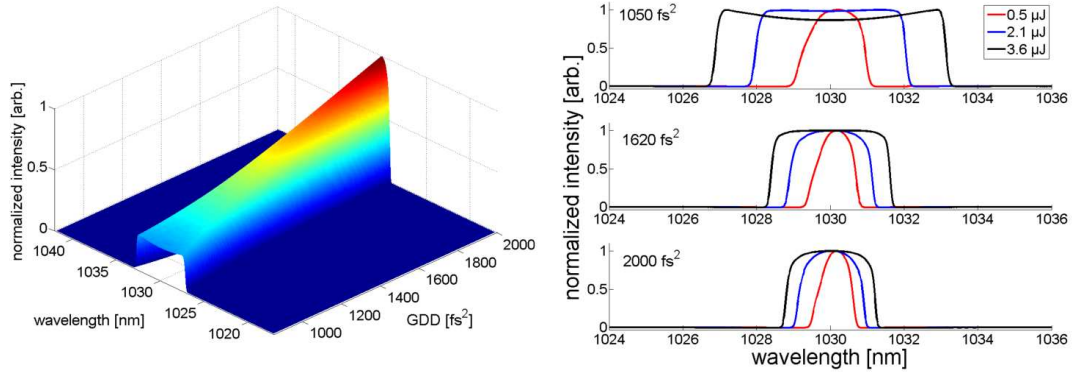
Figure 4.13: Evolution of the pulse spectra for different values of GDD and pulse energy. On the left hand side the evolution of the pulse spectrum for different values of intra-cavity GDD is shown. The right hand side shows the influence the pulse energy has on the spectral shape of the laser pulses.

left. Yet for a pulse energy of 3.6 μJ an intra-cavity GDD of 855 fs^2 is not enough and will result in multiple pulses and other instabilities. Higher levels of GDD do also allow stable mode-locking, but will result in much narrower spectra.

Qualitatively this can be understood by looking at the discussion about pulse shaping in CPOs in Section 3.2. The rectangular shape of the spectra is a result of the SPM and the resulting nonlinear phase-shift generated when a chirped pulse propagates through a nonlinear medium. Consequently, the broadest spectra are generated when the ratio between intra-cavity pulse energy and chirp factor is such that the nonlinear phase-shift is reduced just enough to avoid optical wave-breaking, but still allows for the generation of broad spectra.

This behavior is very similar to that reported in experiments done with the Yb:KYW bulk CPO with cavity dumping [Pal07b] and in general also to that predicted for Ti:sapphire chirped pulse oscillators. [Kal05]. As mentioned above, in Ti:sapphire oscillators theoretical predictions state that the energy scaling is rather limited because 3rd and 4th order dispersion will eventually destabilize the mode-locking. By varying the values of the higher order dispersion over a wide range, the split-step model allows to check whether these limitations also exist for Yb-based gain media. Most likely as a result of the comparatively narrow emission bandwidth it was found that even for values of 10000 fs^3 for the TOD and several 100000 fs^4 for the 4th order dispersion no destabilizing influence of the higher order dispersion was found in the case of Yb:KLuW. This is further supported by the fact that similar behavior has been reported for fiber lasers operating in the positive dispersive regime [Rue07].
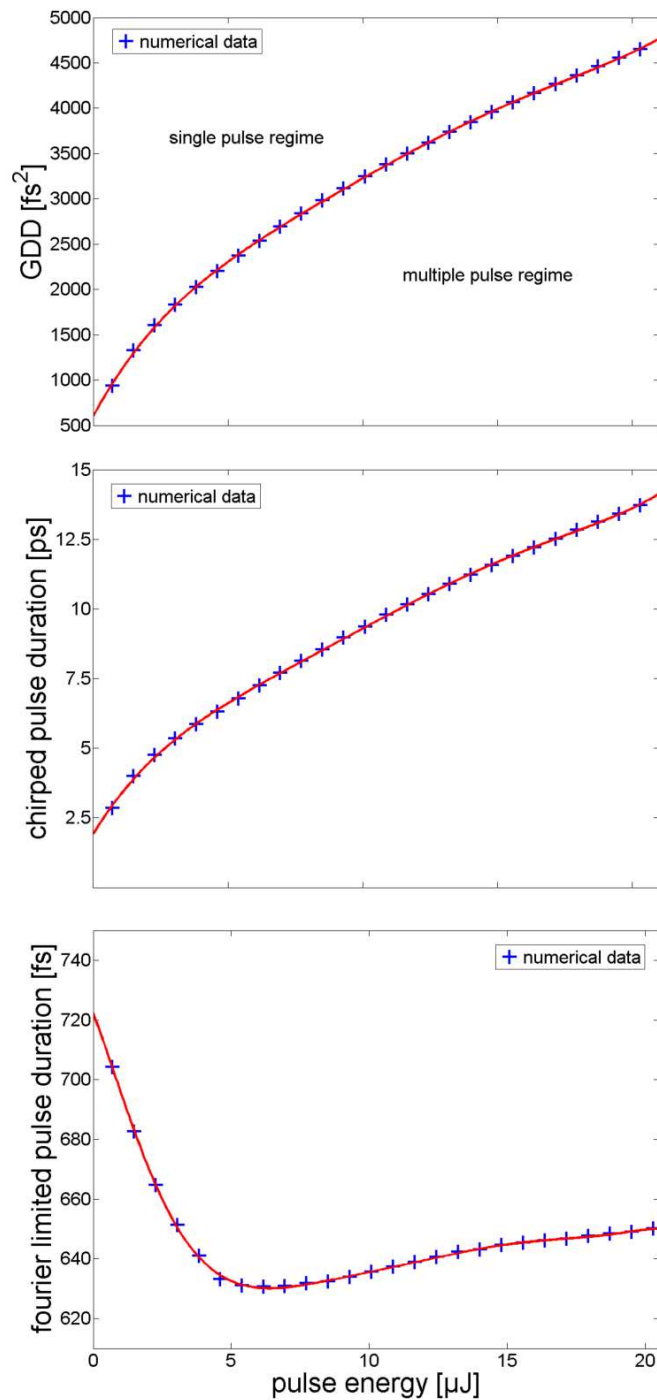
Figure 4.14: Energy dependence of the required GDD (top), the chirped pulse duration (middle) and the Fourier-limit (bottom) in the numerical investigation of the long-cavity Yb:KLuW system. The energies given are the pulse energies coupled out of the oscillator.

The next step in the investigation was to test the properties of these laser systems for higher outcoupled pulse energies and to test how well they are suited for further energy scaling. To this end the pulse energy was scaled to a level exceeding 10 μJ while also increasing the GDD to achieve stable single pulse operation.

Fig. 4.14 shows the results of this numerical investigation up to pulse energies of 20 μJ. The topmost figure shows the GDD required to avoid the buildup of excessive nonlinearities. Above pulse energies of 6 μJ the required increase is almost linearly from several hundred fs^2 to nearly 5000 fs^2 for 20μJ pulses. This figure already shows that the required values of GDD are far higher than those for Ti:sapphire, this again being a result of the more limited spectral bandwidth of the gain material. The plot in the middle of the figure shows the chirped pulse durations resulting from the increase in positive intra-cavity GDD. Not surprisingly, the chirped pulse duration closely follows the intra-cavity GDD starting from below 5 ps for pulse energies below 6 μJ and rising almost linearly for pulse energies above. Following this model a 20 μJ requires a chirped pulse duration of about 14 ps for stable operation. The most interesting aspect of the investigation is shown in the lowest part of the figure. Here the evolution of the Fourier-limit is shown with respect to the pulse energy, interestingly the behavior is much more complex than for the previous two parameters. For pulse energies from 0.5 μJ to about 6 μJ the Fourier-limit actually decreases from above 700 fs to a minimum of about 630 fs despite the increasing pulse chirp. When the pulse energy is further increased, the Fourier-limit rises slowly and almost linearly until it reaches a level of about 650 fs for the 20 μJ pulses. Quantitatively this can be explained in a similar fashion as the spectral narrowing experienced in the Yb:KYW bulk CPO with cavity-dumping. For pulse energies below 6 μJ, the increase in pulse energy results is strong enough that it will result in an increased generation of new frequencies via SPM. However for higher energies the pulse chirp increases until once again the SESAM starts to act as a frequency filter resulting in spectral narrowing [Sie08].

Conclusion and outlook

In the numerical model no principal theoretical limit to the energy scalability could be found so far. While the results presented here are presented only up to 20μJ in the simulations it was actually possible to scale the energy to much higher values. This work clearly shows that Yb-based thin disk oscillators operating have much potential for energy scaling. Besides the promising results in terms of the pulse energy, the numerical investigation also shows that Yb-KYW chirped pulse oscillators should be able to deliver pulse durations below 700 fs even at very high pulse energies. This presents a significant improvement over current active multi-pass systems which are capable of providing similar pulse energies however at pulse durations of nearly 1 ps.

However while the first proof-of-principle experiments with a thin disk CPO based on Yb:KLuW have shown promising results, there remain a number of experimental challenges that have to be dealt with when it comes to scaling the pulse energy to levels observed in the numerical simulations: The high pulse energies and average powers will

put high demands on the optic elements involved especially the thin disk and the SESAM. Here relatively large spot sizes may be necessary to avoid thermal damage which requires a very good surface quality. Experimentally so far the availability of suitable high quality SESAMs has been the greatest hindrance for further energy scaling. While the principal techniques do exist, only few SESAMs are available commercially. Another issue is the relatively high amount of positive intra-cavity GDD required which makes it necessary to actively add dispersion to the cavity. The best way to do this would be the use of positively chirped mirrors which could easily add the required amounts of GDD without adding high levels of additional nonlinearities and which could be produced with the same techniques as current negative dispersive mirrors.

Finally a very intriguing possibility would be the combination of the CPO concept with that of the active multi-pass cell. The high gain of the AMC combined with the reduced nonlinearities of the CPO regime should in principle make it possible to greatly increase the pulse energies available from femtosecond oscillators. Several other drawbacks of the AMC concept might be solved by operation in the positive dispersive regime: On the one hand, instead of having to insert more than -170000 fs^2 for solitary operation the laser could be operated at positive GDD values of only about 5000 fs^2. On the other hand Fig. 4.14 clearly suggests that the Fourier-limit of the laser pulses should be greatly reduced compared to the current value of more than 900 fs.

5 Experimental realization of a Ti:sapphire oscillator with microjoule pulse energy

While the previous chapter has shown the potential for scaling the pulse energy with Yb-based laser systems, these system do have limitations in terms of the achievable pulse durations due to their narrower emission bandwidth. Since shorter pulse durations not only offer the possibility of a better time resolution in pump-probe experiments, but also make it possible to achieve high peak intensities at lower average powers there is much interest in the development of high energy Ti:sapphire oscillators capable of delivering sub-100 fs pulses with energies on the microjoule level. The combination of high pulse energies, ultrashort pulses and MHz-repetition rate make such a laser system especially interesting for experiments in atomic physics such as the generation of high harmonic radiation with MHz repetition rates.

In recent years the pulse energy of standard Ti:sapphire oscillators was significantly increased by employing a Herriott-cell in order to extend the cavity and operating the laser in the positive dispersion regime. This way pulse energies of 500 nJ could be reached at repetition rates of up to 6 MHz [Nau05, Dew06b]. Similar results could also be achieved with a different setup utilizing an AOM for cavity-dumping [Zho06]. However only repetition rates of 800 kHz could be realized in that experiment. Nevertheless since the available pump powers for Ti:sapphire lasers are currently limited to 20 W the cavity-dumping setup is of special interest for further energy scaling as it requires significantly lower pump power compared to the other systems because of the higher outcoupling ratios. However the system presented by Zhou et al. was limited to using 8 W of pump power as higher pump powers resulted in instabilities in the laser operation. The cause for these instabilities are not known exactly. However the authors speculate that the high intra-cavity pulse energies can result in saturation of gain modulation used in the Kerr-lens mode-locking which can then lead to the observed instabilities

In order to investigate the further energy scalability of Ti:sapphire lasers a goal of this thesis was the demonstration of a high energy Ti:sapphire CPO with cavity-dumping. The first section of the following chapter presents the experimental setup of this laser oscillator. Using this system it was possible to generate the highest pulse energies so far achieved with a Ti:sapphire oscillator at 1.1 μJ which will be presented in the second section. The following sections then deal with investigations concerning the cavity-dumping process in an oscillator which relies on both SESAM and Kerr-lens mode-locking for stable pulsed operation. In contrast to the Yb-based laser systems discussed in the previous

chapter numerical simulations for a Kerr-lens mode-locked system are generally not very reliable because the parameters of the Kerr-lens process cannot readily be measured experimentally which makes accurate predictions extremely difficult. Consequently the work presented in this chapter is based only on experimental results.

Lastly the possibility of using a cryogenic post-amplifier for further energy scaling will be discussed and first experimental results are shown.

5.1 Laser setup

Fig. 5.1 shows a schematic drawing of the laser setup. A commercially available Nd:YVO$_4$ laser[1] with a power of 18 W at a wavelength of 532 nm was used as pump source. Using a lens with a focal length of 80 mm the pump light is focused into the gain crystal through one of the folding mirrors. The crystal itself is a Brewster cut Ti:sapphire crystal which is 4 mm long, 5 mm wide and has a height of 1.5 mm. The doping concentration was chosen such that a pump absorption of 80% is achieved over the crystal length of 4 mm. The crystal is then placed in a cooled copper holder for efficient heat removal. The folding mirrors (M_1, M_2) around the crystal each have a radius of curvature (ROC) of 100 mm and are used under an angle of 7° to compensate for astigmatism. The distances from the crystal were experimentally optimized for stable soft aperture Kerr-lens mode-locking. In the upper arm of the laser oscillator three plane mirrors (M_3, M_4, M_5) are used to reflect the laser beam into a Herriott-cell consisting of two concave mirrors (M_6, M_7) each with a ROC of 5000 mm. In the Herriott configuration the mirrors have a separation of 380 mm with 4 reflections on each mirror. Another plane mirror (M_8) is used to couple the laser beam out of the Herriott-cell and reflect it onto another concave mirror (M_9) with a ROC of 750 mm. With the help of this mirror, the laser spot is focused on the SESAM which is used as an end mirror in order to start and assist the mode-locking process in the laser. According to the design parameters, the SESAM has a modulation depth of 2%, a saturation fluence of 20 μJ/cm^2 and a relaxation time of about 10 ps. Also included in the upper arm is an iris diaphragm between M_3 and M_4 which is used to further stabilize the mode-locking by providing hard aperture KLM.

The lower laser arm consists of a pair of focusing mirrors (M_{10}, M_{11}) with an ROC of 100 mm each placed around the fused silica Brag-cell used for cavity-dumping. This results in a tight focus of about 55 μm inside the the AOM which is required for efficient cavity-dumping. From the second mirror, the beam is then reflected onto a partially reflective end mirror which is used to couple out 1% of the intra-cavity laser power. This output-coupler is required in order to create a sufficiently large signal to trigger the AOM as well as to monitor the intra-cavity dynamics.

In order to achieve the maximum dumping depth, the AOM is operated in a double pass configuration and the diffracted laser beam is reflected out of the cavity by means
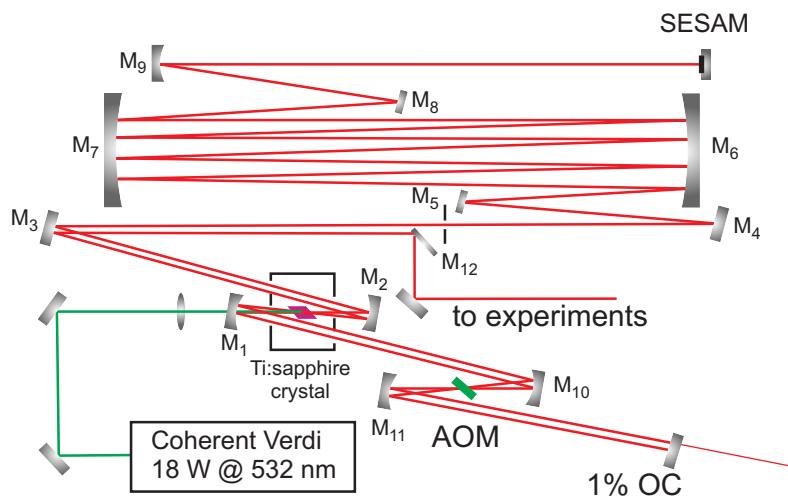
---

1   Coherent Inc. Verdi V-18

Figure 5.1: Comparison of the experimental and simulated pulse spectra obtained for the Yb:KYW CPO with cavity-dumping.

of a plane mirror (M_{12}) in the upper arm of the laser oscillator.

While the mirrors M_1, M_2, M_5 and M_8 double chirped mirrors used to control the intra-cavity dispersion. An optimum value for this parameter was found experimentally by operating the laser with different combinations of double chirped mirrors. This allowed to find the intra-cavity dispersion allowing for the broadest pulse spectra. As a result of this optimization, the total resonator dispersion adds up to 650 fs^2. This value is several times higher than in previous Ti:sapphire based CPO systems. The reason for this is that without the added positive dispersion the increased intra-cavity pulse energies along with the tight focus inside the Bragg-cell would result in higher nonlinearities which would result in optical wave-breaking. By adding more GDD the peak intensities inside the cavity are further decreased so that the build-up of excessive nonlinearities is avoided.

Acousto-optical modulator (AOM)

The AOM used for the cavity-dumping is part of a commercially available cavity-dumping kit[1]. The kit consists of the fused-silica Bragg-cell (6 mm wide, 2.5 mm thick and 5 mm high) and driver electronics which provide up to 16.5 W of rf-power to operate the AOM.

The driver electronics are customized to allow for seed frequencies as low as 25.6 MHz in order to achieve higher intra-cavity pulse energies. To this end the laser cavity was designed to have a length of 5.86 m leading to achieve a matching repetition rate which

---

1   APE GmbH

can be used to trigger the AOM driver. To this end the repetition rate is measured with a photodiode. However because the resulting voltage signal is not sufficiently strong to trigger the AOM directly, it is then fed into a pulse generator[1] where it is used to generate a synchronized pulsed signal which then triggers the AOM electronics.

The dumping frequency is set by choosing a suitable divider ratio, possible dumping frequencies range from the seed frequency f_{seed} down to $f_{seed}/5000$ which for this laser oscillator comes down to a frequency range from 12.8 MHz down to 5.12 kHz. In the current laser setup the divider ratio is set to 1:25 resulting in a dumping frequency of 1.024 MHz. This is the highest repetition rate for which the full rf-power can be used in the dumping process. For higher dumping frequencies the power is automatically reduced in order to prevent damages to the Bragg-cell.

Crystal cooling

As has been established in previous work [Sie05, Dew06b] at pump power levels of 15 W and above effective cooling of the Ti:sapphire crystal becomes necessary to prevent the formation of a thermal lens. Because of this, special care was taken when designing the laser in order to achieve efficient heat removal. As a first measure the crystal dimensions were chosen such that the crystal offers a large surface area to allow good thermal flow between the crystal and the holder. Furthermore the height of the crystal was limited to 1.5 mm in order to allow good heat flow from the laser focus to the sides of the crystal. The next step was the design of a copper crystal holder, shown in Fig. 5.2, into which the crystal was placed. Here Indium foil to ensure good thermal contact between crystal and holder. Active cooling is achieved by means of a Peltier-element placed below the crystal. The Peltier element was chosen such that it allows to generate a maximum temperature difference of 68 K between the hot and the cold side. Heat removal from the hot side of the Peltier-element is provided by means of a copper heat sink flooded with cooled silica oil from a circulation chiller. To prevent water condensation on the Ti:sapphire crystal the holder is placed under a box made from acrylic glass flooded with dehumidified air.

Using this setup it was possible to minimize the thermal effects of the high pump power and to achieve stable laser operation at a temperature of about 5°C. At this temperature a slight thermal lens remains visible. However the laser operation is not affected by this. Compared to previous systems which required a temperature of -45°C for stable operation [Dew06a] this shows that the heat flow away from the laser focus has been greatly improved by the measures described above.

Theoretically temperatures as low as -60°C can be reached at the base of the crystal with the current cooling setup, which would further increase the gain of the laser system as well as completely remove any thermal lensing as explained in Section 2.3.1. However as the dehumidifier delivering the dried air is used for several experiments, it is currently

---

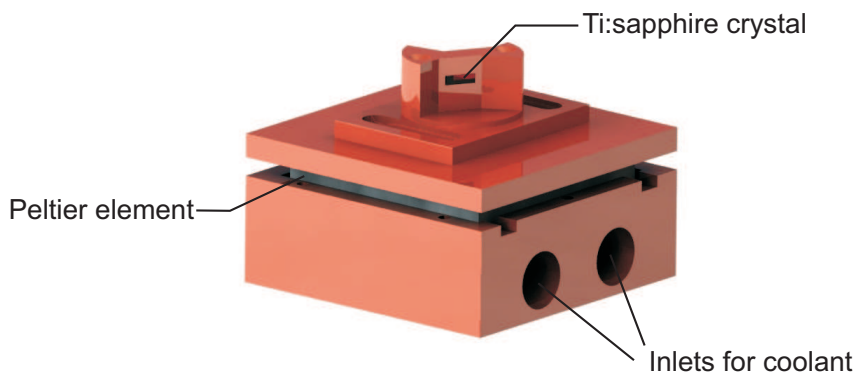1   Agilent GmbH 81110A 165/330-MHz-Impuls-/Bitmustergenerator

Figure 5.2: Crystal holder used in the Ti:sapphire CPO system

operating at near capacity which reduces the effectiveness. Consequently the dehumidified air currently cannot consistently prevent water condensation for temperatures below 5 °C. By using a dehumidifier dedicated to the Ti:sapphire CPO it is expected that the temperatures can be reduced to below -50°C in the near future.

5.2 Experimental results

In the experimental setup a SESAM is used to assist the mode-locking process. By doing so it was possible to overcome any instabilities from a possible saturation of the Kerr-lens in the gain medium. Adding the iris diaphragm into the upper laser arm helped to further stabilize the mode-locking and thus increase the pulse energy. With the pump power set to 18 W a maximum intra-cavity pulse energy of about 2.4 μJ was reached. Setting the AOM driver to maximum rf-power and the divider ratio to 1:25, a dumping depth of about 45% was realized. This leads to an outcoupled average power of 1.1 W which at a repetition rate of 1 MHz results in a pulse energy of 1.1 μJ. Currently the available pulse energy from this laser system is limited only by the available pump power as well as the maximum dumping ratio achievable with the AOM.

This marks the first time, that pulse energies in excess of 1 μJ have been generated directly from a Ti:sapphire oscillator [Sie09]. It needs to be noted that in this setup the laser actually required the cavity-dumping to operate in stable single pulse operation. Without the cavity-dumping either the pump power had to be reduced or an output-coupler with increased transmission has to be used in order to prevent multiple pulsing resulting from excessive nonlinearities. However as the cavity-dumping reduces the intra-cavity energies it allows for the laser to reach stable mode-locked operation.
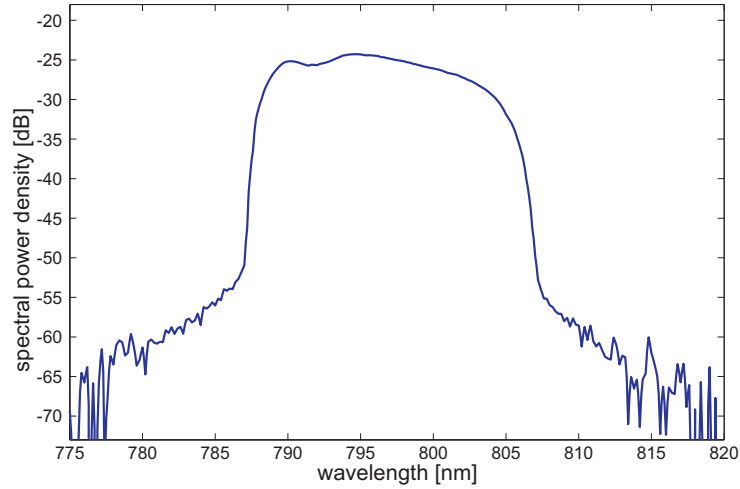
Figure 5.3: Spectrum of the 1 μJ Ti:sapphire oscillator

Fig. 5.3 shows the corresponding spectrum which exhibits a nearly rectangular form characteristic of chirped-pulse oscillators already described in section 3.2.3. The Fourier-limit associated with this spectrum was found to be 74 fs. Like in the case of the Yb:KYW chirped pulse oscillator discussed in Section 4.3.1 there is also a slight oscillation on top of the spectrum. As has been discussed there, a possible cause of this can be found in the dynamics of the SESAM.

When comparing the Fourier-limit to that of other Ti:sapphire based CPOs [Nau05, Dew06b], which achieved pulse durations of about 50 fs, it is obviously somewhat larger. The explanation for this can be found in the relatively high positive dispersion value of 650 fs^2 required to offset the additional intra-cavity nonlinearities induced by the higher pulse energy and the tight focus in the AOM. This behavior is similar to that experienced for the Yb:KYW CPO and agrees very well with the predictions for high power CPOs such as those made in Section 4.3.2 or in [Kal08].

Fig.5.4 shows the evolution of the intra-cavity pulse energy during the cavity-dumping process as measured by a photodiode. The laser exhibits the typical saw-toothed structure of any cavity-dumped system.

The pulse dynamics resulting from the cavity-dumping can also be seen when looking at the rf-spectrum of the leakage behind the outcoupler which is shown in Fig. 5.5. Because of technical restrictions of the rf-spectrometer in question, the measurement was done at the second harmonic of the repetition rate (51.2 MHz). Centered symmetrically around the 2nd harmonic a number of sidebands show up as a result of the cavity dumping and consequently they have a spacing of 1.024 MHz.
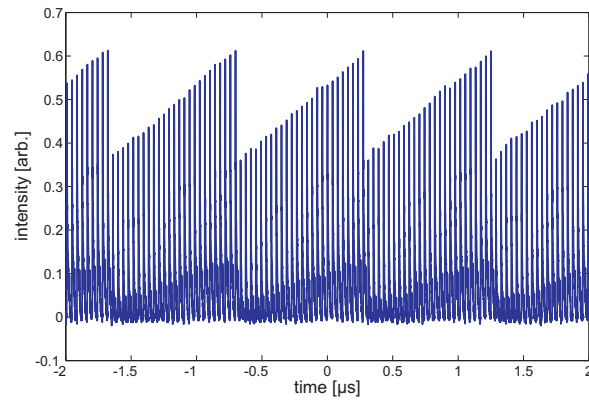
Figure 5.4: Evolution of the intra-cavity pulse energy during cavity-dumping.
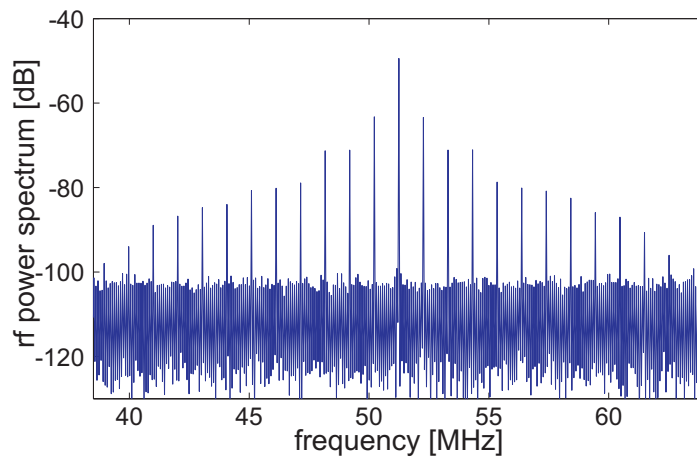
Figure 5.5: RF-spectrum of the intra-cavity laser pulses taken at the 2nd harmonic of the repetition rate. Around the central peak stemming from the repetition rate, a number of needles can be seen each with a spacing of 1 MHz. These are the result of the cavity-dumping shown in Fig. 5.4

5.3 Experimental study of cavity-dumping

In the context of this thesis, the main task with regards to the Ti:sapphire oscillator was to show a way of increasing the pulse energies available from Ti:sapphire, which has already been described above. However the laser oscillator can now be used to gain a better understanding of cavity-dumping in chirped pulse oscillators. The high gain of the Ti:sapphire crystals allows to use output-couplers with up to 10% transmission while at the same time operating the AOM for cavity-dumping. This makes it much easier to study the effects of cavity-dumping on the intra-cavity dynamics than in Yb-based systems such as the ones discussed in Chapter 4. In these systems only the leakage behind high reflective mirrors can be used for such studies because of the relatively small gain provided by the laser crystal.

Keeping this in mind, but also in order to allow stable laser operation even without cavity-dumping, the measurements performed in the following section were done using output-couplers with a 5% transmission rate.

5.3.1 Frequency dependence

Using the divider settings of the AOM controller, it is very easy to change the dumping frequency over a relatively wide range. This makes it possible to test the stability of the dumping process in chirped pulse oscillators and to compare the findings to those already established for laser operation in the negative dispersive regime. Since the laser pulses in CPOs are no soliton-like pulses, it can be expected that the dynamic of the system should be somewhat easier with no influence from specific soliton dynamics. Ideally one would only expect regions of instability when the dumping frequency couples to the eigenfrequency of the relaxation oscillations of the laser system.
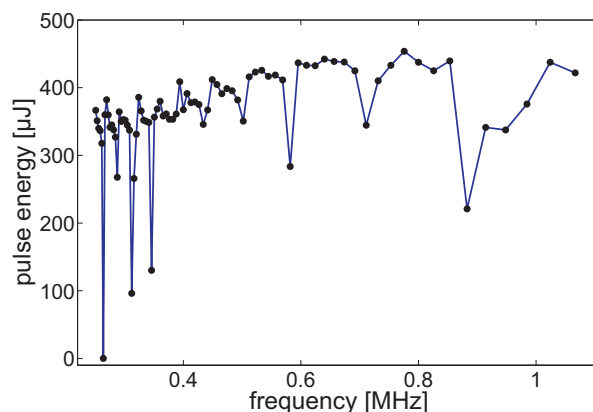
Figure 5.6: Maximum of the outcoupled pulse energy plotted for different dumping frequencies.

Fig. 5.6 shows how the maximum cavity-dumped pulse energy changes when the dumping frequency is varied between 250 kHz and 1.07 MHz. For lower frequencies, the laser entered the relaxed regime and the maximum pulse energy is limited mainly by the available rf-power used to operate the AOM. The frequency scan was done by increasing the divider ratio step by step and then finding the maximum rf-power setting still allowing for stable mode-locking. The outcoupled pulse energy was then calculated by measuring the average output power for that setting.

With the intra-cavity pulse energy already reduced by the use of a more transparent output-coupler, the highest achievable cavity-dumped pulse energies are on the order of 450 nJ. As can be seen in the figure, there are a number of frequencies for which the achievable pulse energy is significantly reduced. For these frequencies it was impossible to achieve stable mode-locking while the AOM was operated at full power. The rf-power was then reduced until the laser became stable again resulting in the reduced pulse energies. This most notably occurs in two frequency ranges, the instability range situated roughly between 250 and 350 kHz can be explained in terms of the relaxation oscillations which for Ti:sapphire oscillators can be expected to be found in this frequency region. Not surprisingly in this region the laser is very susceptible to even slight perturbations caused by the cavity-dumping. Another instability region occurs between 860 and 960 kHz. While this instability region is not as pronounced as the first one, the existence of this instability region is somewhat surprising because in general aside from the relaxation oscillations no other instability was expected for a CPO system. Nevertheless a similar behavior has already been reported by Zhou et al. [Zho06] which seems to confirm the measurements.

An exact cause for these regions of instability is not known. It is possible that the instabilities are only a result of resonances in the AOM electronics which influence the dumping process. However seeing how there are a couple of other frequencies for which the laser exhibits instabilities it is also possible that like in the soliton regime a number of distinct transient regimes do also exist in the positive dispersive regime.

5.3.2 Spectral properties

Besides the frequency dependence of the cavity-dumping it is also of interest to study the effect of cavity dumping in a CPO on the spectral shape of the laser pulses. From work done on cavity-dumped laser systems in the soliton regime it is known that in this regime the dumping ratio significantly influences the spectral width [Emo06]. This influence can be explained by the area theorem governing the ratio between pulse energy, spectral width, nonlinear phase and dispersion. Consequently when the intra-cavity pulse energy is reduced by the cavity-dumping the soliton adapts to this by adopting a narrower spectrum.

Since the area theorem does not apply in the positive dispersive regime it is not intrinsically clear what influence, if any, the cavity-dumping has on the generated pulse spectra.
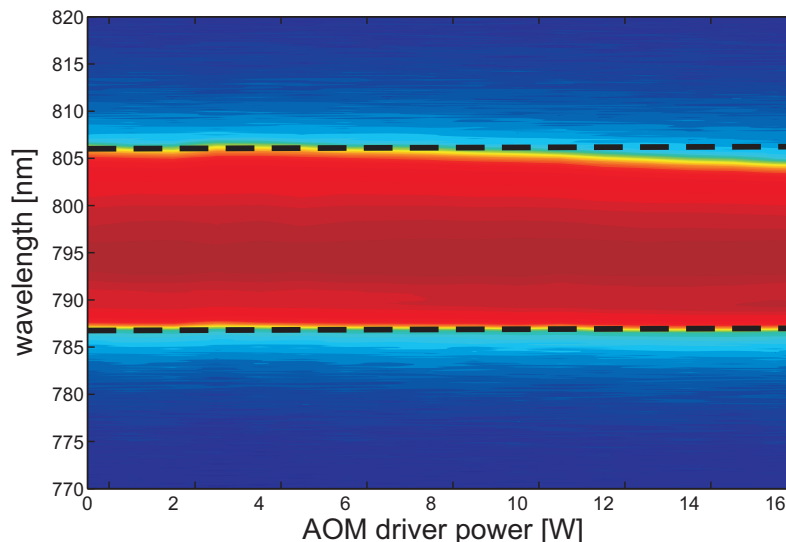
Figure 5.7: Spectral shape of the laser pulses in dependence of the rf-power used for cavity-dumping. The dotted white lines are used to better visualize the slight changes to the spectral shape.

In order to investigate this, the rf-power used to operate the AOM was varied from 0 to the maximum of 16.5 W while all other laser parameters were kept constant again a 5% output-coupler was used to lower the intra-cavity pulse energies during this measurement. In terms of the dumping depth this results in a linear increase from 0 to 45%. Fig. 5.7 shows a 2D projection of this parameter scan. Over the course of the measurement the spectral width is reduced by a total of about 3 nm or 15% when the cavity-dumping is tuned to the maximum value in this laser setup. The same measurement was then repeated with a 10% outputcoupler without any significant changes in the results, again the spectral narrowing was found to be about 15%. This is a factor two less than in the soliton regime where a spectral narrowing of about 30% was observed for dumping depths of about 45% [Emo06].

The reason for the spectral narrowing in the case of the Ti:sapphire CPO most likely lies in the fact that the reduction of the intra-cavity pulse energy by the cavity-dumping leads to less spectral broadening by SPM as explained in Section 3.2.3. The fact that this effect is significantly smaller than the spectral narrowing resulting from the area theorem in the soliton regime again shows that cavity-dumped CPOs offer good potential to be used as sources for highly energetic ultrashort laser pulses. In the future it would be interesting to do a similar experiment with the Yb:KYW CPO with cavity-dumping in order to compare the spectral narrowing for a different gain material.

5.3.3 Pulse characterization

To ensure single pulse operation the rf-spectrum of the laser was detected with a fast photodiode capable of measuring frequencies of up to 20 GHz. For this measurement the leakage behind the 1% outputcoupling mirror was used in order to monitor the whole cavity dynamics and not only the cavity dumped laser pulses. On the left hand side of Fig. 5.8 the rf-spectrum for the maximum frequency range is shown and no sign of any modulation indicative of multiple pulse can be seen. Given the frequency range of the photodiode and the rf-spectrometer used this allows to rule out multiple pulses with a separation of more than 25 ps. The right hand side of the figure shows a high resolution measurement of the internal repetition rate which also shows a very clear needle and very little residual noise.

In order to rule out multiple pulses with a separation of less than 25 ps a long range intensity autocorrelation was performed over a span of ±50 ps. Besides this the autocorrelation also serves to measure the chirped pulse duration of the laser pulses and allows an estimate for the negative GDD required for compression down to the Fourier-limit. The resulting autocorrelation function is shown in Fig. 5.9 along with a Gaussian fit to the experimental data. No sign of multiple pulsing is found in the autocorrelation. The autocorrelation width is measured to be 7.8 ps. A Gaussian fit was applied to the measured data as can be seen in the figure. However because the actual temporal pulse shape depends strongly on the frequency chirp it is difficult to determine the true convolution factor of the pulse. The stronger the chirp, the more the temporal pulse shape will start to resemble that of the frequency spectrum. However since the exact chirp factor is not known the only way to measure the temporal pulse shape would be to use a FROG or SPIDER-setup and calculating the exact convolution factor from this [Kan93, Iac98], but as no such apparatus capable of measuring ps-pulses was available this could not be done. Instead because of the good agreement between the Gaussian fit and the experimental
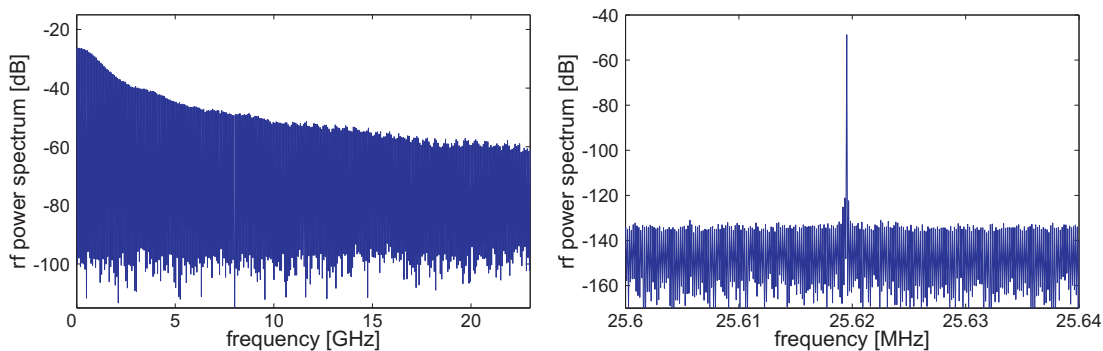

Figure 5.8: The left hand side shows the rf-spectrum of the cavity-dumped laser pulses for the maximum frequency range. While the right hand side shows a high resolution (RBW = 20 Hz) measurement of the intra-cavity repetition rate.
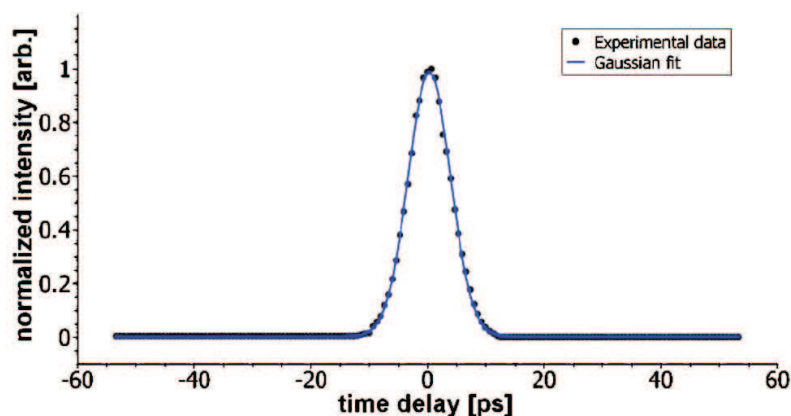
Figure 5.9: Long range autocorrelation of the chirped laser pulses. The black dots signify the measured values while the blue curve is a Gaussian fit to this data. The autocorrelation length resulting from this measurement is $\tau_{ac} = 7.8$ ps.

data the convolution factor of a Gaussian pulse was used. From this the chirped pulse duration can be estimated to be about 5 ps which leads to a required dispersion on the order of 0.10 to 0.12 ps^2.

While the laser pulses ultimately have to be compressed down to their Fourier-limit in order to be used in applications like high harmonic generation, at this point their pulse chirp is actually helpful for another experiment in which the pulse energy will be further increased.

5.4 Cryogenical cw-post amplifier

The initial plans for the laser setup was to use a pump sources capable of providing two beams each with 20 W of pump power[1]. While one of the beams was to be used as pump source for the Ti:sapphire oscillator, the other beam would have been available for further experiments. While the goals set for this part of the thesis have already been achieved with the pulse energies generated by the Ti:sapphire oscillator it was envisioned to demostrate a cryogenic post-amplifier in order to further enhance the pulse energies from the Ti:sapphire CPO. Using the second beam from the pump laser this would have resulted in a compact high energy system with one pump source capable of supplying both the oscillator and the amplifier. Because of the tight focusing required in such systems [Hub03] the high peak intensities of the recompressed laser pulses would result in white light generation in the amplifier crystal. In order to avoid this as well as to counteract the effect of material dispersion from the amplifier, it makes sense to not recompress the

---

1   ELS Gemini 20 W

laser pulses directly behind the oscillator but rather to use the chirped pulses for the amplification process.

However, as a result of technical difficulties, the dual beam pump laser had to be replaced with the 18 W pump laser mentioned in the description of the experimental setup for the Ti:sapphire oscillator. Since the Ti:sapphire oscillator actually requires all of the pump power this laser can provide, a different solution had to be found for the amplifier. It was decided to use a pump laser with 10.5 W of pump power which was available at that time. While this clearly limits possible amplification of the system it at least allows to gather first experimental experiences and results with the system which will help once higher pump powers are available again in the future.

5.4.1 Experimental setup
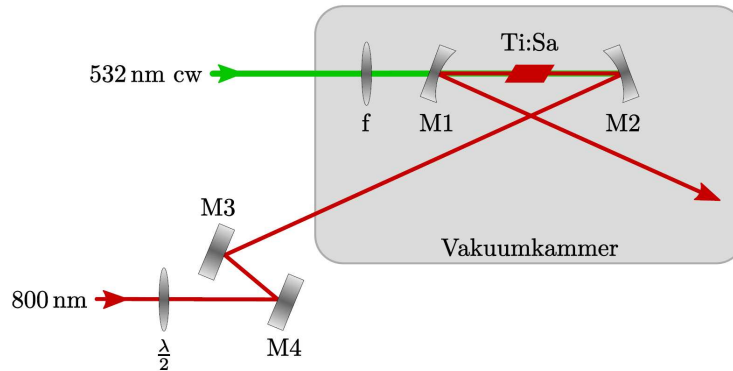
Figure 5.10: Experimental setup of the cryogenical cw-post amplifier.

Fig. 5.10 shows a schematic of the experimental amplifier setup in which the laser beam generated by the CPO system are used as seed. The setup itself is a single-pass geometry centered around a Brewster-cut Ti:sapphire crystal 6 mm long, 5 mm wide and 1.5 mm high which is placed in the focus between two concave mirrors M_1 and M_2 (ROC = 150 mm). In order to compensate the resulting astigmatism, the mirrors are used under an angle of 7°. The mirrors M_3 and M_4 are used in order to direct the seed beam into the amplifier. As explained above, for the current setup a pump power of 10.5 W is used[1] which is focused into the amplifier crystal by a lens (f=80 mm).

The overall optical setup is similar to the one reported in [Hub03]. However in order to accommodate the expected pump powers a cryogenic cooling system was devised for the Ti:sapphire crystal. As explained in Section 2.3.1, both the thermal conductivity and the overall gain increase drastically when cooling the crystal to a temperature of 77 K. To this end the copper crystal holder is mounted on a cooling finger which is connected

---

1   Coherent Inc. Verdi V-10

to a reservoir of liquid nitrogen. To avoid ice formation the laser crystal along with the
pump lens and the focusing mirrors are placed in an evacuated chamber. Because it was
envisioned that the amplifier might in the future also be used in combination with other
laser systems, the vacuum chamber is designed in such a way as to allow for the use
of a variety of crystal sizes and gain media. A sectional view of the amplifier chamber
is provided in Fig. 5.11. The pump and seed lasers are fed into the champer through
two sets of vacuum windows with low-loss anti-reflex coating. Inside the chamber, the
optical pump lens as well as the two mirrors M_1 and M_2 are mounted on an optical rail
for stability reasons. Since the pump power of 10.5 W is relatively low for a single-pass
amplifier, the most vital part of the experimental setup is the overlap of the two laser
beams in order to achieve the highest possible gain. To this end the pump lens as well as
one of the mirrors are set on linear micrometer stages allowing for precise adjustment of
the focus inside the crystal. The crystal itself is mounted in such a way as to allow for
variation of the height by the use of a micrometer gauge. Finally both pump mirrors are
placed in piezo-actuated mirror mounts allowing for adjustment from outside the vacuum
box.
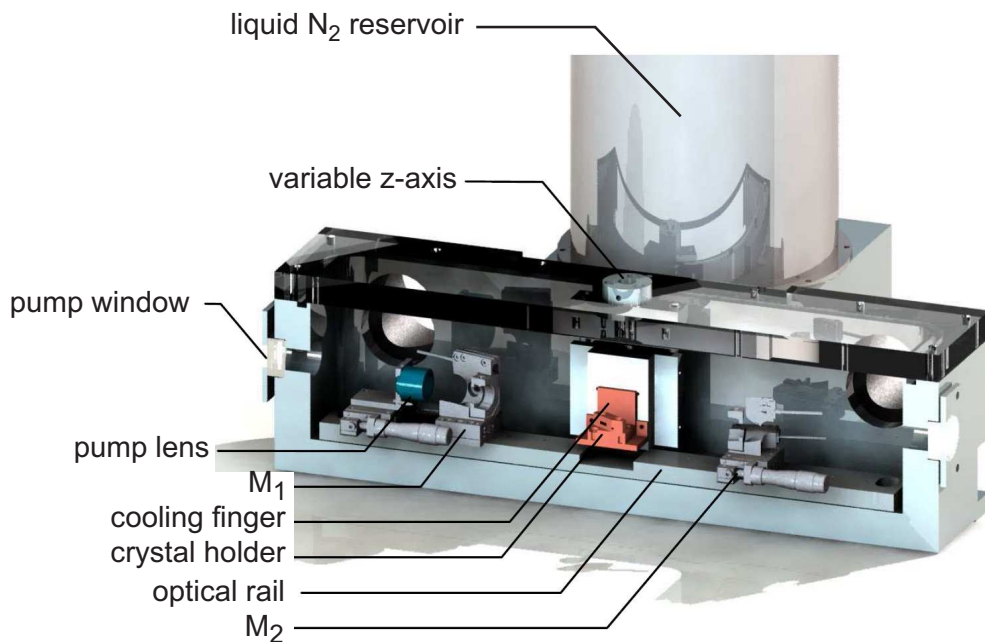
Figure 5.11: Sectional view of the amplifier setup in the vacuum box. The crystal height
as well as the z-position of the pump lens and one of the mirrors can be varied by use of
a micrometer gauge. Both mirrors are also mounted in piezo-driven holders to allow for
adjustment from the outside.

Results

As the result of optical losses between the oscillator and the amplifier, the pulse energy of the seed beam is reduced by about 10% inside the amplifier chamber. With this input and with the pump power set to the maximum of 10.5 W it was possible to achieve an amplified pulse energy of 1.46 μJ with the current setup. These experimental results were tested against a simple numerical calculation based on the rate equations. As it turned out the experimental results are in excellent agreement with the theoretical expectations [Pfu08]. Because the overall amplification is still modest compared to other amplifier systems, no effects of gain narrowing can be observed and both the spectral shape and bandwidth remain unchanged. For these measurements the importance of the cryogenic cooling becomes obvious as the single-pass gain rises sharply from less than 10% for the crystal without any cooling to 46% with liquid nitrogen cooling. The pressure in the vacuum chamber is kept at $10 \cdot 10^{-5}$ mbar, which is sufficient to prevent any ice formation and to allow for stable operation over several hours.

5.4.2 Pulse compression

Having briefly shown first results achieved with the amplifier setting this section will give a short overlook over the grating compressor which will be used for pulse compression of the amplified laser pulses in the future.

As a result of the intensity autocorrelation the negative GDD required for compression of the pulse to the Fourier-limit can be estimated to be on the order of 0.10 to 0.12 ps^2. Since such high values of negative GDD cannot readily be reached in a prism compressor it is necessary to resort to a grating compressor to achieve the necessary recompression of the laser pulses. In order to reach such high dispersion values while also minimizing
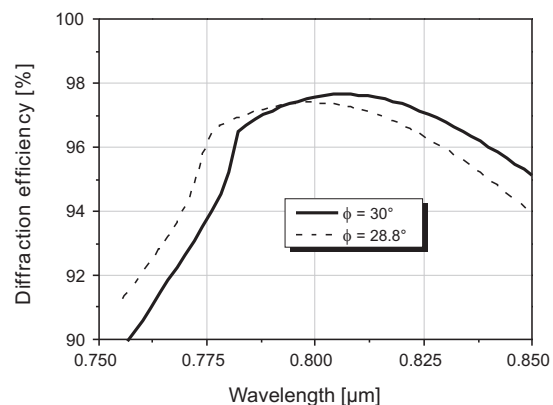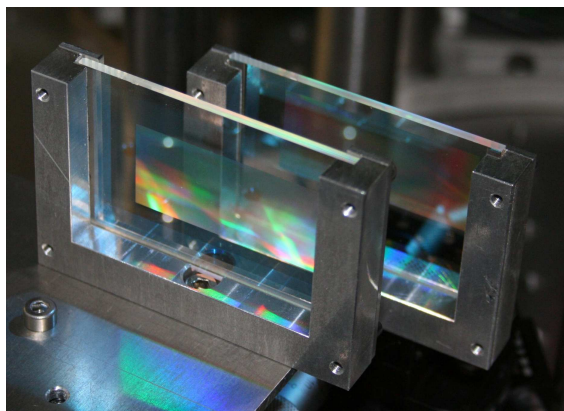

Figure 5.12: The left hand side of the picture shows a picture of the transmission gratings used for recompressing the laser pulses. On the right hand side the theoretical diffraction efficiencies for two slightly different angles of incidence ϕ are shown.

losses a pair of highly efficient transmission gratings with 1250 lines/mm were specifically manufactured for this laser system at the Institute of Applied Physics in Jena. A picture of the transmission gratings is shown on the left hand side of Figure 5.12. The right hand side of the figure shows theoretical curves for the diffraction efficiencies based on design values for two slightly different angles. As can already be seen by the difference resulting from a small deviation of only 0.2° it is important that the grating compressor is aligned very accurately. When this is done the theoretical efficiency of the compressor should be about 90%. First tests in an experimental setup show that at efficiencies of at least 85% can realistically be achieved with this grating compressor.

Figure 5.13 shows a schematic setup of the grating compressor. A $\frac{\lambda}{2}$-waveplate is required to turn the polarization of the laser light as the maximum efficiency of the transmission gratings is only achieved for s-polarization. After the laser beam has passed the gratings it is reflected back through the gratings using a plane HR-mirror, a slight height difference is induced so that that outgoing beam can be separated from the incoming beam by use of another mirror. The actual dispersion value induced by the grating compressor can be varied by changing the distance between the two transmission gratings $l_{grating}$.

The main experiments done so far were aimed at determining the maximum efficiency of the gratings. Currently first tests concerning the recompression of the chirped laser pulses are underway and preliminary results do show that in principle the compression works as pulse durations below 200 fs have been observed.
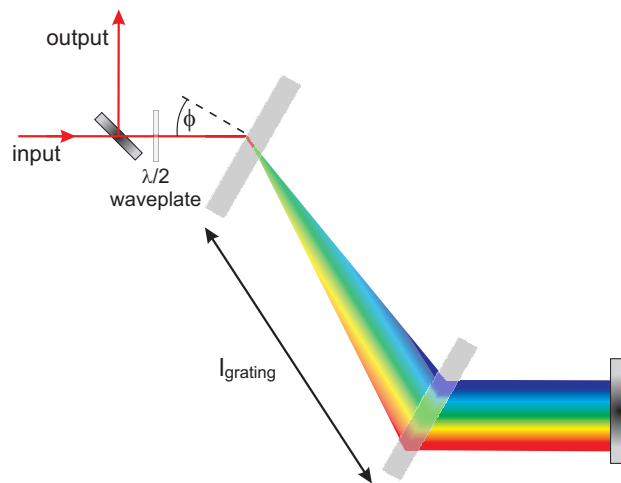

Figure 5.13: Schematic design of a transmission grating compressor. A $\frac{\lambda}{2}$-waveplate is being used to turn the polarization of the laser pulse because the maximum efficiency of the gratings is achieved for s-polarization.

5.4.3 Conclusion

The Ti:sapphire CPO with cavity-dumping presented in this chapter is capable of generating pulse energies of 1.1 μJ at repetition rates of 1 MHz and the pulse spectra support a Fourier-limit of 74 fs. The pulse energies are the highest so far achieved by a Ti:sapphire oscillator. While the recompression of the laser pulses still has to be finalized due to the planned post-amplifier, first experiments as well as the experience with work done on previous CPO systems are very promising [Nau05, Dew06b, Pal07a]. As the current limitation of this system is only given by the pump power as well as the maximum rf-power available for the AOM, this system shows that cavity-dumping in Ti:sapphire chirped pulse oscillators is a promising method for further energy scaling sub-100 fs pulses. Furthermore the preliminary implementation of a cryogenic single-pass amplifier points the way to further increases in terms of the pulse energy. In the future the cryogenic post-amplifier will be upgraded by using higher pump powers up to 20 W and a double pass setup will be implemented. This will further increase the amplification and allow to reach pulse energies of several microjoules. With these upgrades it will then be possible to reach peak powers of several tens of megawatts and reaching peak intensities of close to 10^{15} W/cm^2 in a tight focus which will make this laser system a perfect source for applications in atomic physics such as the generation of high harmonic radiation with MHz repetition rates.

6 Conclusion and Outlook

After having presented the theoretical and experimental results achieved as part of this thesis in the previous chapters, this chapter is going to give a short summary of the results as well as to lay out promising future developments and planned applications. In the first part of the chapter future options of scaling the pulse energy in the different laser systems treated in this thesis will be discussed. The second part then gives an outlook on how the Ti:sapphire laser system can be used for high harmonic generation with megahertz repetition rates in the future. Applications for the Yb-based laser systems will not be presented here, but can instead be found in [Pal09].

6.1 Energy scaling of femtosecond oscillators

6.1.1 Yb-based laser systems

The numerical simulations presented in Chapter 4 predict that there are several methods by which the pulse energy generated with Yb-based laser oscillators can be significantly increased in future setups. In this section a more detailed outlook on the possible experimental realization of such laser systems is given.

Yb:KYW thin disk oscillator with cavity-dumping

As discussed in Section 4.2, the main limitation of the current Yb:KYW thin disk oscillator with cavity dumping in the solitary regime is the limited dumping ratios resulting from the mode radius on the thin disk. Because of the large spot size on the disk, the small-signal gain is decreased while simultaneously the saturation energy is increased making the laser more susceptible to Q-switching instabilities.

By using the numerical simulations it could be shown that it should be possible to increase the outcoupled pulse energy by at least a factor of two when reducing the spot size on the disk. The required tighter focus on the thin disk can be achieved by changing the cavity geometry slightly, e.g. using different focusing mirrors and distances. In order to maintain a constant pump rate, the pump spot size also needs to be adjusted which can be done by using a different pump lens. Together with using a SESAM with a slightly lower modulation depth, this would allow to increase the dumping depth to about 40 % which would be sufficient to couple out pulse energies of about 6 μJ from the oscillator [Sie07].

Ultimately however, the achievable outcoupled pulse energies for this system will be limited by several factors: As described in section 4.2 there exist experimental limits for the reduction of the mode radius and the modulation depth. On the other hand even if these are overcome and the dumping ratio can be increased further, at some point the intra-cavity energy will have to be raised to achieve higher pulse energies. This however is prevented by the nonlinearities in the laser cavity which will ultimately lead to optical wave-breaking in the solitary regime.

Thin disk lasers in the positive dispersion regime

As shown in Section 3.1 a very promising way to overcome these limitations is by operating the thin disk oscillator in the positive dispersive regime. The work done in this thesis marks the first time the dynamics of Yb-based oscillators are investigated in detail. According to the results of the numerical simulations pulse energies of 20 μJ should be achievable with the long-cavity CPO setup described.

While first experimental tests show that CPO operation of thin disk oscillators is indeed possible, some experimental issues remain with respect to demonstrating a high power version of such a setup [Pal08, Sie08]. While the extremely high intra-cavity pulse energies which occur in high energy oscillators simulated in Section 3.1 do not result in excessive nonlinearities due to the CPO operation, they can still damage sensitive optical elements. The most crucial element in this respect is the SESAM used to achieve the mode-locking. Consequently high quality SESAMs with high damage thresholds and good uniformity over a larger area will be required in order to achieve stable laser operation. Lastly in order to achieve the required values of positive intra-cavity GDD the use of positively chirped mirrors might be required.

Another way to achieve even higher power levels can be the combination of the active-multipass concept presented in [Neu08]. The key advantage of the AMC is that by operating with extremely high outcoupling ratios in excess of 70% it significantly reduces the required intra-cavity pulse energies needed which reduces the nonlinearities. This is achieved by increasing the number of passes through the gain medium. The drawback of this method is that as a result of the large number of passes through the disk, even small irregularities (e.g. a slight thermal lens) inevitably add up and significantly reduce the stability region of the laser cavity [Neu09]. Any further increase in pulse energy from this concept has to be accompanied by a higher outcoupling rate in order to avoid excessive nonlinearities. Because of this, ultimately the number of passes through the gain medium will limit the available pulse energy.

By combining the concept of the AMC with that of the CPO it will be possible to increase the intra-cavity pulse energy without having to use a higher outcoupling ratio. No extra passes through the gain medium will be required and the limitation posed by the cumulative effects can be overcome. Based on the simulations done, the use of a gain medium other than Yb:YAG as well as operation in the chirped pulse regime also offers the chance to reduce the pulse duration compared to the 980 fs achieved with the AMC

in the negative dispersive regime.

More numerical and experimental investigations are required to develop a better understanding of such a laser system. Nevertheless based on the numerical simulations done as part of this thesis and in [Neu09] it can be estimated that pulse energies of more than 50 μJ with pulse durations around 700 fs and at repetition rates of 1-3 MHz can be expected from a single oscillator.

6.1.2 Ti:sapphire oscillator

In terms of the Ti:sapphire oscillator presented in Chapter 5 the options for further energy scaling are somewhat more limited, mainly due to the lack of more powerful pump sources than the ones currently used. The identification of parameters for possible improvements is also complicated by another fact: Unlike for the Yb-based systems no numerical simulations exist for the Ti:sapphire oscillator. The reason for this is simply that the parameters of the Kerr-lens mode-locking are not known with sufficient accuracy making it extremely difficult to match the numerical parameters to those of the experiment and rendering any attempts to make accurate predictions even harder. Nevertheless based on the current oscillator design there are a number of improvements that should allow for a further increase in pulse energy.

Cooling system

Due to limitations of the dehumidifier currently used to provide the dry air the cooling system could so far not be operated at full power. Switching to a different dehumidifier will make it possible to operate the laser at far lower temperatures of the gain crystal. First experiments done as part of this thesis show that the pulse energy does in fact rise by about 15% when the crystal is cooled to about -25 °C for a short time before ice formation sets in. Experience with past systems [Dew06a] as well as the thermal properties discussed in 2.3.1 show that by operating the laser crystal at temperatures of -40 °C or below a significant increase in pulse energy can be expected.

AOM

Another possible way to achieve higher pulse energies lies with the AOM. Currently the maximum achievable dumping ratio is 40 %. This is not limited by the laser but rather by the maximum rf-power available from the AOM driver electronics. If it was possible to achieve a higher dumping ratio, this would directly result in higher outcoupled pulse energies.

One possible way to do this would be operating the current AOM with a different driver allowing for higher rf-powers. It is however not intrinsically clear by how much the rf-power can be increased before the AOM gets damaged. In principal it might also be an option to use a different AOM which offers a higher efficiency, however at this point no such AOM is commercially available.

SESAM

Lastly it would be interesting to try to operate the laser with another SESAM instead of the one currently used in order to investigate what influence the SESAM parameters have on a laser system that uses both KLM and SESAM mode-locking. This however is currently not possible because SESAMs for the Ti:sapphire wavelength region are currently no longer commercially available except as part of a complete laser setup. The current SESAM was acquired as part of a scientific corporation with High Q Lasers GmbH. However no other SESAM designs are available from that source.

If new designs were to become available it might be interesting to test SESAMs with shorter relaxation times and different values for the modulation depth. Possibly this could allow for broader pulse spectra or even higher pulse energies.

Ti:sapphire post-amplifier

Besides possible improvements to the Ti:sapphire oscillator the post-amplifier descried in Chapter 5 will also help increase the pulse energy further. As explained earlier, technical problems with the pump laser were responsible for limiting the pump power to 10.5 W. As these problems are overcome, power will be increased to 20 W which will greatly increase the amplification of the system. Initial experiments using a pump laser with 18.5 W of pump power have already been performed and single pass gains as high as 80% have been achieved.

Also with the use of an optical isolator the amplifier setup will be changed from a single to a double pass which according to numerical simulations done as part of [Pfu08] should result in pulse energies in excess of 2 μJ for seed powers similar to the one used before. When higher seed energies are realized as a result of improvements made to the oscillator, even higher amplified pulse energies will be available.

Pulse compression

Once the setup of the post-amplifier is completed it will be necessary to recompress the pulses using the grating compressor. First tests have already shown promising results. However careful adjustments to the compressor will be required in order to achieve compression close to the Fourier-limit.

In this respect it might also be an interesting experiment to recompress the laser pulses partially prior to the amplification process. As has been discussed before complete recompression would result in white-light generation in the amplifier crystal. In contrast to that a partial recompression of the pulse could be used to allow for some SPM to take place in the amplifier crystal in order to achieve spectral broadening. Since the laser pulses have to be recompressed after the amplifier anyway this might open up a possibility for further pulse shortening.

6.2 Applications in high harmonic generation (HHG)

When the system consisting of the Ti:sapphire CPO and the post-amplifier is finalized it is going to be a convenient source of multi-microjoule, sub-100 fs laser pulses with MHz repetition rate. This combination makes it ideally suited for a number of applications including wave-guide writing or micro-machining, but even more so in atomic physics where it can be used in ionization experiments in noble gases [Dew06a, Liu07, Liu08] or the generation of high harmonic radiation.

Especially the latter is of great interest because currently only three systems worldwide have been show to generate high harmonic generation with MHz repetition rates [Goh05, Yos08, Kim08]. The systems by Gohle et al. and Yost et al. rely on enhancement cavities in order to achieve the necessary peak intensities for HHG. In contrast the concept presented by Kim et al. uses a method relying on plasmonic enhancement of the peak intensities in gold nanostructures which will be discussed below.

Using the Ti:sapphire system developed in this thesis it should be possible to either generate high harmonic generation directly in a gas jet. However in order to achieve good conversion efficiencies the most promising approach and the one planned for the future is the plasmon enhanced HHG developed by Kim et al.

6.2.1 Plasmon-enhanced high harmonic generation

The technique of plasmon-enhanced high harmonic generation is a newly developed method that has been shown to allow the generation of EUV radiation using a standard Ti:sapphire oscillator with a pulse energy of less than 2 nJ and pulse durations of 10 fs [Kim08]. Fig. 6.1 shows a schematic of the process. The basic principle is that a laser beam is focused onto an array of gold nano-antennas. When the geometry of the nanostructure is chosen correctly, the laser pulse will excite a plasmonic resonance in the gold tips. This resonance will then result in an electric field enhancement of more than 10^3 in the gaps between the gold antennas. If a noble gas such as Argon or Xenon is applied to the nanostructure the field enhancement will then be strong enough to generate high harmonic radiation in the EUV region.

The left hand side of the figure shows the laser beam being focused on the nanostructure from below through a sapphire substrate. The EUV radiation is then generated in the gaps between the nano-antennas and radiated in the same direction as the laser beam. The gas beam as well as the outgoing laser beam are omitted for reasons of clarity. The right hand side of the figure shows a close up of the process taking place between a single pair of gold tips. As the laser pulse irradiates the nanostructure the field enhancement is induced and the high harmonic radiation is generated.
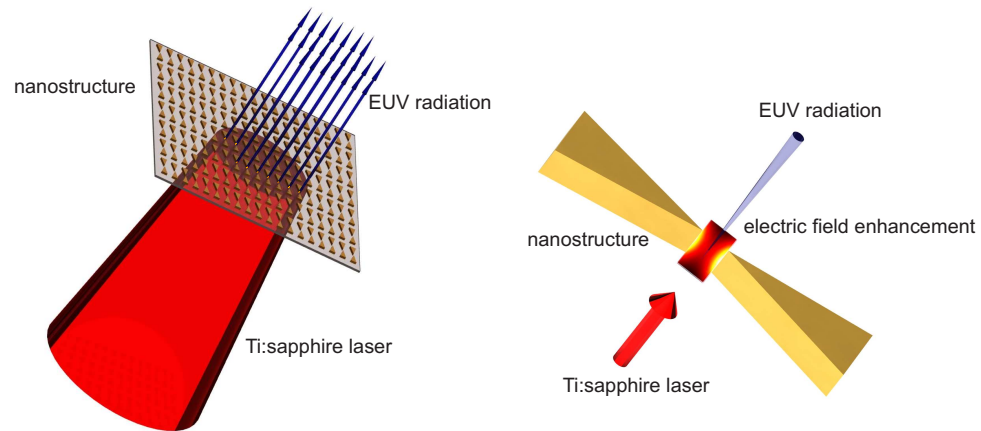
Figure 6.1: Schematic diagram of plasmon enhanced HHG. The left hand side of the picture shows a the Ti:sapphire beam hitting the gold nanostructure and generating EUV radiation at the irradiated gold tips. The right hand side shows a close up of the interaction between the laser beam and a single nanostructure along with the resulting field enhancement. The gas beam is omitted for reasons of clarity.

While the pulse duration of the Ti:sapphire CPO is longer than that used by Kim et al., the peak intensities will be far higher due to the higher pulse energy. As a result it should be possible to achieve a far higher conversion ratio and a much higher power in the different harmonic orders that are generated.

6.2.2 Experimental setup

As part of this thesis a first design for a vacuum chamber which can be used for the plasmon enhance HHG was developed. First experimental tests were conducted. In order to reproduce the results shown by Kim et al. a laser source similar to the one reported in [Kim08] was used[1].

The required nanostructure was manufactured at the PTB in Braunschweig in cooperation with Dr. Thomas Weimann. A picture of a sample structure on a fused silica substrate taken with a scanning electron microscope is shown in Fig. 6.2. The separation of the gold tips in the picture is on the order of 20 nm while the length of each individual tip is about 200 nm with a width of about 50 nm. The probe was manufactured using the e-beam lithography technique. After the preparation of this test sample, a first experimental probe was manufactured using a sapphire substrate similar to the ones used by Kim et al.

---

1 VENTEON Pulse One PE
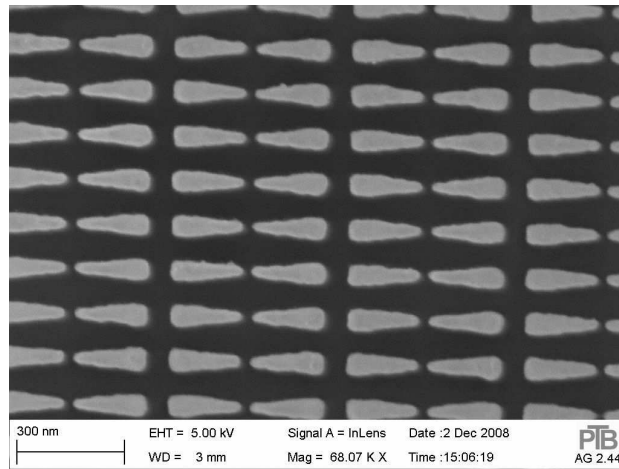
Figure 6.2: Sample of the gold nanostructure used for the plasmon enhanced high harmonic process. In contrast to the sample used in the experiment the substrate in this case is fused silica.

A schematic of the experimental setup is shown in Fig. 6.3. The incoming laser beam is focused into the vacuum chamber through a fused silica window with an off-axis parabolic mirror which has a gold coating for higher efficiency. Inside the vacuum chamber the sapphire substrate with the gold nanostructure is placed in a holder which can be adjusted in the by means of two piezo-electric linear stages. The chamber is aligned in such a way that the EUV radiation leaves the main chamber through a KF-port located behind the sapphire substrate. For detection of the high harmonic radiation a multi-channel plate is connected to the port during the experiments which is omitted in the figure. Also not shown is the gas inlet which is realized by means of a aluminium tube inserted from the top of the chamber and pointed towards the substrate. Inside the aluminum tube a glass capillary with a diameter of several micrometers is glued which acts as a nozzle for the gas jet. For the purpose of evacuating the chamber a turbo molecular pump is connected to the bottom of the chamber.

6.2.3 First experiments and outlook

In first tests, no high harmonic radiation could be detected. After further investigation the reason for this is most likely that the nanostructure used in the experiments was far less regular in shape than the test sample grown on fused silica and shown in Fig. 6.2. This was caused by the change from a fused silica to a sapphire substrate which changes the electron backscattering rate in the e-beam lithography and requires adjustments to the manufacturing process which will be done in the future.

The next step after manufacturing better quality nanostructures will be another attempt to reproduce the results achieved by Kim et al. The results from this can then be used to enhance the detection scheme as well as to increase the efficiency of the setup.
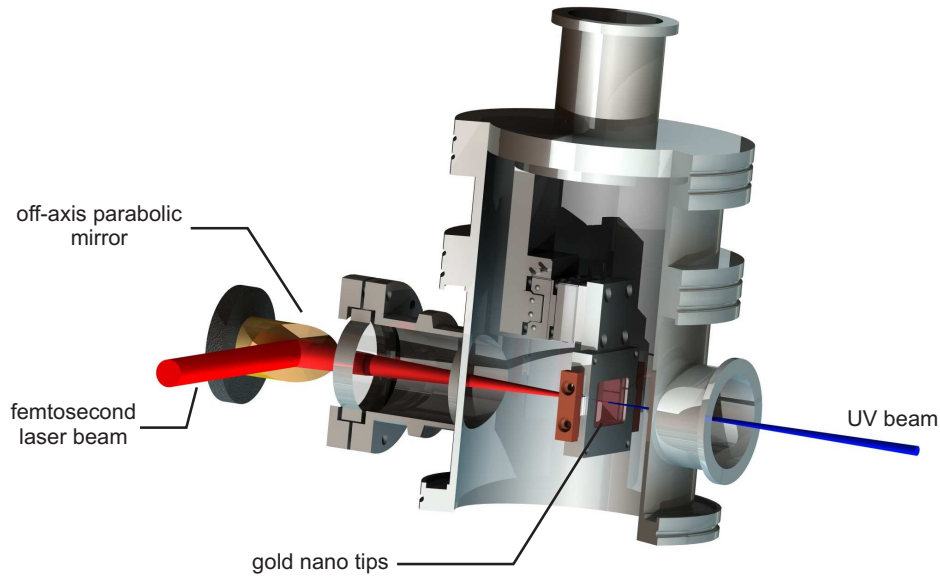
Figure 6.3: Sectional view of the experimental setup for the plasmon enhanced HHG.

Already in the first tests a number of possible points for improvements were found such as the focusing of the laser beam as well as the placing of the substrate inside the vacuum chamber. Once these improvements are implemented the microjoule Ti:sapphire CPO can be used along with the post-amplifier in order to efficiently generate high harmonic radiation with MHz repetition rates for the first time. The high repetition rate makes this system particularly interesting for applications like Fourier-spectroscopy [Kov05] or the generation of a frequency comb in the UV-region [Goh05]. Another intriguing experimental application is to use the 5th harmonic of the Ti:sapphire for the purpose of nuclear spectroscopy on the Thorium-229 nucleus [Pei03]. If successful, this will represent the first ever measurement of a nuclear transition by a laser system.

List of Figures

List of Tables

Bibliography

[Agr95]   AGRAWAL, G.P.: *Nonlinear Fiber Optics*, San Diego Academic Press (1995)

[Alb86]   ALBERS, P.; STARK, E. and HUBER, G.: Continuous-wave laser operation and quantum efficiency of titanium-doped sapphire. *J. Opt. Soc. Am. B* (1986), vol. 3(1): pp. 134 – 139

[And93]   ANDERSON, D.; DESAIX, M.; KARLSSON, M.; LISAK, M. and QUIROGA-TEIXEIRO, M. L.: Wave-breaking-free pulses in nonlinear-optical fibers. *J. Opt. Soc. Am. B* (1993), vol. 10: pp. 1185–1190

[Bal97]   BALTUSKA, A.; WEI, Z.; PSHENICHNIKOV, M. S.; WIERSMA, D.A. and SZIPOCS, R.: All-solid-state cavity-dumped sub-5-fs laser. *Applied Physics B* (1997), vol. 65: pp. 175–188

[Bar96]   BARENBLATT, G. I.: *Scaling, self-similarity, and intermediate asymptotics*, Cambridge University Press (1996)

[Bra91]   BRABEC, T.; SPIELMANN, C. and KRAUSZ, F.: Mode locking in solitary lasers. *Opt. Lett.* (1991), vol. 16: pp. 1961–1963

[Bra92a] BRABEC, T.; SPIELMANN, C.; CURLEY, P. F. and KRAUSZ, F.: Kerr lens modelocking. *Opt. Lett.* (1992), vol. 17: pp. 1292–1294

[Bra92b] BRABEC, T.; SPIELMANN, C. and KRAUSZ, F.: Limits of pulse shortening in solitary lasers. *Opt. Lett.* (1992), vol. 17: pp. 748–750

[Bra93]   BRABEC, T.; CURLEY, P. F.; SPIELMANN, C.; WINTNER, E. and SCHMIDT, A. J.: Hard-aperture Kerr-lens mode locking. *J. Opt. Soc. Am. B* (1993), vol. 10: pp. 1029–1034

[Cer94a] CERULLO, G.; SILVESTRI, S. De and MAGNI, V.: Self-starting Kerr-lens mode locking of a Ti:sapphire laser. *Opt. Lett.* (1994), vol. 19(14): pp. 1040–1042

[Cer94b] CERULLO, G.; SILVESTRI, S. De; MAGNI, V. and PALLARO, L.: Resonators for Kerr-lens mode-locked femtosecond Ti:sapphire lasers. *Opt. Lett.* (1994), vol. 19(11): pp. 807–809

[Che99]   CHEN, Y.; KÄRTNER, F. X.; MORGNER, U.; CHO, S. H.; HAUS, A.; IPPEN, E. and FUJIMOTO, J. G.: Dispersion-managed mode locking. *J. Opt. Soc. Am. B* (1999), vol. 16: pp. 1999–2004

[Cho99]   CHO, S. H.; BOUMA, B. E.; IPPEN, E. P. and FUJIMOTO, J. G.: Low-repetition-rate high-peak-power Kerr-lens mode-locked TiAl2O3 laser with a multiple-pass cavity. *Opt. Lett.* (1999), vol. 24: pp. 417–419

[Cho01]   CHO, S. H.; KÄRTNER, F. X.; MORGNER, U.; IPPEN, E. P. and FUJIMOTO, J. G.: Generation of 90-nJ pulses with a 4-MHz repetition-rate Kerr-lens mode-locked Ti:Al2O3 laser operating with net positive and negative intra-cavity dispersion. *Opt. Lett.* (2001), vol. 26: pp. 560–562

[Dew02]   DEWALD, S.: *Aufbau eines Ti:Saphir Laseroszillators zur Erzeugung ultrakurzer Laserpulse mit hohen Pulsenergien*, diploma thesis, Universität Karlsruhe (2002)

[Dew06a]   DEWALD, S.: *Erzeugung intensiver Lichtfelder mit einem Laseroszillator und deren Wechselwirkung mit Atomen*, Ph.D. thesis, Universität Heidelberg (2006)

[Dew06b]   DEWALD, S.; SIEGEL, M.; SCHRÖTER, C. D.; MOSHAMMER, R.; ULLRICH, J.; LANG, T. and MORGNER, U.: Ionization of noble gases with laser pulses directly from a laser oscillator. *Opt. Lett.* (2006), vol. 31: p. 2072

[Die06]   DIELS, J.C. and RUDOLPH, W.: *Ultrashort Laser Pulse Phenomena - 2nd Edition*, Academic Press, San Diego (2006)

[Dud07]   DUDLEY, J. M.; FINOT, C.; RICHARDSON, D. J. and MILLOT, G.: Self-Similarity in ultrafast nonlinear optics. *Nature Physics* (2007), vol. 3: pp. 597–603

[Ell03]   ELL, R.: *Sub-Two Cycle Ti:Sapphire Laser and Phase Sensitive Nonlinear Optics*, Ph.D. thesis, Universität Karlsruhe (2003)

[Emo06]   EMONS, M.: *Mikrojoule-Laserpulse aus einem Femtosekunden-Laseroszillator mit Cavity-Dumping*, diploma thesis, Fachhochschule Koblenz (2006)

[Fer04]   FERNANDEZ, A.; FUJI, T.; POPPE, A.; FÜRBACH, A.; KRAUSZ, F. and APOLONSKI, A.: Chirped-pulse oscillators: a route to high-power femtosecond pulses without external amplification. *Opt. Lett.* (2004), vol. 29(12): pp. 1366–1368

[Gib96]   GIBSON, G. N.; KLANK, R.; GIBSON, F. and BOUMA, B. E.: Electro-optically cavity-dumped ultrashort-pulse Ti:sapphire oscillator. *Opt. Lett.* (1996), vol. 21: pp. 1055–1057

[Gie94]   GIESEN, A.; HÜGEL, H.; VOSS, A.; WITTIG, K.; BRAUCH, U. and OPOWER, H.: Scalable concept for diode-pumped high-power solid-state lasers. *Applied Physics B* (1994), vol. 58: pp. 365–372

[Gie07]   GIESEN, A. and SPEISER, J.: Fifteen Years of Work on Thin-Disk Lasers: Results and Scaling Laws. *IEEE Journal of Selected Topics in Quantum Electronics* (2007), vol. 13: pp. 598–609

[Goh05]   GOHLE, C.; UDEM, T.; HERRMANN, M.; RAUSCHENBERGER, J.; ANDN H. A. SCHUESSLER, R. Holzwarth; KRAUSZ, F. and HAENSCH, T. W.:

A frequency comb in the extreme ultraviolet. *Nature* (2005), vol. 436: pp. 234 – 237

[Gra06] GRANGE, R.: *Near Infrared Semiconductor Saturable Absorber Mirrors For High Repetition Rate Lasers*, Ph.D. thesis, ETH Zürich (2006)

[Gri05] GRIEBNER, U.; RIVIER, S.; PETROV, V.; ZORN, M.; ERBERT, G.; WEYERS, M.; MATEOS, X.; AGUILÓ, M.; MASSONS, J. and DÁZ, F.: Passively mode-locked Yb:KLu(WO4)2 oscillators. *Opt. Exp.* (2005), vol. 13: pp. 3465–3470

[Har73] HARDIN, R. H. and TAPPERT, F. D.: Applications of the split-step Fourier method to the numerical solution of nonlinear and variable coefficient wave equations. *SIAM Rev. Chronicle* (1973), vol. 15: p. 423

[Hau75a] HAUS, H.: A theory of forced mode locking. *IEEE Journal of Quantum Electronics* (1975), vol. QE 11: pp. 323–330

[Hau75b] HAUS, H.: Theory of mode locking with a fast saturable absorber. *Journal of Applied Physics* (1975), vol. 46: pp. 3049–3058

[Hau75c] HAUS, H.: Theory of Mode Locking with a Slow Saturable Absorber. *IEEE Journal of Quantum Electronics* (1975), vol. QE 11: p. 736

[Hau02] HAUMESSER, P.-H.; GAUMÉ, R.; VIANA, B. and VIVIEN, D.: Determination of laser parameters of ytterbium-doped oxide crystalline materials. *J. Opt. Soc. Am. B* (2002), vol. 19: pp. 2365–2375

[Hec06] HECHT, J.: A proliferation of petawatt lasers. *Laser Focus World* (2006), vol. 42

[Her64] HERRIOT, D.; KOGELNIK, H. and R.KOMPFNER: Off-Axis Paths in Spherical Mirror Interferometers. *Appl. Opt.* (1964), vol. 3(4): pp. 523–526

[Hön99] HÖNNINGER, C.; PASCHOTTA, R.; MORIER-GENOUD, F.; MOSER, M. and KELLER, U.: Q-switching stability limits of continuous-wave passive mode locking. *J. Opt. Soc. Am. B* (1999), vol. 16: pp. 46–56

[Hub03] HUBER, R.; ADLER, F.; LEITENSTORFER, A.; BEUTTER, M.; BAUM, P. and RIEDLE, E.: 12-fs pulses from a continuous-wave-pumped 200-nJ Ti:Sapphire amplifier at a variable repetition rate as high as 4 MHz. *Opt. Lett.* (2003), vol. 28(21): pp. 2118 – 2120

[Iac98] IACONIS, C. and WALMSLEY, I. A.: Spectral phase interferometry for direct electric-field reconstruction of ultrashort optical pulses. *Opt. Lett.* (1998), vol. 32: pp. 792–794

[Ild04a] ILDAY, F. Ö.; BUCKLEY, J. R.; CLARK, W. G. and WISE, F. W.: Self-Similar Evolution of Parabolic Pulses in a Laser. *Physical Review Letters* (2004), vol. 92(21): p. 213902

[Ild04b] ILDAY, F. Ö.; WISE, F. W. and KÄRTNER, F. X.: Possibility of self-similar pulse evolution in a Ti:sapphire laser. *Opt. Exp.* (2004), vol. 12(12): pp. 2731–2733

[Kal05]   KALASHNIKOV, V.L.; PODIVILOV, E.; CHERNYKH, A.; NAUMOV, S.; FERNAN-
          DEZ, A.; R.GRAF and APOLONSKI, A.: Approaching the microjoule frontier
          with femtosecond laser oscillators: theory and comparison with experiment.
          New Journal of Physics (2005), vol. 7(217): p. 217

[Kal07]   KALASHNIKOV, V. L. and CHERNYKH, A.: Spectral anomalies and stability of
          chirped-pulse oscillators. *Physical Review A* (2007), vol. 75: p. 033820

[Kal08]   KALASHNIKOV, V. L.; FERNANDEZ, A. and APOLONSKI, A.: High-order dis-
          persion in chirped-pulse oscillators. *Opt. Exp.* (2008), vol. 16(6): pp. 4206 –
          4216

[Kal09]   KALASHNIKOV, V. L. and APOLONSKI, A.: Chirped-pulse oscillators: A unified
          standpoint. *Physical Review A* (2009), vol. 79

[Kan93]   KANE, D. and TREBINO, R.: Characterization of arbitrary femtosecond pulses
          using frequency-resolved optical gating. *IEEE Journ. of Quantum Electron-
          ics* (1993), vol. 29: p. 571

[Kär95]   KÄRTNER, F. X. and KELLER, U.: Stabilization of solitonlike pulses with a
          slow saturable absorber. *Opt. Lett.* (1995), vol. 20: pp. 16–18

[Kel92]   KELLY, S. M.: Characteristic sideband instability of periodically amplified av-
          erage soliton. *Electronics Letters* (1992), vol. 28: p. 806

[Kel96]   KELLER, U.; WEINGARTEN, K. J.; KÄRTNER, F. X.; KOPF, D.; BRAUN, B.;
          JUNG, I. D.; FLUCK, R.; HÖNNINGER, C.; MATUSCHEK, N. and AUS DER
          AU, J.: Semiconductor Saturable Absorber Mirrors (SESAM's) for Fem-
          tosecond to Nanosecond Pulse Generation in Solid State Lasers. *IEEE Jour-
          nal of selected Topics in Quantum Electronics* (1996), vol. 2: pp. 435–543

[Kel02]   KELLER, U.: *Ultrakurzzeit-Laserphysik* (2002)

[Kil04a] KILLI, A. and MORGNER, U.: Solitary pulse shaping dynamics in cavity-
          dumped laser oscillators. *Opt. Exp.* (2004), vol. 12: pp. 3297–3307

[Kil04b] KILLI, A.; MORGNER, U.; LEDERER, M. J. and KOPF, D.: Diode-pumped
          femtosecond oscillator with cavity dumping. *Opt. Lett.* (2004), vol. 29: pp.
          1288–1290

[Kil05a] KILLI, A.: *Cavity-Dumping in solitär modengekoppelten Femtosekunden-
          Laseroszillatoren*, Ph.D. thesis, Universität Heidelberg (2005)

[Kil05b] KILLI, A.; STEINMANN, A.; DÖRRING, J.; MORGNER, U.; LEDERER, M. J.;
          KOPF, D. and FALLNICH, C.: High peak power pulses from a cavity-dumped
          Yb:KYW oscillator. *Opt. Lett.* (2005), vol. 30: pp. 1891–3

[Kim08]   KIM, S.; JIN, J.; KIM, Y-J.; PARK, I-Y; KING, Y. and KIM, S-W.: High-
          harmonic generation by resonant plasmon field enhancement. *Nature* (2008),
          vol. 453: pp. 757–760

[Koe06]   KOECHNER, W.: *Solid State Laser Engineering*, Springer (2006)

[Kov05]   KOVACEV, M.; FORMICHEV, S. V.; PRIORI, E.; MAIRESSE, Y.; MERDJI, H.; MONCHICOURT, P.; BREGER, P.; NORIN, J.; PERSSON, A.; L'HUILLIER, A.; WAHLSTRÖM, C.-G.; CARRE, B. and SALIERES, P.: Extreme Ultraviolet Fourier-Transform Spectroscopy with High Order Harmonics. *Phys. Rev. Lett.* (2005), vol. 95: p. 223903

[Kow03]   KOWALEVICZ, A. M.; ZARE, A. Tucay; KÃ¤RTNER, F. X.; FUJIMOTO, J. G.; DEWALD, S.; MORGNER, U.; SCHEUER, V. and ANGELOW, G.: Generation of 150-nJ pulses from a multiple-pass cavity Kerr-lens modelocked Ti:Al2O3 oscillator. *Opt. Lett.* (2003), vol. 28(17): pp. 1597–1599

[Kow06]   KOWALEVICZ, A. M.; SENNAROGLU, A.; ZARE, A.T. and FUJIMOTO, J.G.: Design principles of q-preserving multipass-cavity femtosecond lasers. *Opt. Lett.* (2006), vol. 23: pp. 760–770

[Kru00]   KRUPKE, W. F.: Ytterbium solid-state lasers - the first decade. *IEEE Journal of Selected Topics in Quantum Electronics* (2000), vol. 6: pp. 1287–1296

[Kul97]   KULESHOV, N.V.; LAGATSKY, A. A.; PODLIPENSKY, A. V.; MIKHAILOV, V. P. and HUBER, G.: Pulsed laser operation of Yb-doped KY(WO4)2 and KGd(WO4)2. *Opt. Lett.* (1997), vol. 22: p. 1317

[Liu07]   LIU, Y.; TSCHUCH, S.; DÜRR, M.; RUDENKO, A.; MOSHAMMER, R.; ULLRICH, J.; SIEGEL, M. and MORGNER, U.: Towards non-sequential double ionization of Ne and Ar using a femtosecond laser oscillator. *Opt. Exp.* (2007), vol. 15: pp. 18103–18110

[Liu08]   LIU, Y.; TSCHUCH, S.; DÜRR, M.; RUDENKO, A.; MOSHAMMER, R.; ULLRICH, J.; SIEGEL, M. and MORGNER, U.: Strong field double ionization of Ar below the recollision threshold. *Phys. Rev. Lett.* (2008), vol. 101

[Liu09]   LIU, J.; HAN, W.; ZHANG, H.; MATEOS, X. and PETROV, V.: Comparative Study of High-Power Continuous-wave Laser Performance of Yb-Doped Vanadate Crystals. *IEEE Journal of Quantum Electronics* (2009), vol. 45: pp. 807–815

[Mac09]   MACLEAN, A. J.; ROTH, P.; VALENTINE, G. J.; KAEMP, A. J. and BURNS, D.: Direct Diode Laser Pumping of a Ti:Sapphire Laser, Advanced Solid-State Photonics, OSA Technical Digest Series (CD), Optical Society of America, paper WE2

[Mar06]   MARCHESE, S. V.; SÜDMEYER, T.; GOLLING, M.; GRANGE, R. and KELLER, U.: Pulse energy scaling to 5 μJ from a femtosecond thin disk laser. *Opt. Lett.* (2006), vol. 31: pp. 2728–2730

[Mar08]   MARCHESE, S. V.; BAER, C. R.; ENGQVIST, A. G.; HASHIMOTO, S.; MAAS, D. J.; GOLLING, M.; SÜDMEYER, T. and KELLER, U.: Femtosecond

thin disk laser oscillator with pulse energy beyond the 10-microjule level. *Opt. Exp.* (2008), vol. 16: pp. 6397–6407

[Mol80]   Mollenauer, L. F.; Stolen, R. H. and Gordon, J. P.: Experimental observation of picosecond pulse narrowing and solitons in optical fibers. *Phys. Rev. Lett.* (1980), vol. 45: p. 1095

[Mol84]   Mollenauer, L. F. and Stolen, R. H.: The soliton laser. *Opt. Lett.* (1984), vol. 9: pp. 13–15

[Mor03]   Morgner, U.: *Erzeugung und Propagation optischer Laserpulse - Optische Nachrichtentechnik IV*, Vorlesungsskript (2003)

[Mou86]   Moulton, P. F.: Spectroscopic and laser characteristics of Ti:Al$_2$O$_3$. *J. Opt. Soc. Am. B* (1986), vol. 3: pp. 125–133

[Nau05]   Naumov, S.; Fernandez, A.; R.Graf; Dombi, P.; Krausz, F. and Apolonski, A.: Approaching the microjoule frontier with femtosecond laser oscillators. *New Journal of Physics* (2005), vol. 7(216): p. 216

[Neu08]   Neuhaus, J.; Bauer, D.; Zhang, J.; Killi, A.; Kleinbauer, J.; Kumkar, M.; Weiler, S.; Guina, M.; Sutter, D. H. and Dekorsy, T.: Subpicosecond thin-disk laser oscillator with pulse energies of up to 25.9 microjoules by use of an active multipass geometry. *Opt. Exp.* (2008), vol. 16: pp. 20530–20539

[Neu09]   Neuhaus, J.: *Passively mode-locked Yb:YAG thin-disk laser with active multipass geometry*, Ph.D. thesis, Universität Konstanz (2009)

[Ort09]   Ortac, B.; Baumgartl, M.; Limpert, J. and Tünnermann, A.: Approaching microjoule-level pulse energy with mode-locked femtosecond fiber lasers. *Opt. Lett.* (2009), vol. 34: pp. 1585–1587

[Pal07a]   Palmer, G.; Emons, M.; Siegel, M.; Steinmann, A.; Schultze, M.; Lederer, M. and Morgner, U.: Passively mode-locked and cavity-dumped Yb:KY(WO4)2 oscillator with positive dispersion. *Opt. Exp.* (2007), vol. 15: pp. 16017–16021

[Pal07b]   Palmer, G.; Siegel, M.; Steinmann, A. and Morgner, U.: Microjoule pulses from a passively mode-locked Yb:KY(WO4)2 thin-disk oscillator with cavity dumping. *Opt. Lett.* (2007), vol. 32: pp. 1593–1595

[Pal08]   Palmer, G.; Schultze, M.; Siegel, M.; Emons, M.; Bünting, U. and Morgner, U.: Passively mode-locked Yb:KLu(WO4)2 thin-disk oscillator operated in the positive and negative dispersion regime. *Opt. Lett.* (2008), vol. 33: pp. 1608–1610

[Pal09]   Palmer, G.: *Hoch-Energie Ytterbium-Laseroszillatoren mit Cavity-Dumping*, Ph.D. thesis, Leibniz Universität Hannover (2009)

[Pas01]   PASCHOTTA, R.; DER AU, J. AUS; SPÜLER, G. J.; ERHARD, S.; GIESEN, A. and
           KELLER, U.: Passive mode locking of thin-disk lasers: effects of spatial hole
           burning. *Applied Physics B* (2001), vol. 72: pp. 267–278

[Pei03]   PEIK, E. and TAMM, C.: Nuclear laser spectroscopy of the 3.5 eV transition in
           Th-229. *Europhys. Lett.* (2003), vol. 61: pp. 181–186

[Pet07]   PETROV, V.; PUJOL, M. C.; MATEOS, X.; SILVESTRE, O.; RIVIER, S.; AGUILÓ,
           M.; SOLÉ, R. M.; LIU, J.; GRIEBNER, U. and DIÁZ, F.: Growth and prop-
           erties of KLu(WO4)2, and novel ytterbium and thulium lasers based on this
           monoclinic crystalline host. *Laser & Photonics Review* (2007), vol. 1: pp.
           179–212

[Pfu08]   PFULLMANN, Nils: *Kryogene Nachverstärkung von Mikrojoule-Laserpulsen*,
           diploma thesis, Leibniz Universität Hannover (2008)

[Pic93]   PICHE, M. and SALIN, F.: Self-mode locking of solid-state lasers without aper-
           tures. *Opt. Lett.* (1993), vol. 18: pp. 1041–1043

[Pro93]   PROCTOR, B.; WESTWIG, E. and WISE, F.:   Characterization of a Kerr-
           lens mode-locked Ti:sapphire laser with positive group-velocity dispersion.
           Opt. Lett. (1993), vol. 18(19): pp. 1654–1656

[Psh93]   PSHENICHNIKOV, M.S.; DE BOEIJ, W. P. and WIERSMA, D. A.: Generation
           of 13-fs, 5-MW pulses from a cavity-dumped Ti:sapphre laser. *Opt. Lett.*
           (1993), vol. 19: pp. 572–574

[Ram93]   RAMASWAMY, M.; ULMAN, M.; PAYE, J. and FUJIMOTO, J.G.: Cavity-dumped
           femtosecond Kerr-lens mode-locked Ti:Al2O3. *Opt. Lett.* (1993), vol. 18: pp.
           1822–1824

[Rau08]   RAUSCH, S.; BINHAMMER, T.; HARTH, A.; KIM, J.; ELL, R.; KÄRTNER, F. X.
           and MORGNER, U.: Controlled waveforms on the single-cycle scale from a
           femtosecond oscillator. *Opt. Exp.* (2008), vol. 16(13): pp. 9739–9745

[Rue07]   RUEHL, A.; PROCHNOW, O.; SCHULTZ, M.; WANDT, D. and KRACHT, D.:
           Impact of third-order dispersion on the generation of wave-breaking free
           pulses in ultrafast fiber lasers. *Opt. Lett.* (2007), vol. 32: pp. 2590–2592

[Rue08]   RUEHL, A.: *The normal dispersion regime in passively mode-locked fiber oscil-
           lators*, Ph.D. thesis, Leibniz Universität Hannover (2008)

[SC97]   SOTO-CRESPO, J. M.; AKHMEDIEV, N. N.; AFANASJEV, V. V. and WABNITZ,
           S.: Pulse solutions of the cubic-quintic complex Ginuburg-Landau equation
           in the case of normal dispersion. *Phys. Rev. E* (1997), vol. 55: pp. 4783–4796

[Sch07]   SCHULTZE, M.: *Pump-Abfrage-Experimente an Halbleiterstrukturen im nahen
           Infraroten*, diploma thesis, Leibnitz Universität Hannover (2007)

[Sel06]   SELIANOV, A. G.; DENISOV, I. A. and KULESHOV, N. V.: Nonlinear refractive properties of Yb3+-doped KY(WO4)2 and YVO4 laser crystals. *Applied Physics B* (2006), vol. 83: pp. 61–65

[SG04]   SAINT-GOBAINCRYSTALS: Reference Guide Saphikon (2004)

[Shc01]   SHCHESLAVSKIY, V.; YAKOVLEV, V. V. and IVANOV, A.: High-energy self-starting femtosecond Cr4:Mg2SiO4 oscillator operating at a low repetition rate. *Opt. Lett.* (2001), vol. 26: pp. 1999–2001

[Sie05]   SIEGEL, M.: *Ein Titan-Saphir-Laseroszillator zur Erzeugung von Laserpulsen mit Pulsenergien im Mikrojoule-Bereich*, diploma thesis, Universität Heidelberg (2005)

[Sie07]   SIEGEL, M.; PALMER, G.; STEINMANN, A.; POSPIECH, M. and MORGNER, U.: Theoretical and experimental limits of cavity-dumping in passively mode-locked thin-disk oscillators. *Opt. Exp.* (2007), vol. 15: pp. 16860–16869

[Sie08]   SIEGEL, M.; PALMER, G.; EMONS, M.; SCHULTZE, M.; RUEHL, A. and MORGNER, U.: Pulsing dynamics in Ytterbium based chirped-pulse oscillators. *Opt. Exp.* (2008), vol. 16: pp. 14314–14320

[Sie09]   SIEGEL, M.; PFULLMANN, N.; PALMER, G.; RAUSCH, S.; BINHAMMER, T.; KOVACEV, M. and MORGNER, U.: Microjoule pulse energy from a chirped-pulse Ti:sapphire oscillator with cavity dumping. *Opt. Lett.* (2009), vol. 34: pp. 740–742

[Smo98]   SMOLORZ, S. and WISE, F.: Time resolved nonlinear refraction in femtosecond laser gain media. *Opt. Lett.* (1998), vol. 23: pp. 1381–1383

[Spe91]   SPENCE, D. E.; KEAN, P. N. and SIBBETT, W.: 60-fsec pulse generation from a self-mode-locked Ti:sapphire laser. *Opt. Lett.* (1991), vol. 16(1): pp. 42–44

[Ste00]   STEWEN, C.; CONTAG, K.; LARIONOV, M.; GIESEN, A. and HÜGEL, H.: A 1-kW CW Thin Disc Laser. *IST* (2000), vol. 6: pp. 650–657

[Ste08]   STEINMANN, A.: *Doktorarbeit Andy*, Ph.D. thesis, Leibniz Universität Hannover (2008)

[Str85]   STRICKLAND, D. and MOUROU, G.: Compression of amplified chirped optical pulses. *Optical Communication* (1985), vol. 62: p. 419

[Süd08]   SÜDMEYER, T.; MARCHESE, S. V.; HASHIMOTO, S.; BAER, C. R. E.; GINGRAS, G.; WITZEL, B. and KELLER, U.: Femtosecond laser oscillators for high-field science. *Nature Photonics* (2008), vol. 2: pp. 599–604

[Sve98]   SVELTO, O.: *Principles of Lasers*, Plenum Press, New York, 4 edn. (1998)

[Tho99]   THOEN, E. R.; KOONTZ, E. M.; JOSCHKO, M.; LANGLOIS, P.; SCHIBLI, T. R. and KÄRTNER, F. X.: Two-photon absorption in semiconductor saturable absorber mirrors. *Applied Physics Letters* (1999), vol. 74: pp. 3927–2929

[Tom85]   Tomlinson, W. J.; Stolen, R. H. and Johnson, A. M.: Optical wave break-ing of pulses in nonlinear optical fibers. *Opt. Lett.* (1985), vol. 10: pp. 457–459

[Yos08]   Yost, D. C.; Schibli, T. R. and Ye, J.: Efficient output coupling of intracavity high harmonic generation. *Opt. Lett.* (2008), vol. 33: pp. 1099–1101

[Zay95]   Zayhoski, J. J. and Dill, C.: Coupled cavity electro-optically Q-switched Nd:YVO4 microchip lasers. *Opt. Lett.* (1995), vol. 20: pp. 716–718

[Zho06]   Zhou, X.; Kapteyn, H. and Murnane, M.: Positive-dispersion cavity-dumped Ti:sapphire laser oscillator and its application to white light gen-eration. *Opt. Exp.* (2006), vol. 14(21): pp. 9750–9757

Curriculum Vitae

Personal Data

Name:	Martin Siegel
Date of birth:	17.07.1979
Place of birth:	Mannheim
Nationality:	German
Marital status:	married

Education

08/1986 - 07/1990	Wilhelm-Wundt Grundschule, Mannheim
08/1990 - 07/1999	Moll-Gymnasium, Mannheim

University Education

10/1999 - 12/2005	Physics at the University of Heidelberg
08/2002 - 06/2003	Exchange student at the University of New Mexico, Albuquerque, USA
2005	Diploma thesis at the Max-Planck Institute for Nuclear Physics, Heidelberg, title of the thesis: 'Ein Titan-Saphir-Laseroszillator zur Erzeugung von Laserpulsen mit Pulsenergien im μJ-Bereich'

Alternative Service

1998 - 2003	Technisches Hilfswerk Mannheim, 1. Technischer Zug
2003 - 2006	Technisches Hilfswerk Heidelberg, FG Führung und Kommunikation

Ph.D. studies

01/2006 - 08/2006	Ph.D. student at the Max-Planck Institute for Nuclear Physics, Heidelberg
08/2006 - present	Ph.D. student at the Institute of Quantum Optics, Leibniz Universität Hannover

List of Publications

Journal Papers

1. S. Dewald, T. Lang, C.D. Schröter, R. Moshammer, J.Ullrich, M. Siegel, and U. Morgner
   Ionization of noble gases with pulses directly from a laser oscillator,
   Optics Letters, Vol. 31 Issue 13, pp. 2072-2074 (2006)

2. G. Palmer, M. Siegel, A. Steinmann and U. Morgner
   Microjoule pulses from a passively mode-locked Yb:KY(WO$_4$)$_2$ thin-disk oscillator with cavity dumping,
   Optics Letters, Vol. 32 Issue 11, pp. 1593-1595 (2007)

3. G. Palmer, M. Emons, M. Siegel, A. Steinmann, M. Schultze, M. Lederer, and U. Morgner
   Passively mode-locked and cavity-dumped Yb:KY(WO$_4$)$_2$ oscillator with positive dispersion, Optics Express, Vol. 15 Issue 24, pp. 16017-16021 (2007)

4. M. Siegel, G. Palmer, A. Steinmann, M. Pospiech, and U. Morgner
   Theoretical and experimental limits of cavity dumping in passively mode-locked thin-disk oscillators,
   Optics Express, Vol. 15 Issue 25, pp. 16860-16869 (2007)

5. Y. Liu, S. Tschuch, M. Dürr, A. Rudenko, R. Moshammer, J. Ullrich, M. Siegel, and U. Morgner
   Towards non-sequential double ionization of Ne and Ar using a femtosecond laser oscillator,
   Optics Express 2007, Vol. 15, Issue 26, pp. 18103-18110

6. A. Steinmann, G. Palmer, M. Emons, M. Siegel, and U. Morgner
   Generation of 9 µJ, 420 fs pulses by fiber-based amplification of a cavity-dumped Yb:KYW laser oscillator,
   Laser Physics 18, pp. 527-529, 2008

7. G. Palmer, M. Schultze, M. Siegel, M. Emons, U. Bünting, and U. Morgner
   Passively mode-locked Yb:KLu(WO$_4$)$_2$ thin-disk oscillator operated in the positive and negative dispersion regime,
   Optics Letters, Vol. 33 Issue 14, pp. 1608-1610 (2008)

8. Y. Liu, S. Tschuch, M. Dürr, A. Rudenko, R. Moshammer, J. Ullrich, M. Siegel, and U. Morgner
Strong field double ionization of Ar below the recollision threshold,
Phys. Rev. Lett. 101, 053001 (2008)

9. M. Siegel, G. Palmer, M. Emons, M. Schultze, A. Ruehl, and. U. Morgner
Pulsing dynamics in Ytterbium based chirped-pulse oscillators,
Optics Express, Vol. 16 Issue 19, pp. 14314-14320 (2008)

10. M. Siegel, N. Pfullmann, S. Rausch, T. Binhammer, G. Palmer, and U. Morgner,
Microjoule pulse energy from a chirped-pulse Ti:Sapphire oscillator with cavity-dumping,
Optics Letters, Vol. 34 Issue 6, pp. 740-742 (2009)

International Conferences

1. S. Dewald, M. Siegel, R. Moshammer, and U. Morgner
Generation of Intense Laser Fields by a Long-Cavity Oscillator,
Conference on Lasers and Electro-Optics (CLEO) 2006, Long Beach, USA, paper: CMG1

2. U. Morgner, G. Palmer, S.Dewald, A. Steinmann, and M. Siegel
High-energy laser pulses directly from the oscillator,
16th International Laser Physics Workshop 2007, León, Mexiko

3. U. Morgner, G. Palmer, A. Steinmann, M. Emons, M. Pospiech, M. Schultze, and M. Siegel
High-energy laser pulses directly from the oscillator - from thin-disk to positive dispersion,
Advanced Solid-State Photonics (ASSP) 2008, Nara, Japan, paper: ME3

4. G. Palmer, M. Emons, M. Siegel, A. Steinmann, M. Pospiech, and U. Morgner,
Passively Mode-Locked and Cavity-Dumped Yb:KY(WO$_4$)$_2$ Oscillator with Positive Dispersion,
Conference on Lasers and Electro-Optics (CLEO) 2008, San José, USA, paper: CFB2

5. G. Palmer, M. Siegel, A. Steinmann, M. Schultze, and U. Morgner,
Passively Mode-Locked Yb:KY(WO$_4$)$_2$ Thin Disk Oscillator with Cavity-Dumping
Conference on Lasers and Electro-Optics (CLEO) 2008, San José, USA, paper: CThFF7

6. M. Siegel, G. Palmer, A. Steinmann, M. Pospiech, and U. Morgner,
Theoretical and Experimental Limits of Cavity-Dumping in Passively Mode-Locked

Thin-Disk Oscillators,
Conference on Lasers and Electro-Optics (CLEO) 2008, San José, USA, paper:
JWA73

7. M. Siegel, G. Palmer, M. Emons, M. Schultze, A. Ruehl, and U. Morgner,
Pulsing dynamics in Ytterbium based chirped-pulse oscillators,
Advanced Solid-State Photonics (ASSP) 2009, Denver, USA, paper: MB10

8. M. Siegel, N. Pfullmann, S. Rausch, T. Binhammer, G. Palmer, and U. Morgner,
Microjoule pulse energy from a chirped-pulse Ti:Sapphire oscillator with cavity-dumping,
Advanced Solid-State Photonics (ASSP) 2009, Denver, USA, paper: WE3

9. G. Palmer, M. Schultze, M. Siegel, M. Emons, A. Steinmann, and U. Morgner,
Chirped-Pulse and Solitary Mode-Locked Yb:KLuW Thin-Disk Laser Oscillator,
Advanced Solid-State Photonics (ASSP) 2009, Denver, USA, paper: MC2

10. M. Siegel, N. Pfullmann, S. Rausch, T. Binhammer, G. Palmer, and U. Morgner,
Microjoule pulse energy from a chirped-pulse Ti:Sapphire oscillator with cavity-dumping,
CLEO/Europe-EQEC 2009, München, paper: CA7.5

11. G. Palmer, M. Schultze, M. Siegel, A. Steinmann, and U. Morgner,
Yb:KLuW thin disk oscillator in solitary and chirped pulse operation,
CLEO/Europe-EQEC 2009, München, paper: CA2.4

12. S. Rausch, T. Binhammer, A. Harth, M. Siegel, and U. Morgner,
Ti:sapphire Frequency Comb with Octave-Spanning Spectrum for Spectroscopy and Few-Cycle Pulse Shaping,
CLEO/Europe-EQEC 2009, München, paper: EG.P.2

Spring Meeting of the German Physical Society (DPG)

1. S. Dewald, M. Siegel, T. Lang, and U. Morgner,
Erzeugung hoher Pulsspitzenleitungen direkt aus einem Laserresonator,
DPG - Frühjahrstagung 2005, Berlin, Germany

2. S. Dewald, M. Siegel and, U. Morgner,
Erzeugung intensiver Laserfelder mit einem langen Laseroszillator,
DPG - Frühjahrstagung 2006, Frankfurt, Germany

3. M. Siegel, J. Meyer-Ilse, U. Morgner, and S. Tschuch
Erzeugung hoher Pulsspitzenleistungen direkt aus einem Laserresonator
DPG - Frühjahrstagung 2007, Düsseldorf, Germany

4. S. Tschuch, Y. Liu, M. Dürr, R. Moshammer, J. Ullrich, M. Siegel, and U. Morgner
   Ionisation von Atomen mit Lichtpulsen aus einem 6 MHz Laseroszillator,
   DPG - Frühjahrstagung 2007, Düsseldorf, Germany

5. M. Siegel, G. Palmer, A. Steinmann, N. Pfullmann, and U. Morgner
   Theoretische und experimentelle Limits von modengekoppelten Scheibenlasern mit Cavity-Dumping
   DPG - Frühjahrstagung 2008, Darmstadt, Germany

6. Y. Liu, S. Tschuch, M. Dürr, A. Rudenko, R. Moshammer, J. Ullrich, M. Siegel, and U. Morgner,
   Experiments on non-sequential double ionization of Ne and Ar using a femtosecond laser oscillator,
   DPG - Frühjahrstagung 2008, Darmstadt, Germany

7. G. Palmer, M. Emons, M. Siegel, A. Steinmann, and U. Morgner,
   Passiv modengekoppelter Yb:KYW-Oszillator mit Cavity- Dumping im positivem Dispersionsregime,
   DPG - Frühjahrstagung 2008, Darmstadt, Germany

8. M. Siegel, N. Pfullmann, G.Palmer, F. Schewe, and U. Morgner,
   Titan-Saphir Laseroszillator mit Mikrojoule Pulsenergie,
   DPG - Frühjahrstagung 2009, Hamburg, Germany

9. N. Pfullmann, M. Siegel, and U. Morgner
   Kryogene Nachverstärkung von μJ-Laserpulsen,
   DPG - Frühjahrstagung 2009, Hamburg, Germany

10. G. Palmer, M. Schultze, A. Steinmann, A. L. Lindemann, M. Siegel, and U. Morgner
   Femtosekunden Yb:KLuW-Scheibenoszillator im solitären und positiv dispersiven Dispersionsregime,
   DPG - Frühjahrstagung 2009, Hamburg, Germany

Acknowledgements

First of all I would like to thank Prof. Uwe Morgner for supervising my thesis and giving me the opportunity to work in this field.

It was fascinating to see the group grow, starting with only handful of people at the beginning of my thesis in Heidelberg, to nearly 30 people working in Hannover right now. Special thanks belong to Thomas Binhammer, Guido Palmer, Stefan Rausch and Andy Steinmann who also made the move from Heidelberg to Hannover and have been great friends and colleagues throughout the last couple of years. Since supervising diploma students always is a learning experience for both sides, I would also like to thank my diploma students Nils Pfullmann, Anne Harth and Julia Meyer-Ilse for the time we spent working together. The same thanks of course go out to all the other former and current members of the Ultrafast Optics group at the Institute of Quantum Optics, which by now are too many for them all to be named here.

Thanks are also due to the team of the institute's workshop without whose work none of the experimental results of this thesis could have been achieved. To the team of the secretariat at IQ belong my thanks, as they were always available to help with any of the numerous questions concerning the bureaucratical stuff that comes with such a work.

Last but not least I want to thank my wife Stefanie, my parents Konrad and Roswitha as well as my sister Eva, for all the support they have given me over the years. None of this would have been possible without them.